MODULATION OF NEURONAL RYANODINE RECEPTOR-MEDIATED CALCIUM SIGNALING BY CALSENILIN

A DISSERTATION IN
Cell Biology and Biophysics
and
Molecular Biology and Biochemistry

Presented to the Faculty of the University
of Missouri-Kansas City in partial fulfillment of
the requirements for the degree

DOCTOR OF PHILOSOPHY

by
MICHAEL ANTHONY GRILLO

M.S., University of Missouri-Kansas City, Kansas City, MO 2010
B.S., Texas Wesleyan University, TX, 2000

Kansas City, MO
2013

MODULATION OF NEURONAL RYANODINE RECEPTOR-MEDIATED CALCIUM SIGNALING BY CALSENILIN

Michael Anthony Grillo, Candidate for the Doctor of Philosophy Degree

University of Missouri-Kansas City, 2013

ABSTRACT

Calsenilin is calcium (Ca^{2+}) ion Ca^{2+} binding protein found in the nucleus, plasma membrane, and endoplasmic reticulum of neuronal cells. Calsenilin was first found to interact with two proteins involved in early-onset familial Alzheimer disease (AD), presenilin 1 and presenilin 2. Several studies have shown overexpression of calsenilin to alter Ca^{2+} signaling and cell viability in several neuronal cell models of AD. In this study, we show that calsenilin directly interacts with the ryanodine receptor (RyR) modulating Ca^{2+} release from this intracellular Ca^{2+}-activated Ca^{2+} release channel.

Co-expression, co-localization, and protein-protein interaction of calsenilin and RyR in primary neurons and in central nervous system tissue were determined using immunoblotting, immunohistochemistry and co-immunoprecipitation. Mechanisms of intracellular Ca^{2+}- signaling controlled by the interaction of calsenilin and RyR, including changes in the release of Ca^{2+} from intracellular stores, were measured with single channel electrophysiology and live-cell optical imaging techniques.

Immunohistochemical studies showed a high degree of co-localization between calsenilin and the RyR in neurons of the central nervous system. Additionally,

successful immunoprecipitation of a RyR-calsenilin protein complex from brain tissue provided evidence of a functional interaction. Using electrophysiological and Ca^{2+} imaging techniques the modulatory effects of calsenilin on Ca^{2+} release in a single RyR channel or in a cellular system with a population of RyR channels, respectively, whereby RyR-mediated intracellular Ca^{2+} release by calsenilin was determined under physiological and pathophysiological intracellular Ca^{2+} concentrations.

Calsenilin directly interacts with the RyR, modulating Ca^{2+} induced Ca^{2+} release (CICR) pathways in neuronal cells. Further characterization of this interaction and its pharmacological and molecular biological control could provide insight into altered Ca^{2+} signaling in neurodegenerative and other diseases controlled by CICR and aid in developing novel alternative therapies using these newly identified mechanisms as targets.

APPROVAL PAGE

The faculty listed below, appointed by the Dean of the School of Graduate Studies, have examined a dissertation titled, “Modulation of neuronal ryanodine receptor-mediated calcium signaling by calsenilin”, presented by Michael Anthony Grillo, candidate for the Doctor of Philosophy degree, and certify that in their opinion it is worthy of acceptance.

Supervisory Committee

Peter Koulen, Ph.D., Committee Chair
Cell Biology and Biophysics

Lawrence Dreyfus, Ph.D.,
Cell Biology and Biophysics

Anthony Persichini, Ph.D.,
Molecular Biology Biochemistry

Ann Smith, Ph.D.,
Molecular Biology and Biochemistry

Simon Kaja, Ph.D.,
Ophthalmology

TABLE OF CONTENTS

TABLE OF FIGURES

Figure Page

LIST OF TABLES

Table Page

ACKNOWLEDGEMENTS

This thesis would not have been possible without the help and support of my colleagues in the University of Missouri-Kansas City.

I am especially indebted to Dr. Peter Koulen, whose seemingly inexhaustible encouragement, guidance and long hours of supervision proved invaluable throughout the course of this research.

I would also like to express my appreciation to my committee members and fellow lab members for their conversation and advice whilst undertaking long hours of laboratory work.

Finally, I wish to thank my wife, Stephanie, for providing me with love and encouragement throughout my years of study. Without her understanding and support it would have been impossible to cope with the many peaks and troughs that are involved in completing a dissertation. Not only has her role as a spouse been instrumental in completing my dissertation, but her knowledge as a scientist has helped to overcome the many research hurdles I have faced. Without her in my life I would not be the scientist or person I am today.

CHAPTER 1

INTRODUCTION

General overview of Ca^{2+} signaling: functions, mechanism, and channels

Calcium (Ca^{2+}) is a tightly regulated signaling molecule in cells [11]. Localized increases in Ca^{2+} concentration initiate different signaling pathways [11, 12, 22, 30, 51, 92, 126, 134, 135, 142, 163, 164]. The ability of Ca^{2+} to initiate multiple signaling pathways depends on the source of Ca^{2+} entry [11]. Ca^{2+} entry into the cytoplasm occurs through multiple ion channels in the plasma and endoplasmic/sarcoplasmic reticulum membrane [11]. Ca^{2+} ion channels possess distinct protein ensembles responsible for transmitting Ca^{2+} signals from the source of Ca^{2+} entry to the site of action [11].

For most cell types, the resting intracellular Ca^{2+} concentration is between 50nM-150nM [11]. The Ca^{2+} concentration in the endoplasmic/sarcoplasmic reticulum is approximately 100μM, and the Ca^{2+} concentration outside the cell is in the mM range [11]. The high concentration of Ca^{2+} outside the cell and in the endoplasmic/sarcoplasmic reticulum creates a steep concentration gradient between cytoplasmic Ca^{2+}, extracellular Ca^{2+}, and endoplasmic/sarcoplasmic Ca^{2+} [11]. Activating Ca^{2+} ion channels on the plasma membrane rapidly increases Ca^{2+} concentrations in the intracellular loci surrounding the ion channels [12]. The increase in Ca^{2+} concentration surrounding the plasma membrane Ca^{2+} ion channels is amplified by the release of Ca^{2+} from Ca^{2+} induced Ca^{2+} release (CICR) ion channels on the endoplasmic/sarcoplasmic reticulum [12]. The increased Ca^{2+}

concentration surrounding the plasma membrane ion channels creates several microdomains of elevated Ca^{2+} that can reach high μM concentrations. [134]. The elevation in Ca^{2+} concentration in these microdomains along the plasma membrane can last from milliseconds to minutes [158]. The microdomains of elevated Ca^{2+} can remain localized, which can result in activation of Ca^{2+} sensitive proteins, or they can move throughout the cell by activating regenerating waves of increased Ca^{2+} throughout the cytoplasm through CICR [134]. Ca^{2+} signaling is regulated by the composition of proteins within close proximity of these elevated Ca^{2+} microdomains [126]. Ca^{2+} binding proteins, Ca^{2+} buffering proteins, Ca^{2+} ATPase pumps, exchangers, and Ca^{2+} ion channels (both plasma and endoplasmic/sarcoplasmic reticulum membrane) surrounding the increased Ca^{2+} microdomains can bind Ca^{2+} [12, 23, 30]. The binding of Ca^{2+} to Ca^{2+} binding proteins can initiate signaling pathways through the activation, or inactivation, of the Ca^{2+} binding proteins. The binding of Ca^{2+} to Ca^{2+} buffering proteins lowers the amount of free Ca^{2+} present in microdomains of elevated Ca^{2+}, therefore limiting the spread of increased Ca^{2+} in the cytoplasm. Ca^{2+} ATPase pumps, both on the plasma membrane and endoplasmic/sarcoplasmic reticulum membrane, rapidly extrude Ca^{2+} from the cytoplasm to subsequently lower the availability of free Ca^{2+}, therefore returning intracellular Ca^{2+} concentration to resting levels [30, 54]. The binding of Ca^{2+} to CICR channels in the endoplasmic/sarcoplasmic reticulum amplifies and propagates the initial increase in Ca^{2+} concentration through plasma membrane Ca^{2+} ion channels [52]. Understanding Ca^{2+} signaling in cells begins with the activation mechanisms of plasma membrane Ca^{2+} ion channels [59, 126, 156, 171].

Plasma membrane Ca^{2+} ion channels activate in response to extracellular stimuli [92]. The mechanism of plasma membrane Ca^{2+} ion channel activation is specific for each family of plasma membrane Ca^{2+} ion channels [92]. Membrane depolarization activates voltage operated Ca^{2+} channels (VOCC) on the plasma membrane [92]. Activation of VOCCs on the plasma membrane generates rapid increases in intracellular Ca^{2+} in excitable cells [104]. The rapid influx of Ca^{2+} through VOCCs on the plasma membrane control muscle contraction and exocytosis of neurotransmitters [30]. Receptor operated Ca^{2+} channels on the plasma membrane are activated by binding ligands produced from extracellular signals. N-Methyl-D-Aspartate (NMDA) receptors and α-amino-3-hydroxy-5-methylisoxazole-4-propionate acid (AMPA) receptors are activated through binding of the neurotransmitter glutamate [142]. Glutamate is released from presynaptic neurons into the synaptic cleft where it binds to postsynaptic NMDA and AMPA receptors activating them [116]. The influx of Ca^{2+} through NMDA and AMPA receptors in response to glutamate is one mechanism of neuron to neuron communication. Another source of Ca^{2+} entry is through plasma membrane store operated Ca^{2+} channels that refill endoplasmic/sarcoplasmic reticulum Ca^{2+} stores [116]. The transient receptor potential plasma membrane Ca^{2+} ion channels represents a large family of ion channels that are activated in different ways depending on the type of channel [115]. Some of the transient receptor potential ion channels are stretch sensitive, responding to mechanical disruption of the plasma membrane, while others bind agonists for activation [115]. The wide variety of plasma membrane Ca^{2+} channels is the cells first response to extracellular stimuli propagating distinct

Ca^{2+} signals throughout the cell [115]. The amplification of these signals by CICR channels in the endoplasmic/sarcoplasmic reticulum increases Ca^{2+} locally ,or transmits these signals throughout the cell[115].

The major CICR ion channels in the endoplasmic/sarcoplasmic reticulum are ryanodine receptors (RyRs) and Inositol-1, 4, 5-trisphophate receptors (IP_3Rs) [149]. The binding of Ca^{2+} to intracellular CICR channels, within the microdomains of increased Ca^{2+} concentration, results in activation of these channels and subsequent Ca^{2+} release into the cytoplasm [11, 12, 30]. The release of Ca^{2+} from intracellular CICR channels can then activate Ca^{2+} release from adjacent intracellular CICR channels [11, 12, 30]. This process of activation allows the influx of Ca^{2+} from the plasma membrane Ca^{2+} channels to be amplified by the CICR release from RyR- and IP_3R- sensitive stores [134]. The adjacent stimulation of clusters of RyRs creates frequent repetitive oscillations of increased Ca^{2+} [134]. The phenomenon of frequent repetitive oscillations of increased Ca^{2+} has been extensively studied in heart tissue [26, 71, 183]. In heart tissue, the coupling of RyRs to L-type VOCC regulate excitation contraction coupling [26, 71, 183]. Ca^{2+} influx through L-type VOCCs activate clusters of RyRs that release Ca^{2+} creating a localized increase in Ca^{2+}, or Ca^{2+} “spark” [26, 71, 183]. The “spark” enlists adjacent clusters of RyRs to release Ca^{2+}, creating discrete spatiotemporal increases in Ca^{2+} concentration that coordinate muscle contraction throughout the heart [118]. In neurons, NMDA receptor activation in dendrites causes metabatropic glutamate receptors to mobilize Inositol 1, 4, 5-trisphosphate (IP_3) [94, 150]. IP_3 along with Ca^{2+} activate IP_3Rs in apical dendrites of neurons initiating a Ca^{2+} wave that creates

discrete spatiotemporal patterns along dendrites [94, 150]. In dendrites of layer II/III and V pyramidal cortical neurons, the amplification and transmission of Ca^{2+} along apical dendrites has a RyR component as well as an IP_3R component [94, 150]. The amplification and propagation of Ca^{2+} signals by RyRs and IP_3Rs coordinates the activity of adjacent cells. The coordination of signals occurs through the specific spatiotemporal pattern of Ca^{2+} release throughout the cells [94]. In excitable cells, Ca^{2+} plays a pivotal role in induction and transmission of signals within the cell that lead to short and long term alterations in protein expression and activity [205]. These alterations have a profound effect on cell to cell communication, most notably in the central nervous system where Ca^{2+} is involved in every aspect of pre- and post- synaptic communication between neurons [10].

The spatiotemporal release of Ca^{2+} in neurons contributes to neuronal plasticity and memory

Ca^{2+} signaling in neurons involves the integration and communication of multiple incoming neuronal messages [138]. Neuronal signaling is processed through complex hierarchies of distinct cell populations creating networks of related processing units [138]. The organization of neuronal networks is achieved through definitive spatial and temporal patterns of increased cytoplasmic Ca^{2+} [138]. The distinct patterns of increased Ca^{2+} release in neurons regulates transcription [31, 156], membrane excitability [163], neurotransmitter release [142], apoptosis [111, 171] , and memory formation [11, 142, 168].

Ca^{2+} signaling directly effects transcription in neurons through Ca^{2+} binding transcriptional modulators such as calsenilin [31], or by initiating Ca^{2+} dependent signaling cascades that effect transcription [208]. The activation of adenylyl cyclase by Ca^{2+} to produce cyclic AMP (cAMP) causes cAMP to directly enter the nucleus and effect transcription [208]. Cyclic AMP activation of protein kinase A (PKA) leads PKA to phosphorylate target proteins that alter transcription [5]. The activation of Ca^{2+}/calmodulin-dependent protein kinase IV (CAMKIV) can phosphorylate Ca^{2+}/cAMP response element binding protein (CREB) altering hippocampal gene transcription [19]. Activation of the ras signaling pathway alters long term plasticity, and occurs in a Ca^{2+} dependent fashion [133]. In CA1 neurons, large Ca^{2+} signals occur at the synapse and cause a Ca^{2+} wave to travel from apical dendrites to the nucleus [21]. This increase in nuclear Ca^{2+} that originates in dendrites can change neuronal plasticity [6]. Plasticity and memory formation occur between pre- and post-synaptic neurons through the spatial and temporal aspects of Ca^{2+} signaling [105, 138]. Regulation of membrane excitability in neurons can increase or decrease firing patterns between neuronal synapses [3]. A backpropagating action potential is a process where an action potential is generated in the soma of neurons traveling through the axon, and through proximal and apical dendrites [104]. Studies in dendritic spike timing and back-propagation of signals have shown that VOCC location as well as Ca^{2+} influx from VOCC's effects communication in hippocampal neurons [55]. The amplification of pre- and post-synaptic signals by ryanodine sensitive stores can effect membrane potential therefore altering the spatiotemporal firing of neurons [10, 55, 104, 149]. These alterations in firing pattern

underlie the major contribution of Ca^{2+} signal integration during the formation of long term potentiation (LTP) and long term depression (LTD) [10, 54, 105]. LTP and LTD are processes in neurons, whereby the specific spatiotemporal pattern of intracellular Ca^{2+} can consolidate or erase temporary memories [10, 163]. The release of vesicles containing neurotransmitter in pre-synaptic cells are controlled by Ca^{2+} intrusion through VOCCs, and amplification of the Ca^{2+} signal by internal release from ER stores [10, 163].

Ca^{2+} signaling can initiate apoptosis by activating caspases [171]. In neurodegenerative disorders, abnormal alterations in Ca^{2+} homeostasis can increase apoptosis through different mechanisms based on disease and cell type [9, 11, 83, 109, 111, 165]. The integration of simultaneous neuronal signaling pathways can be transmitted by modest alterations in CICR dynamics [50]. RyRs are one of the major CICR channels of the ER [13]. RyRs have multiple binding sites for modulation of Ca^{2+} release including signaling molecules, ions, proteins, and other ion channels [13]. The different modulatory molecules that bind to RyRs allow multiple signaling pathways to be shaped by Ca^{2+} release l[13].

Structure, modulation, function, and role of ryanodine receptors in neurodegeneration

RyRs are CICR channels consisting of four-approximately 550kDa subunits located on the ER [118, 149, 172, 180]. This approximately 2200 kDa channel has a large N –terminal cytoplasmic domain [61, 73, 90, 93]. The N-terminal domain acts

as a scaffold for multiple modulatory substances that integrate different cellular pathways by modulating the release of Ca^{2+} through CICR [61, 73, 90, 93]. The RyR has three receptor subtypes, RyR1 [198], RyR2 [122], and RyR3 [60] that share 65% sequence homology [43, 60, 66, 125]. The two major RyR in the brain are the type 2 and type 3 isoforms found in the hippocampus, cortex, and cerebellum [53, 60, 89, 119, 150]. RyRs have a bell shaped response curve to cytosolic Ca^{2+}, with maximum activity between 1-100uM depending on receptor subtype [17]. RyR2 and RyR3 are active over a wide range of cytosolic Ca^{2+} values, while RyR1 is activated and inhibited at higher cytosolic Ca^{2+} levels [17, 77, 85, 114, 124, 154]. The biophysical modulation of the RyRs can be characterized by a change in the frequency of channels openings, the gating time of ON and OFF channel events, and the conductance of Ca^{2+} through the channel [67, 137]. Signaling molecules such as ATP [14, 153], cADPR [58, 84], small molecules such as magnesium [92, 93] and Ca^{2+} [17, 77, 85, 154] have an effect on RyR channel function by altering the affinity of RyRs for Ca^{2+}. Phosphorylation of RyRs by protein kinase A (PKA) [29, 113, 185] and Ca^{2+}/calmodulin-dependent protein kinase II (CaMKII) [186, 189] can increase Ca^{2+}-dependent activation of RyRs. Phosphorylation of RyRs allows distinction of different Ca^{2+} sensitive pathways through phosphorylation of specific kinase sensitive domains [132] [186, 191]. The macromolecular complex formed by RyRs involves the cytoplasmic N-terminal domain that accounts for 90% of the total mass of the receptor [155]. The structural proteins FKBP12 and FKBP 12.6 bind to RyRs stabilizing the closed conductance state and coordinating gating between adjacent receptor clusters [57, 106, 107, 127]. Homer proteins competitively bind to

RyRs and effect channel activity [71, 82]. The long isoform of Homer increases the channel conductance of RyRs, while the short isoform of Homer has no effect on channel activity [188]. During single channel electrophysiology experiments additive increases in the concentration of the short isoform of Homer dose-dependently decreased the heightened activation of RyRs due to the interaction of the long-isoform of Homer [46, 72, 188]. In cardiac muscle cells, the direct interaction of L-type Ca^{2+} channels with RyRs couples the Ca^{2+} influx through the plasma membrane to CICR [52] [42]. The estrogen receptor beta binds to the RyR stimulating single channel activity [136]. Binding of calmodulin (CaM) to RyRs in both the Ca^{2+} bound and unbound form inhibits the activity of RyR2 at all Ca^{2+} concentrations [148, 174]. The association of RyRs and the N-terminus of the Alzheimer's associated proteins presenilin 1 (PS1) and presenilin 2 (PS2) potentiate RyR activity [67, 137]. Alzheimer's disease mutations in PS1 associated with Alzheimer's disease further increase Ca^{2+} release [34, 162]. The diversity of proteins regulating RyRs including signaling molecules, kinases, other channels, and Ca^{2+} binding proteins shape Ca^{2+} transients by altering CICR of RyRs [178].

Structure, expression, and multiple cellular roles of calsenilin

The NCS family of Ca^{2+} binding proteins contain canonical EF hand $Ca2^{+}$-binding domains. The EF hand domain transmits Ca^{2+} signals through the cell via Ca^{2+}-bound activation [23]. The binding of Ca^{2+} to these molecules can cause conformational changes within the proteins themselves, and upon binding the target

proteins. These conformational changes induce cellular responses that initiate multiple signaling pathways [23]. One such molecule CaM, that is closely related to NCS proteins, transmits Ca^{2+} signals to multiple proteins throughout the cell and directly alters CICR through an interaction with RyRs [23, 178]. Another NCS protein, calsenilin, has been shown to alter the dynamics of Ca^{2+} signaling [98, 100] through a yet unidentified protein interaction.

Calsenilin/KChIP3/DREAM (hereafter called calsenilin) is a 31kD protein that is part of the (NCS) family [23]. Calsenilin contains a C-terminus with 4 EF-hand motifs -reminiscent of the frequenin NCS-1 subfamily, however calsenilin has a unique amino terminus [24]. Calsenilin binds to Ca^{2+} with high affinity at EF hands 3 and 4, magnesium at physiological concentrations at EF-hand 2, and contains a CPXG sequence on the first EF-hand that prevents Ca^{2+} binding [41, 120, 193]. Ca^{2+} binding to the EF hands of calsenilin cause the formation of homodimers and homotetramers that translate Ca^{2+} dependent activity to target molecules [41, 103, 120, 121]. Calsenilin is found in human brain extracts [25], and in all mouse nervous tissue with particularly high expression levels in the hippocampal layers (dentate gyrus, CA1-3), layers V & VI in the cerebral cortex, granule layers of the cerebellum, and olfactory centers [44, 62, 157, 159, 190, 192, 194]. Calsenilin is expressed throughout mouse development with the highest expression levels in adults [194].

Calsenilin was first identified to interact with the C-termini of Alzheimer's disease related proteins PS1 and PS2. This interaction regulates the level of a 20kDa specific caspase cleavage product of PS2 [24]. Calsenilin itself is a substrate for caspase 3 cleavage [37] which is regulated by phosphorylation of Ser63 in

calsenilin [36]. In neuroglioma cells, calsenilin preferentially interacts with the 20kDa PS2 C-terminal fragment which is increased in AD and associated with PS2 Familial Alzheimer's Disease (FAD) associated mutations in this protein [37]. Though not directly a part of the γ-secretase complex [48], calsenilin affects the γ-secretase cleavage of N-cadherin [74] and increases the γ-secretase production of Aβ [79]. In calsenilin knockout mice the levels of Aβ as well as Aβ induced apoptosis is decreased [99]. The pro-apoptotic function of calsenilin, which is associated with increased cytosolic Ca^{2+} concentration [80], is coordinated with presenilin/ γ-secretase activity and enhanced in the presence of PS1 gain of function AD mutants [78].In neuroglioma cells overexpression of calsenilin, enhances apoptosis in response to serum withdrawal and thapsigargin treatment is [100]. This enhancement in apoptosis is thought to occur through altered Ca^{2+} release and correlates with increased caspase activity [100]. Calsenilin can alter IP_3R mediated Ca^{2+} signaling and Ca^{2+} stores in the ER, which directly effects Ca^{2+} levels within the cell [49, 98].

Calsenilin regulates the expression of the human prodynorphin gene in a Ca^{2+} dependent manner [31]. Prodynorphin is distributed throughout the CNS and involved in pain and memory acquisition [146]. Calsenilin regulates prodynorphin through an interaction with the downstream regulatory element (DRE) hence the name DRE-antagonist regulator (DREAM) [31]. Calsenilin, in the absence of Ca^{2+}, is bound to the DRE site silencing prodynorphin gene expression. Upon Ca^{2+}, and c-AMP elevation, calsenilin binding to the DRE site is abolished [31, 41, 103, 121]. Prodynorphin expression alters several signaling pathways due to the fact it is a

precursor for several opioid receptor agonists. Opioid receptor activation can influence phosphorylation and Ca^{2+} concentrations within the cell [146]. In hematopoietic cells, calsenilin binding to a DRE site in the 3' untranslated region of the pro-apoptotic HRK gene represses HRK expression [140]. Elevation in Ca^{2+}, PI-3 kinase phosphorylation of calsenilin, and apoptotic inducers all reduce calsenilin binding to the DRE site increasing apoptosis [139, 140]. In cerebellar neurons calsenilin binding to a DRE site in the sodium Ca^{2+} exchanger (NCX3) gene decreases NCX3 expression levels in the cell [56]. This decrease in NCX3 causes increased susceptibility to Ca^{2+} induced apoptosis [56]. Furthermore, in PC12 cells, calsenilin binding to peroxiredoxin, an antioxidant enzyme that functions as a redox sensor, enhances calsenilin binding to DRE sites [130]. Knockdown of calsenilin in PC12 cells increases oxidative stress induced damage [130]. The transcription of glial fibrillary acidic protein (GFAP), an astrocyte expressed stress marker, is controlled through a calsenilin interaction in the promoter region [32, 177]. This interaction is regulated through a pituitary adenylate cyclase-activating polypeptide–cAMP-Ca^{2+}-calsenilin interaction [32, 177]. This occurs in Mueller glial cells in the retina in a NMDA - cAMP response element binding protein (CREB) phosphorylation dependent manner [35, 91, 129]. Binding of calsenilin to phosphorylated CREB decreases the interaction with DRE sites, and regulates the production of the early response gene c-fos in a cAMP dependent manner [28, 47, 95, 96]. In spinal inflammation the production of brain derived neurotrophic factor is controlled by calsenilin [131, 196], and in kainite and pentylenetetrazol induced seizure the levels

of calsenilin in dentate gyrus, cerebral cortex, and piriform complex are altered providing evidence for calsenilin in inflammatory responses [70, 108].

Calsenilin directly interacts with rapidly inactivating voltage gated potassium channel ($Kv_{4.2}$) potassium channels on the plasma membrane. The interaction with $Kv_{4.2}$ channels occurs in the α pore forming subunit altering the biophysical release properties of the channel [182]. The interaction of calsenilin with $Kv_{4.2}$ channels stabilizes tetramerization of the four $Kv_{4.2}$ subunits [7, 27, 75, 117, 181]. This interaction occurs in a 1:1 ratio between each $Kv_{4.2}$ subunit and calsenilin. This interaction includes DPP 10, a cell adhesion related protein, that form a multiprotein complex regulating channel activity [7, 27, 75, 117, 181]. Calsenilin aides in the tetrameric assembly of $Kv_{4.2}$ channels, and rescues zinc mutants that do not form tetramers and remain in the ER/Golgi [87]. Co-expression of $Kv_{4.2}$ and calsenilin in Chinese hamster ovary (CHO) cells alters $Kv_{4.2}$ activity by increasing peak current, peak current density, inactivation time constant, and recovery from inactivation [2]. The increase in channel density can be attributed to calsenilin to trafficking $Kv_{4.2}$ channels from the ER to the plasma membrane [151]. $Kv_{4.2}$ channels are found at high density in proximal and distal dendrites [18]. The modification of $Kv_{4.2}$ channel activity by calsenilin returns resting dendritic membrane potentials faster, eliminating back propagation of action potentials from the soma [18]. In the presence of a constitutively active form of Ca^{2+}-calmodulin-dependent kinase II (CaMKII) and calsenilin, $Kv_{4.2}$ current amplitudes and surface expression were increased linking $Kv_{4.2}$ channel activity to calsenilin and Ca^{2+} [179]. Alterations in the inactivation time constant of $Kv_{4.2}$ channels are transmitted to $Kv_{4.2}$ by arachidonic acid and PKA

phosphorylation only in the presence of calsenilin [69, 143]. Signaling between T-type Ca^{2+} channels (Cav3) and $Kv_{4.2}$ channels through a calsenilin interaction is thought to link Ca^{2+} signaling and $Kv_{4.2}$ channels [3]. Finally, calsenilin binds to the C0 domain of the NR1 subunit of NMDA receptors causing an inhibition of NMDA receptor currents and reduction of NMDA receptor activated Ca^{2+} currents [197].

Calsenilin has a myriad of functions that alter Ca^{2+} signaling and cell viability in neurons [31]. Calsenilin affects Ca^{2+} levels in cells, excitability in neurons, transcription, and cleavage products AD related-proteins. The similar roles of calsenilin and CICR channels in the maintenance of physiological Ca^{2+} and the perturbation of Ca^{2+} in pathological states is striking.

Perturbations of Ca^{2+} homeostasis in Alzheimer's disease

Subtle changes Ca^{2+} homeostasis can affect cell viability, transcriptional regulation of apoptotic proteins, and neuronal connectivity [9]. In the progression of AD all of these processes are altered [9]. There is also an increase in the production of Aβ plaques and tau neurofibrillary tangles [9]. The linking of FAD with sporadic Alzheimer's disease (SAD) could provide clues into the etiology and progression of nongenetic SAD.

AD is a neurodegenerative disorder that is clinically characterized by a loss of higher cognitive function and memory with marked behavioral abnormalities [63]. Pathologically, AD is characterized by the presence of β amyloid (Aβ) plaques, neurofibrillary tangles, and progressive neuronal loss [63]. One type of AD which

accounts for approximately 5% of AD cases is early onset familial AD (FAD) [63]. FAD occurs in people before 65 years of age and is correlated with missense mutations in the amyloid precursor protein (APP), γ-secretase proteins, PS1 and PS2 [63]. The second type of AD, which accounts for the remainder of the cases, is sporadic AD (SAD) [63]. SAD occurs later in life, usually after 65 years of age, and has genetic and non-genetic factors [63]. Typical disease etiology of SAD includes a slow decline in cognition and memory, and increase in cell loss in the hippocampus and cortex [63]. Alterations in Ca^{2+} signaling occur before these changes become evident [16], suggesting that Ca^{2+} dysregulation plays a role in the pathogenesis of AD. The Ca^{2+} hypothesis of AD states that a remodeling of Ca^{2+} homeostasis in response to altered β-amyloid accumulation is an underlying cause of memory loss and cell death associated with AD [9, 109, 165]. Increased β-amyloid accumulation, as well as normal aging, can cause an increase in the resting Ca^{2+} concentration within neurons [86, 102, 173]. This alteration in normal Ca^{2+} concentration induces oxidative stress [88, 110], increases cell death from excitotoxicity [4], and effects learning and memory (reviewed [9]). Cortical neurons from triple AD mutant transgenic mice show increased resting Ca^{2+} levels [102]. Neocortical neurons from triple AD mutant transgenic mice also show elevations in resting Ca^{2+} levels in dendrites and spines as a function of proximity to Aβ deposits [86]. In young and aged transgenic mouse models of AD there is a correlation between increased Aβ and aberrant expression and release of RyR sensitive Ca^{2+} stores [83, 166]. Mutations in PS1 and PS2 increase recruitment, expression, and Ca^{2+} release from RyRs in transgenic mouse models of AD in cortical, and hippocampal neurons [33,

34, 97, 152, 161]. The increase in Ca^{2+} content and Ca^{2+} release from ER mediated stores causes an increase in apoptosis in several models of AD [51, 97, 161]. These alterations in intracellular Ca^{2+} signaling suggest that abnormal activities of RyRs may play a part in the progression of AD. Modulation of RyRs by AD related proteins such as PS1, PS2 and calsenilin could help dissect the role of RyRs in AD, and provide possible targets for the modulation of intracellular Ca^{2+} release.

Identification of a direct protein-protein interaction between calsenilin and neuronal RyRs as a potential mechanism for the alteration of CICR

The goal of the present study is to identify a direct interaction of calsenilin with neuronal RyRs describing a mechanism of action for the underlying modulation of CICR. By identifying an interaction and describing the modulatory effect we will describe whether this interaction alters intracellular Ca^{2+} levels in physiological and pathophysiological states. Calsenilin and neuronal RyRs directly interact with the AD related proteins PS1 and PS2 to alter the Ca^{2+} levels within the cell in normal physiological cell signaling [24, 49, 67, 81, 98, 100, 137]. In several models of AD, the interaction between calsenilin and PS1 and PS2, as well as RyRs and PS1 and PS2, cause increased apoptosis, abnormal Ca^{2+} signaling, and vulnerability to various cellular insults [33, 78-80, 83, 99, 100, 152, 161, 166]. The ability of NCS to modulate RyRs and alter CICR suggests a possible role for calsenilin and RyRs in shaping neuronal cell signaling [155]. The fact that calsenilin binds with PS1 and PS2 in the ER [172], and multiple targets of several Ca^{2+} signaling pathways [31,

79, 96, 100, 195] including modulation and tetramerization of plasma membrane $Kv_{4.2}$ channel that is directly linked to T-type Ca^{2+} channels [2, 3, 75], suggests a possible interaction between calsenilin and RyRs. To date, the link between altered Ca^{2+} release and calsenilin has not been studied in depth and is widely seen as a consequence of alterations in transcription, $Kv_{4.2}$ channel action, and γ-secretase activity.

Targets for the modulation of Ca^{2+} have proved effective in slowing the progression of neuronal loss in several neurodegenerative diseases [45], but this approach is applied to whole receptor populations in the body affecting countless signaling pathways. Targeting a modulatory protein rather than a whole ion channel population would allow for tunable manipulations of specific cells populations. For the current study, we hypothesize that calsenilin and RyRs directly interact to modulate RyR Ca^{2+} release. To test this hypothesis we used immunological, electrophysiological and live imaging techniques in neuronal cells and tissue to 1) determine whether there is colocalization of RyR and calsenilin, 2) to determine whether a direct protein-protein interaction of RyR and calsenilin exists, 3) to test the effect calsenilin has on single RyR channels, and 4) to test the effect calsenilin has on a population of RyR channels, *in vitro*.

CHAPTER 2

MATERIALS AND METHODS

In order to verify that calsenilin and neuronal RyRs interact, the expression pattern of these two proteins was assessed in neuronal cells and whole brain tissue sections using fluorescent immunohistochemistry. The quantification of co-localization was calculated using standard algorithmic formulas, Pearson's and Mander's coefficients. Once co-localization was established, testing for direct protein-protein interactions was verified using co-immunoprecipitation studies reported with Western blot analysis. The alterations in biophysical Ca^{2+} release from single brain RyRs in the presence of calsenilin were measured using planar lipid electrophysiology. The changes in single channel RyRs biophysical release was assessed utilizing a whole cell paradigm using overexpression of calsenilin in order to determine how the changes in single channel RyR Ca^{2+} release translated into whole cell Ca^{2+} release signals.

Growth and preparation of the SH-SY5Y neuroblastoma cell line: an experimental neuronal cell model for Ca^{2+} release studies

SH-SY5Y neuroblastoma cells (ATCC, Manassas, VA) were thawed from cryo-storage (-80°C), and grown in a T-150 cell culture flask (TPP, MidSci, St. Louis, MO) using SH-SY5Y media (10% fetal bovine serum (PAA, Piscataway, NJ), 1:200 penicillin/streptomycin, 50% Ham's F-12 media, 50% eagle minimum essential

media (Lonza, Walkersville, MD)) where cells were maintained in a maintained in a 37ºC, 5%CO_2, 95% O_2 incubator. Once 50%-70% confluency was reached, media was removed and placed into a 50mL conical Falcon tube where 5mL of Trypsin-EDTA (Mediatech, Manassas, VA) was added to the flask and allowed to incubate a 37^{o}C for 2-5 minutes. Following incubation, 5mL of the removed media was placed back into the flask to inhibit the trypsin digestion. The flask was washed three times with the removed media and placed into the 50mL Falcon tube. The sample was spun at 200xg for 3 minutes and the supernatant was removed. The pellet was resuspended in 1 mL of cell media and 20 µL of the suspension was counted using a Cellometer Auto T4 (Nexcelom Bioscience, Lawrence, MA). The cells were plated at 25,000 cells per laminin/poly-d lysine coverslips (BD Biocoat, Bedford, MA) and maintained in a 37ºC, 5%CO_2, 95% O_2 incubator.

Growth and preparation of rat cortical neurons: an *in vitro* model to establish endogenously expressed calsenilin and RyRs

NeuroPure™ embryonic day 18 (E18) Sprague Dawley rat cortical cells (Genlantis, San Diego, CA) were prepared following the according to manufacturer's protocol. The shipping media from the vial containing the E18 rat brain tissue was removed and replaced with 5mg of NeuroPapain™ enzyme dissolved in NeuroPrep™ medium (Genlantis), and incubated for 15 minutes at 37^{o}C (to breakdown the extracellular matrix). The tissue was then centrifuged at 200xg for 1 min and supernatant removed and discarded, and replaced with the original shipping

media. The tissue was resuspended with a fire polished glass pipette by triturating approximately 15 times in (Genlantis). Subsequently, the cells were centrifuged at 200xg for 1 minute and resuspended in NeuroPure™ plating medium (Genlantis). In order to determine the cell density, the cell suspension was mixed with a trypan blue at a 1:1 ratio, and counted using a Cellometer Auto T4 (Nexcelom Bioscience). The cells were plated at 25,000 cells per laminin/poly-d lysine coverslips (BD Biocoat) and maintained in a 37ºC, 5%CO_2, 95% O_2 incubator.

Immunocytochemistry: to establish the expression pattern and co-localization of calsenilin and RyRs in neuronal cell models

SH-SY5Y cells or primary cortical neurons were allowed 1 or 7 days, respectively, to adhere to laminin/poly-d lysine coverslips (BD Biocoat), then were washed three times in phosphate buffered saline (PBS) (Lonza), and fixed for 15 min in 4% paraformaldehyde (PFA) (4% PFA w/v, 0.1M NaOH, 0.1M NaH_2PO_4, pH 7.3 (Sigma-Aldrich)) to preserve cellular structures by methylene crosslinking. Following the removal of PFA, three 10 min washes with PBS were performed. In order to block nonspecific secondary antibody binding, a serum buffer from the secondary antibody host species was applied (donkey serum blocking buffer (1% BSA fraction V (EMD Millipore, Gibbstown, NJ), 0.5% Triton x -100 (Sigma-Aldrich), 10% donkey serum (PAA) in PBS at pH of 7.4)), where cells were incubated for 1 hour at room temperature. The block was removed and the cells were incubated with goat anti-calsenilin monoclonal antibody raised against the full length human calsenilin (1:50;

Santa Cruz Biotechnologies, Dallas, TX) and rabbit RyR2 antibody raised against a synthetic peptide variant from the transmembrane region of human RyR2 (1:10000, Chemicon Biotechnologies, Temecula, CA) or a rabbit ryanodine type 3 receptor raised against a synthetic peptide variant from the transmembrane region of human RyR3 (1:5000; Chemicon Biotechnologies) diluted in incubation buffer (1% BSA fraction V, 0. 5% Triton x-100, 3% donkey serum in PBS at a pH of 7.4) and incubated for 36-48 hours at 4°C. The primary antibody was removed, and the cells were washed three times in PBS. Cells were incubated for 1 hour in the dark at room temperature with AlexaFluor 488 donkey anti-goat secondary antibody (1:2000; Life Technologies, Carlsbad, CA; the calsenilin primary antibody was raised in goat and therefore anti-goat secondary antibody will bind specifically to the primary antibody) and AlexaFluor 594 donkey anti-rabbit (1:2000; Life Technologies; used for both of the RyR antibodies because the species specific label of the primary antibody). AlexaFluor 488 fluorescent antibody has a peak excitation wavelength of 490nm- 495nm and AlexaFluor 594 fluorescent antibody has a peak excitation wavelength of 590nm. The non-overlapping excitation and emission spectra of the two secondary antibodies used allows acquisition of both signals without the use of complex spectral unmixing software. Following secondary antibody incubation, the cells were washed in PBS with 1:10000 4', 6-diamidino-2-phenylindole (DAPI) (which binds strongly to A-T regions in DNA) for three minutes. The cells underwent three subsequent 10 minute washes in PBS, followed by one 10 min wash in deionized water (to remove excess phosphate), and the coverslips were mounted to microscope slides with Aqua-Polymount (Polysciences, Warrington, PA).

Collection and preparation of mouse brain sections: to establish endogenously expressed calsenilin and RyRs in the intact mouse brain

C57BL/6 mice (Jackson Laboratories, Bar Harbor, MA) were used in this study as a model for human brain physiology. Mice were euthanized using IACUC approved methods of carbon dioxide overdose. The heads of the mice were removed from the body by a lateral incision above the C4 cervical segment but below the brain stem. After removal of the skull from the body, the fur and skin over the crown of the skull was removed, and an incision through the medial line of cranium was made from the most posterior to the most anterior portion. Further incisions were made in the posterior and anterior portions of the skull perpendicular to the medial incision. The crown of the skull was then removed allowing access to the brain. The brains were removed from the cranial cavity using a spatula, and immersion fixed in 4% PFA overnight. Following the removal of PFA, the brain was rinsed in PBS. The tissue was then sequentially cryoprotected in a graded series of 10% sucrose, then 20% sucrose, then 30% sucrose, in order to ensure the preservation of cellular structures within the tissue. Each cryoprotection step was done at 4^{o}C overnight. Tissue was then removed from the final sucrose solution and placed in a mold, where the tissue was incubated in Tissue-Tek Optimal Cutting Temperature (OCT) Embedding Medium (Tissue Tek, Torrance CA) for 1hr at 4^{o}C. The samples were then placed in -80^{o}C isopentane (Alfa Aesar, Ward Hill, MA) to solidify the OCT compound and snap-freeze the tissue. Molds were sectioned at

30μm using a Leica model CM 3050S Cryostat. Sections were placed in PBS and stored at 4^{o}C until immunohistochemistry was performed.

Immunohistochemistry: in order to establish the expression pattern and co-localization of calsenilin and RyRs in intact mouse brain tissue

The sectioned tissue was placed in 1mg/ml sodium borohydride (Sigma Aldrich) 3 times for 10 minutes to reduce reversible Schiff's bases that may have formed during PFA-fixation [8]. In order to eliminate nonspecific binding, blocking buffer using serum from the same host species of the secondary antibody was applied (donkey serum blocking buffer (1% BSA fraction V (EMD Millipore), 0.5% Triton x -100 (Sigma-Aldrich), 10% donkey serum (PAA) in PBS at pH of 7.4)), where brain sections were incubated for 1 hour at room temperature. The block was removed and the cells were incubated with goat anti-calsenilin monoclonal antibody raised against the full length human calsenilin protein (1:50; Santa Cruz Biotechnologies) and rabbit RyR2 antibody raised against a synthetic peptide variant from the transmembrane region of human RyR2 (1:10000, Chemicon Biotechnologies) or a rabbit RyR3 raised against a synthetic peptide variant from the transmembrane region of human RyR3 (1:5000; Chemicon Biotechnologies) diluted in incubation buffer (1% BSA fraction V, 0. 5% Triton x-100, 3% donkey serum in PBS at a pH of 7.4) and incubated for 36-48 hours at 4°C. The primary antibody was removed, and the brain sections were washed three times in PBS.

Brain sections were incubated for 1 hour in the dark at room temperature with AlexaFluor 488 donkey anti-goat secondary antibody (1:2000; Life Technologies; used to label the calsenilin primary antibody) and AlexaFluor 594 donkey anti-rabbit (1:2000; Life Technologies; used for both of the RyR antibodies). AlexaFluor 488 fluorescent antibody has a peak excitation wavelength of 490nm-495nm and AlexaFluor 594 fluorescent antibody has a peak excitation wavelength of 590nm. The non-overlapping excitation and emission spectra of the two secondary antibodies used allows acquisition of both signals without the use of complex spectral unmixing software. Following secondary antibody incubation, the brain sections were washed in PBS with 1:10000 4', 6-diamidino-2-phenylindole (DAPI) (which binds strongly to A-T regions in DNA) for three minutes. The brain sections underwent three subsequent 10 minute washes in PBS, followed by one 10 min wash in deionized water (to remove excess phosphate). The brain sections were then incubated in 25mM $CuSO_4$ for 10 minutes in order to mask the fluorescent pigment lipofuscin, which are pigment granules that accumulate in the cytoplasm of cell in the central nervous system. The sections were subsequently washed three times with PBS for 10 minutes, followed by a 10 min wash in deionized water (to remove excess phosphate), where coverslips were mounted to microscope slides with Aqua-Polymount and allowed to dry overnight.

Confocal microscopy: imaging of calsenilin and RyR immunoreactivity in neuronal cells and tissue

Confocal imaging settings for accurate data acquisition

Images were acquired using a Leica laser-scanning TCS SP5X confocal microscope with tunable pulsed White Light Laser, at 63x oil objective. Collection and visualization of images were done with Leica Acquisition Software. All cell images were acquired with the following settings: 95.5 µm pinhole, xyz scan mode, 107.0 µm width and height, 1.6 µm depth with step sizes of 0.13 µm, voxel width and height 52.3 nm and depth at 125.9 nm, 2048 by 2048 pixels with a 4x line average and 2.3 zoom. Laser power, offset and gain remained constant throughout all cells imaged. All brain images were acquired with the following settings: 102.8 pinhole, xyz scan mode, 8 bit resolution, 60.0 µm width and height, 1.0 µm depth with a step size of 0.13 µm, voxel width and height 58.7 nm and depth at 125.9nm, 1024 by 1024 pixels with a zoom of 4.1. Laser power, offset and gain remained constant throughout all experiments. AlexaFluor 488 was excited at a wavelength of 495nm and emission was collected at 496nm-647nm. AlexaFluor 594 was excited at a wavelength of 590nm and collected at 602-760nm. The collection of each of the fluorophores was done sequentially to avoid crosstalk, which is the excitation of one fluorophore causing a spillover emission signal of the other fluorophore. Due to the excitation of AlexaFluor 594 being 590nm, which is in the emission spectra of AlexaFluor 488, AlexaFluor 488 was always excited first, then AlexaFluor 594, and lastly DAPI.

Acquisition theory to ensure maximum resolution and contrast sensitivity of confocal image acquisition settings

The optimizing of imaging parameters allows a precise definition of the sampling frequency used by a particular microscope. By calculating the correct sampling frequency for the microscopes hardware any sample can be accurately visualized. By defining the sampling frequency, we avoid false positives that occur from under sampling, and avoid superfluous collection of data due to oversampling. All imaging was done in such a way as to maximize the resolution and contrast sensitivity of the microscope. In order to identify the maximum resolution of each objective used an Airy disk calculation was done. The Airy disk is a calculation of the diffraction pattern of light, and can be visualized as a sine curve of the maximum and minimum intensity of the signal. The Airy Disk is calculated for each objective separately, using the formula $r=0.61\ \lambda/NA$ (where λ is the emission wavelength of the secondary antibody and NA is the numerical aperture of the objective). The numerical aperture for each objective takes into account the half angle of the cone of light that enters the lens, and the refraction index for the medium used (i.e. Oil=1.56, water=1.33, air=1). The Airy disk calculation quantifies the distance with which the objective used can resolve a single point of light. To maximize spatial resolution, or contrast, of two points the Rayleigh criterion was applied. The Rayleigh criterion states that the maximum spatial resolution that can be expected in an image (the minimum distance that can accurately determine the separation of two objects in close proximity) is achieved by the lining up of the zero point of one Airy disk with the maximum point of the next objects Airy disk. This criterion becomes applicable

when the sampling frequency used to collect the image is to be determined. In microscopy the sampling frequency is the pixel size. Utilizing the Nyquist theorem, which states that to accurately reproduce a sine curve sampling, must be done at 2.3 times the frequency, the optimum pixel size as related to the maximum resolution, or Airy disk, can be chosen. To maximize the spatial resolution that can be expected from two objects that are in close proximity as defined by the Rayleigh criterion, the application of the Nyquist theorem to the half curve of the Airy disk will ensure accurate reproduction of the areas of the curve that derive maximum contrast. These parameters were applied to the collection of all confocal images in all imaging experiments [20, 147].

Co-localization software was used to analyze and discriminate between the true immunoreactivity signal over background signal

Fiji ImageJ was used to quantify co-localization between calsenilin and the RyR utilizing the 'Intensity Correlation Analysis' plugin. The output of this analysis program was a Pearson's coefficient (R^r) and the Mander's coefficients (M1, M2) for each protein. To ensure that the co-localization output was true and not due to a random overlap of pixels, the Costes method was applied to the images. To ensure signal accuracy, several control staining/collections were done to set a fluorescent threshold level. The threshold level is a value that describes fluorescence that is due to nonspecific signals. Only values above these levels were considered true signals. Nonspecific values are tissue/cell autoflourescence (no antibodies, inherent fluorescents of tissue/cells), nonspecific secondary fluorescence (due to the

secondary antibody binding to tissue/cell), crosstalk (e.g. fluorescent signals collected in 602-760nm from 495 excitation (AlexaFluor 488 excitation in AlexaFluor 594 emission)), and background fluorescence.

Pearson's coefficient: to measure the linear relationship of calsenilin and RyR immunoreactivity

The Pearson's coefficient is an algorithm that measures the covariance of two fluorophores within the analyzed image. The covariance is described as a linear relationship between the signals in the two channels. The values are from -1 to 1 with a value of -1 describing an inverse relationship between signals (as one signal increases the other decreases) and defined as no colocalization. A value of 1 describes a relationship in which the two channels are perfectly colocalized (as one signal increases the other increases), and a value of 0 is defined as a nonlinear relationship between the two species. The Pearson's coefficient is not affected by background, but can be affected by noise. This limitation can be overcome by applying a threshold during analysis, and correctly setting the gain and offset function during image acquisition. The Pearson's coefficient allows the correlation of how two signals interact but does not take into account the contribution of each of the fluorophores separately as the Mander's coefficient does.

Mander's overlap coefficient: a measurement of the overlap of calsenilin and RyR immunoreactivity

The Mander's coefficient is an algorithm that measures the proportion of overlap of each channel with the other [38]. The values of the Mander's coefficient are between 0 to 1, with a value of 0 describing no co-localization and a value of 1 describing perfect co-localization. The Mander's coefficient allows us to establish the percentage of each protein that is co-localized with each other. A value of 1 means that the two proteins of interest are localized together 100% of the time, while a value of 0 means that the two proteins are never localized together. For most proteins with multiple binding partners and activities in the cell, we would expect a value between 0.3 - 0.7, indicating the proteins are sometimes localized together, but also to have other proteins they associate with. The Mander's coefficient is not influenced by the intensity of the two signals, but is sensitive to high background. This limitation can be overcome by applying a threshold during analysis, and correctly setting the gain and offset function during image acquisition. The Mander's coefficient allows us to quantify the percentage of each species that is expressed within a certain image.

Costes method: to determine if the co-localization established between calsenilin and RyRs was due to random chance.

The Costes method is an approach to test the validity of the co-localization values with respect to the co-localization values that would be calculated by random overlap [40]. This method allows us to verify whether proteins are contained within the same area, or if they are randomly associated due to a captured event during fixation, the random association of background signal to real signal, and happenstance detritus on coverslips. In this method, one of the channels pixels are scattered randomly and the Pearson's value derived from this overlap is compared to the co-localization value derived from the true sample. The values are compared and the significance of the true co-localization is indicated by a P-value of > 95%. In this study 200 randomization patterns were compared to the value from the true localization.

Co-immunoprecipitation: to determine a direct protein-protein interaction between calsenilin and RyRs

Protein-A (*Staphylococcus aureus*) coated magnetic beads (EMD Millipore) were coated with antibodies used for co-Immunoprecipitation experiments. Protein A magnetic beads were used due to their high affinity for the rabbit IgG_2 of the precipitating antibody rabbit anti-RyR2 antibody (Millipore, MA, USA, raised against the synthetic peptide from the variant TM region of human RyR2). ER microsomes

(250µg; method detailed later in the chapter) alone or with rabbit anti-RyR antibody (1:200; #AB9080; Millipore) or control rabbit IgG (2mg/ml magnetic beads), with or without recombinant calsenilin protein (20nM, 40nM, 60nM, 80nM and 100nM; Mus musculus; transcript variant 1, mRNA; accession number, NM_019789; protein was obtained and purified by Brian Gerdes in the Vision Research Center), and were incubated under constant shaking at 4^{o}C for 12hrs. The recombinant calsenilin protein carries a glutathione S-transferase (GST) tag, therefore instead of detection of calsenilin protein its actual weight of approximately 29-30kDa, the protein is detected at the combined calsenilin and GST molecular weight of between 51-55kDa (see Figure 1). Following incubation, the slurry of antibodies and proteins were incubated at room temperature with protein A magnetic beads (50ul) for 10 minutes, washed 3 times in PBS with 0.1% Tween 20, and eluted with Western Blot Sample Buffer sodium dodecyl sulfate (SDS): 10%, glycerol: 10%, β-mercaptoethanol: 1%, bromophenol blue: 0.004%, tris (hydroxymethyl) aminomethane (Tris)-HCl: 0.5 M, pH 6.8) and heated for 10 min at 80^{o}C. Samples were then probed using the western blot technique.

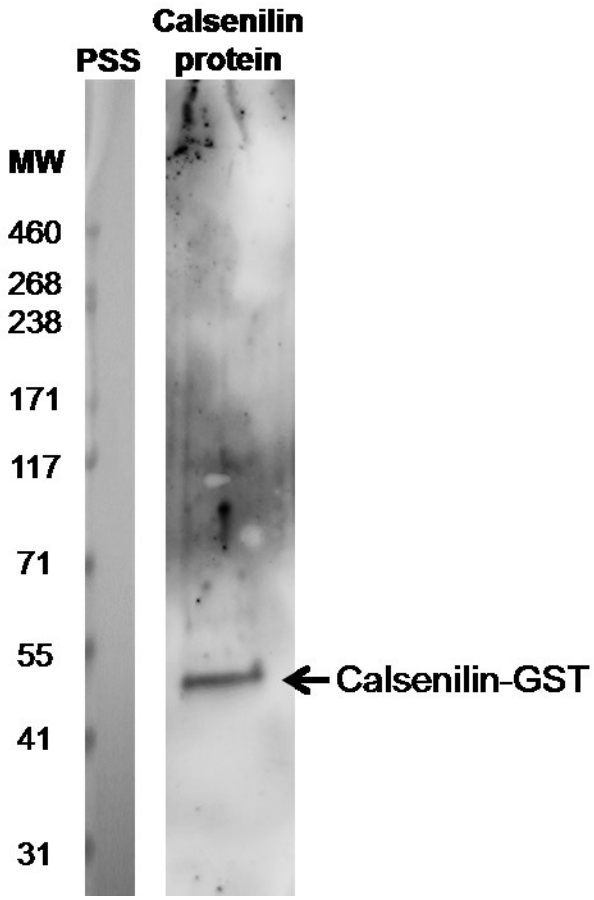

Figure 1. Immunoblot of calsenilin recombinant protein with a GST tag, detected at approximately 51 kDa.

Immunoblot image of calsenilin protein with a GST tag probed with ***mouse monoclonal calsenilin antibody (1:500; clone 40A5; #05-756; Upstate, NY, USA)*** overnight at 4°C with an ***horseradish peroxidase (HRP) linked anti-mouse secondary antibody (1:5000; #31430; Thermo Scientific, Glen Burnie, MD, USA)***, and ***imaged on*** the ***Syngene G:BOX using Syngene GeneSnap acquisition software***

Western blotting: to detect the protein-protein interactions following co-immunoprecipitation

Samples prepared from co-immunoprecipitation were loaded on a 3-8% NuPAGE® Novex® Midi Tris-acetate gel (Life Technologies) for electrophoresis in tris-acetate buffer (Life Technologies). Protein size was determined using Spectra Multicolor High Range Protein Ladder (Fermentas, Glen Burnie, MD). Proteins were separated at 100V, 50-60mA for 1.5-2hrs and then transferred to Amersham Hybond-ECL blotting paper (0.45µm, GE Healthcare) in transfer buffer (25mM Tris-Base, 192mM Glycine, 20% methanol, 0.01% SDS (Sigma)) at 50V/250-300mA for 2hrs at 4°C. Membranes were blocked for 1 hour at room temperature in blocking buffer (5% BSA, 0.2% Tween 20 (Sigma) in tris buffer saline (TBS, Blots were then incubated for 12-16hrs in washing buffer (0.2% Tween 20 in TBS) with mouse monoclonal calsenilin antibody (1:500; clone 40A5; #05-756; Upstate, NY, USA) and mouse RyR2 antibody (1:100; clone C3:33, Millipore, MA; raised against canine cardiac ryanodine receptor). Blots were washed 3 times for ten minutes in washing buffer and incubated with horseradish peroxidase (HRP) linked anti-mouse secondary antibody (1:5000; #31430; Thermo Scientific, Glen Burnie, MD, USA) in washing buffer at room temperature for 1 hour. Membranes were washed three times in washing buffer and developed using SuperSignal West Femto Chemiluminescent Substrate (Thermo Scientific) and imaged on the Syngene G:BOX using Syngene GeneSnap acquisition software.

Planar lipid bilayer electrophysiology: testing the effects of the calsenilin and RyRs direct protein-protein interaction on individual RyR channel activity

Isolation of endoplasmic reticulum microsomes for the electrophysiological testing of native brain RyRs

C57BL/6 mouse brains (n=8-15) were thawed and washed in ice cold PBS. The washed brains were minced on ice in homogenization buffer (260mM sucrose, 5mM HEPES, 1mMEGTA, 1mMDTT, and 10 µg/mL protease inhibitor cocktail (PMSF, aprotinin, pepstatin, trypsin inhibitor), at pH 7.35 with KOH) using a straight razor. The minced tissue was then diluted in ice cold homogenization buffer, and placed in a Dounce glass homogenizer, homogenized for 10-15 strokes, and placed in an ultracentrifuge tube. The sample was then centrifuged in a Sorvall ULTRA 80 ultracentrifuge for 10 minutes at 1000xg to remove the nuclear fractions and cellular debris. The supernatant was collected and spun at 1000xg for 10 minutes to ensure removal of all cellular debris and nuclear fraction. The supernatant was collected and centrifuged at 5000xg (to remove mitochondrial fraction) for 10 minutes. This step was repeated once more. Following the second centrifugation step, the supernatant was collected a further time and centrifuged at 100,000xg for 50 minutes (to collect the ER microsomal fraction). The supernatant was removed and discarded and the pellet was resuspended in homogenization buffer without EGTA, snap frozen in liquid nitrogen, and stored at -80^{o}C until use.

Planar lipid bilayer experimental setup

Planar lipid bilayer electrophysiology involves forming an artificial bilayer across an aperture which links two fluid filled chambers. The system consists of two distinct chambers (Warner Instruments, Hamden, CT; see Figure 2): the cis chamber, representing the cytoplasm of the cell (containing 93mMTrisOH/190mM HEPES, (Sigma-Aldrich) pH 7.35, approx. 285 mOsm) and the trans chamber representing the ER lumen (containing 50mM Ba (OH) 2/245mM HEPES (Sigma-Aldrich), pH 7.35, approx. 285 mOsm). The trans chamber contains a bilayer cup with a 150μm aperture which a lipid bilayer containing phosphatidylethanolamine and phosphatidylserine (3:1 w/w dissolved in decane; Avanti Polar Lipids, Alabaster, AL) is spread across. Prior to the spreading of the artificial bilayer, the aperture is primed by dispersing lipids containing phosphatidylcholine and phosphatidylserine (3:1 w/w dissolved in decane; Avanti Polar Lipids) within the aperture. This priming prepares the aperture to receive the lipid bilayer by providing the extra lipids to anchor the bilayer to the bilayer cup. Two salt agar bridges (5% agar in 1MKCL (Sigma) (w/v)) connect the cis and trans chamber to a headstage that transfers the signals to a BCD525 Warner Instruments amplifier. After bilayer formation a capacitance test is then performed to access the relative thickness of the bilayer. The capacitance measurement allows an indirect measure of the artificial bilayer thickness ensuring the pore region of the receptor can pass completely through the bilayer. The trans chamber is grounded and the cis chamber is clamped at 0mV. The integrity of the bilayer is accessed by monitoring the current between the two

chambers before microsome incorporation. At this time a current of 0mV connotes a bilayer with no contact between chambers.

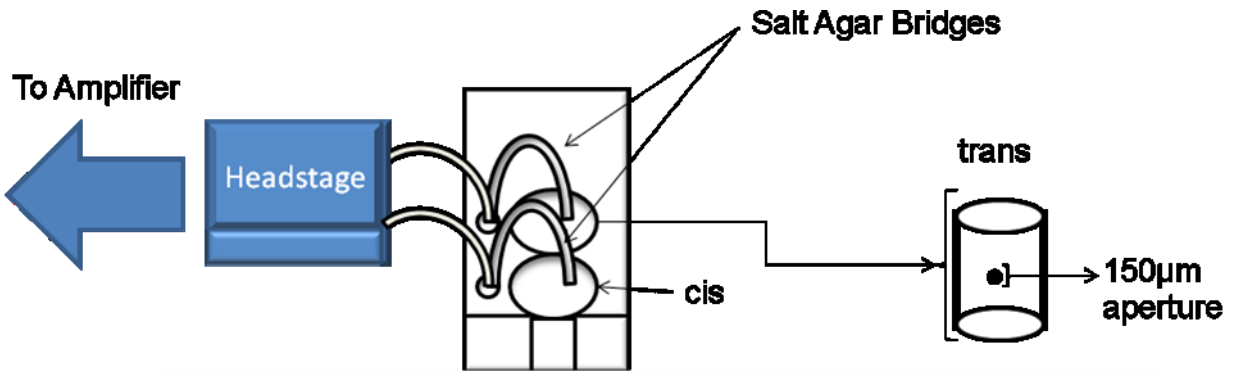

Figure 2. Schematic representation of Planar lipid bilayer electrophysiology: experimental set up.

Two chambers (cis and trans) are separated by a 150µm aperture in which an artificial bilayer is formed across. Salt agar bridges connect the two chambers to a headstage that transfers the electrical activity to an amplifier. The trans side of the chamber is grounded and the cis side of the chamber is clamped at a 0mV holding potential.

Testing for proper channel incorporation, stability, and experimental procedures for the measurement of RyRs biophysical activity

When a stable bilayer was formed, ER microsomes containing RyRs were added to the cis chamber and incubated for 10-20 minutes. The purpose of the incubation is to place the microsomes in a pre-fusion state where the lipids of the bilayer and microsome are in close proximity. When incubation was complete, microsomes were fused to lipid bilayers by addition of 3M KCl. The addition of the hyperosmotic solution creates an osmotic gradient and induces microsomal swelling. The hydrostatic pressure created within the microsome induces fusion. Fusion is monitored by the appearance of channel activity. Upon channel incorporation the cis chamber was washed with 10 volumes of cis solution. To ensure all channels are correctly oriented with the cytoplasmic portion of the RyR facing the cis chamber the current carrier used is Ba^{2+}. Ba^{2+} as a charge carrier cannot activate RyR; therefore any channels oriented with the cytoplasmic portion facing the trans chamber will not be activated. RyR currents were activated by adding Ca^{2+}/EGTA in molar proportions, calculated by MaxChelator software (Stanford University) and verified by Ca^{2+} electrode measurements. Once activated at the specific Ca^{2+} concentration to be tested, the channel activity was recorded for three minutes. After this baseline activity was recorded, calsenilin recombinant protein was added to the cis side of the chamber and allowed to incubate with constant stirring for one minute. Following incubation, the channel activity was recorded for three minutes. The range of calsenilin concentrations we used represents possible physiological concentrations of calsenilin within the cell. All experiments were performed at room temperature.

Software settings for the acquisition and filtering of single channel experiments

Single channel recordings were performed using BCD525 Warner Instruments amplifier, and filtered to reduce the amplitude of high-frequency noise at 500Hz. Digitization was done at 10 kHz using Digidata 1322A acquisition system and Molecular Devices pClamp 10 software. Analysis of recordings was done using Molecular Devices ClampFit 10 software, lowpass filtered at 320 Hz to reduce lower frequency noise associated with digitization. Baselines were set at zero, and single channel events were recorded for the conductance states of -2pA and -4pA. Clampfit software calculated all of the following statistics for 3 minutes of recording: number of events (how many times the channel opens), average amplitude (current for single channel opening), dwell time (the amount of time per each single channel opening), and open probability (the probability of a channel being open per time period).

Comparing single channel biophysical data of RyRs in the presence and absence of calsenilin

Due to the variable nature of single channel activity, all recordings were normalized to control values and reported as percentage of controls. Graphpad prism 5 software was used for all analysis and data presentation. Nonlinear curve fitting was performed using the Levenberg–Marquardt algorithm and tested for goodness of fit using the chi squared algorithm. A one-way ANOVA with a Dunnett's post hoc test was used to test significance (Mean ± SEM; $p< 0.05$*, $p< 0.01$**,

p<0.001***). One-way ANOVA analysis with a Dunnett's post hoc test was used because it is the most appropriate analysis for comparing multiple groups and normalized data.

Ca^{2+} imaging: to test the effect of calsenilin modulation of single RyR channels in a whole cell paradigm by overexpressing calsenilin in SH-SY5Y cells

Overexpression of calsenilin recombinant protein in SH-SY5Y cells

SH-SY5Y cells were grown as previously stated in section of materials and methods. Cells were stripped using trypsin-EDTA as described earlier, and 2 million cells were used for each reaction. Cells were co-transfected with the tdTomato to allow identification of transfected cells. Cells were suspended in Lonza transfection media with 2 µg of calsenilin. pcDNA3. 1 (+) Zeo mammalian expression vector and 0.5 µg of tdTomato (reporter protein) pcDNA3.1 (+) Zeo mammalian expression vector, then transfected using a Lonza 4D-nucleofector transfection unit. After transfection was carried out, the cells were plated at 25,000 cells per laminin/poly-d-lysine coverslip and maintained for 36-48 hours, and subsequently used for Ca^{2+} imaging experiments.

Verification of co-transfection using fluorescent markers

SH-SY5Y cells were co-transfection with green fluorescent protein (GFP; emission wavelength 509nm) and tdTomato fluorescent protein (emission wavelength 581nm) in order to verify the transfection protocol (described in the

preceding section). The ratio of GFP: tdTomato plasmid co-transfection was the same as that used for calsenilin: tdTomato. The cells were then fixed and imaged as previously stated. Figure 3 shows that all cells expressing the fluorescent marker tdTomato also express the GFP fluorescent marker. These results verify that cells are successfully transfected using our protocol, and that GFP can be used as a transfection-verification tool.

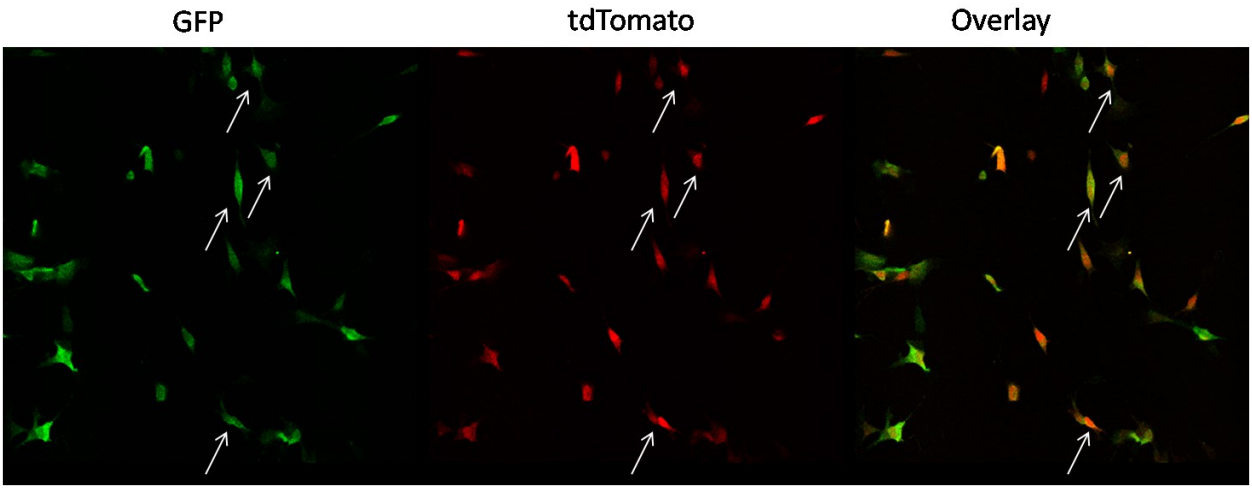

Figure 3. Validation of Co-transfection using fluorescent markers.

Co-transfection of GFP and tdTomato fluorescent markers into SH-SY5Y cells verifies that all cells transfected with the fluorescent marker protein (tdTomato) are also transfected with the GFP protein (ratio GFP: tdTomato 4:1). The first panel shows transfected cells with GFP fluorescence, the second panel shows tdTomato fluorescence, and the third panel displays an overlay of the two fluorescent signals. The arrows indicate representative cells showing similar levels of expression for both proteins.

Verification of tdTomato as an indicator for overexpression of calsenilin in cells using confocal microscopy

SH-SY5Y cells were co-transfected with calsenilin (no emission or fluorescence) and tdTomato (emission wavelength 581nm) plasmids were prepared, stained using immunocytochemistry, and imaged (see earlier section describing the immunocytochemistry protocol). Images were processed using the Image J heat map plugin which measures relative fluorescent values of specified channels and displays results using a color coded figure legend. Figure 4 shows cells that are tdTomato positive have a higher calsenilin expression level that cells that are tdTomato negative. The calsenilin expression in cells that are tdTomato negative are likely to be endogenous levels of calsenilin as they are expected to be untransfected. These results verify that by co-transfecting the cells with tdTomato enables visualization of the transfected cells with a fluorescent marker, making it possible to distinguish between successful transfection of calsenilin and consequently enabling selection of calsenilin overexpressing cells. Therefore, based on this rationale, only cells that were tdTomato positive (fluorescing cells) were chosen for Ca^{2+} imaging experiments.

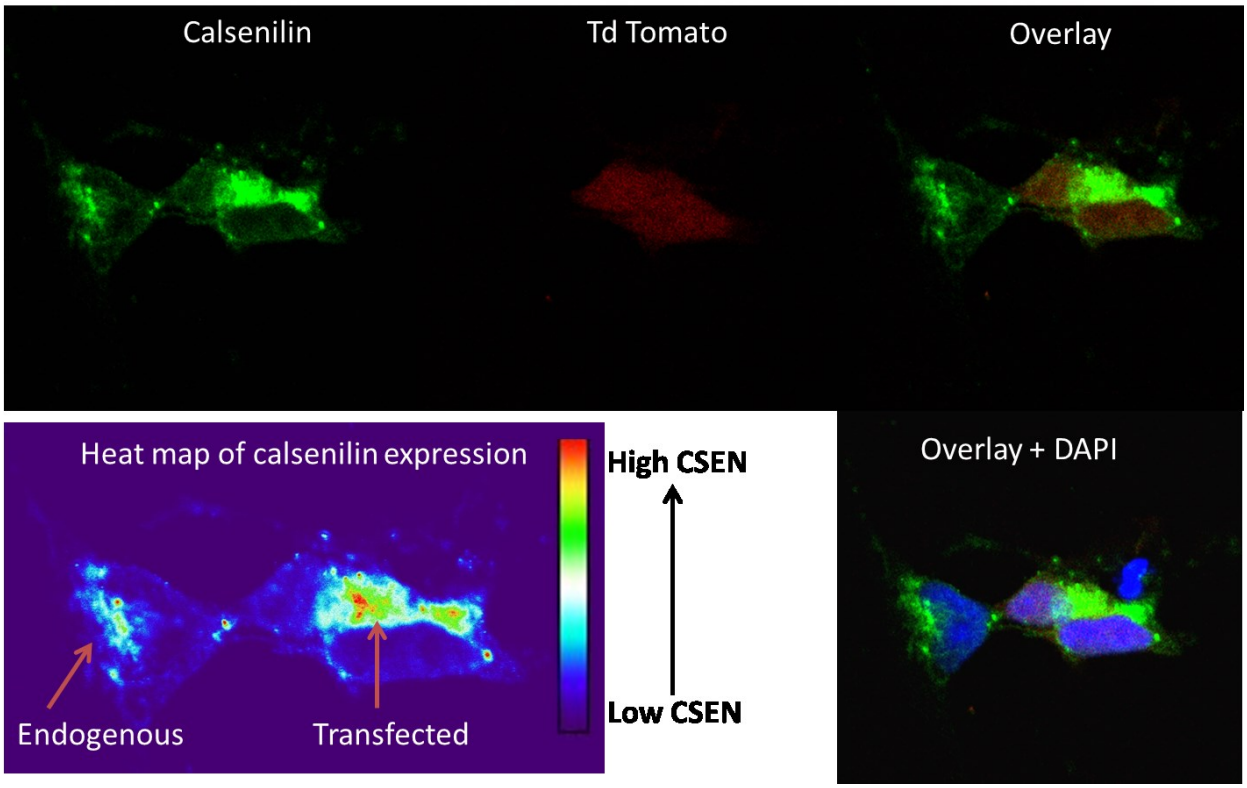

Figure 4. Confocal images showing tdTomato incorporation as an indicator for successful calsenilin transfection in SH-SY5Y cells.

SH-SY5Y cells co-transfected with calsenilin and tdTomato showed that tdTomato positive cells display increased calsenilin expression compared to cells absent of tdTomato. The first panel displays calsenilin expression, the second panel tdTomato expression, and the third panel displays and overlay of the two channels. The heat map shows that the cells expressing tdTomato have an increased expression of calsenilin as opposed to cells showing no tdTomato expression. The two red arrows in the heat map panel indicate expression of calsenilin. The fifth panel is an overlay plus the nuclear stain DAPI, indicating that overexpression of calsenilin does not alter the perinuclear expression pattern.

Calibration of the Fura-2 Ca^{2+} indicator dye K_d for Ca^{2+} binding in order to accurately translate changes in fluorescence to biological changes in Ca^{2+} concentration

Fura-2 pentapotassium salt (Life Technologies) Ca^{2+} indicator dye was used as an *in vitro* calibration for K_d calculations that mimicked experimental conditions of pH 7.35, temperature of 37^{o}C, and imaged on a Leica DM6000 FS fluorescent microscope (Leica, Wetzlar, Germany) with an Orca-R2 C10600 digital camera (Hamamatsu, Bridgewater, NJ) and DG5 illuminator and fast wavelength switcher (Sutter, Novato, CA) controlled by MetaFluor (Molecular Devices, Sunnyvale, CA), Fura-2 filter set 71000av2 (D340xv2, D380xv2, 400DCLP, D510/40m; Chroma, Bellows Falls, V) with a HCX PL APO 40x/1.25-0.75 oil objective (Leica, Wetzlar, Germany). Collection of the ratiometric fluorescent dye Fura-2 was done by exciting alternately at 340nm and 380nm and collecting at 510nm. Fluorescent values were calculated using a 340nm/380nm ratio which indicates the change in Ca^{2+} concentration. Cell free calibration of Fura-2 was done to achieve relative values of Ca^{2+} concentration for changes in fluorescence within these experimental conditions, as opposed to absolute values that would be achieved using a cell based calibration. The *in vitro* calibration was used to ensure that the minimum value of the fluorophore was achieved Reciprocal dilutions were used to calibrate Fura-2 Ca^{2+} indicator dye. This technique is based on the notion that defines free [Ca^{2+}] as the K_d of EGTA at a particular pH, temperature, and osmolarity when Ca^{2+} and EGTA concentrations are equitably close [176]. To ensure the purity of compounds used in the calibration, a commercially available calibration kit was used (calibration buffer kit # 1; Invitrogen).

The amount of free Ca^{2+} was calculated by the ratio of supplied K_2 EGTA (10mM) and CaEGTA (10mM), added to fixed amount of Fura-2 pentapotassium salt. The free Ca^{2+} concentrations tested were 0, 0.006μM, 0.0137μM, 0.0234μM, 0.0365μM, 0.0547μM, 0.0821μM, 0.128μM, 0.219μM, 0.492μM, and 36μM. Ratio measurements at 0μM and 36μM were considered min and max values, respectively. K_2 EGTA (10mM) and CaEGTA (10mM) solutions with Fura-2 pentapotassium salt (2μM) were brought to a pH of 7.35, a temperature of 37^{o}C, and placed on the microscope for data collection. Ratios of K_2 EGTA (10mM) and CaEGTA (10mM) solutions with 2μM Fura-2 pentapotassium salt were sequentially added and measured for all free Ca^{2+} values mentioned. After collection, values were plotted as the log of free Ca^{2+} concentrations (X-axis) and the log of $(F-F_{min})/(F_{max}-F)$ (y-axis). The double log plot gives an x-intercept that is the log of the K_d of Fura-2 (see Figure 5). The slope of 1 reflects the 1:1 binding of fura-2 with Ca^{2+} (Figure 5). The *in vitro* K_d of Fura-2 in these conditions was calculated to be 0.118 μM.

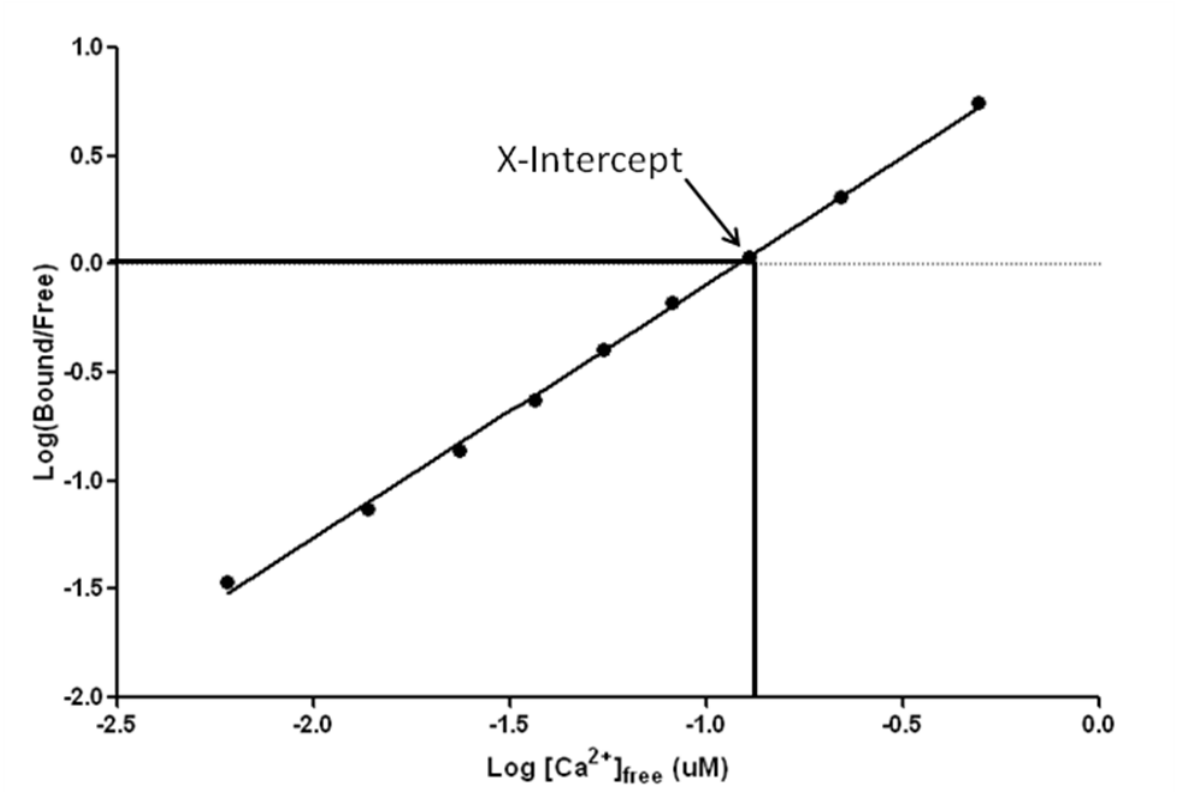

Figure 5. Calculated graph for the calibration of Fura-2 K_d value.

The y-axis displays the log of the bound/ free Ca^{2+} as reported by the fluorescent ratio of Fura-2 (340nm/380nm). The x-axis is the log of the free Ca^{2+} as calculated previously using the K_d of EGTA and a known ratio of Ca^{2+} /EGTA (x-axis; 0.006μM, 0.137μM, 0.234μM, 0.365μM, 0.547μM, 0.821μM, 0.128μM, 0.219μM, 0.492μM) at a pH of 7.35 and temperature of 37°C. The x-intercept represents the log of the K_d of Fura-2.

Ca^{2+} imaging: Quantifying the effect of calsenilin and RyR interaction on Ca^{2+} release in calsenilin-transfected SH-SY5Y cells

The media from mock- or calsenilin-transfected SH-SY5Y cells (maintained, plated and transfected as described in previous sections) was removed and washed in extracellular solution buffer (ECS; 137mM NaCl, 5mM KCl, 1mM Na_2HPO_4, 1mM $MgSO_4$ (anhydrous), 10mM HEPES, 22mM D-(+)-glucose, and 1.8mM $CaCl_2$ (anhydrous); 7.3pH at 37°C) three times, then incubated in 2μM fura-2 AM (Invitrogen) in ECS for 30 minutes. Coverslips were then washed with ECS containing 55mM KCl to empty and subsequently refill their intracellular Ca^{2+} stores, then washed a further two times with ECS. Coverslips were assembled to the imaging platform as previously described, and continually perfused with ECS at a constant temperature of 37°C by Temperature Controller TC-344B (Warner Instruments, Hamden, CT) and SC-20 inline heater/cooler (Warner Instruments). ECS containing caffeine (30mM, caffeine is a selective ryanodine receptor activator [175]) was perfused using VC-8T perfusion system (Warner Instruments, Hamden, CT) by MetaFluor and driven by P720/66 high flow peristaltic pumps (Instech, Plymouth Meeting, PA) at 2ml/minute. Time from perfusion channel opening to full chamber incubation was consistently measured at approximately 60 seconds. Perfusion protocols were the same for all experiments and controlled through MetaFluor sequential journals. The perfusion protocol was a simple 3 step sequence: 1 minute of ECS to establish a baseline, 3 minutes of 30mM caffeine in ECS to stimulate the RyRs, 3 minute of ECS to return the response to baseline (see Figure 6). Regions of Interest (ROIs) were selected following Ca^{2+} imaging, in order

to adjust for drift, and background ROI's (N=4 for each coverslip) were selected using a region of the optical field not occupied by cells.

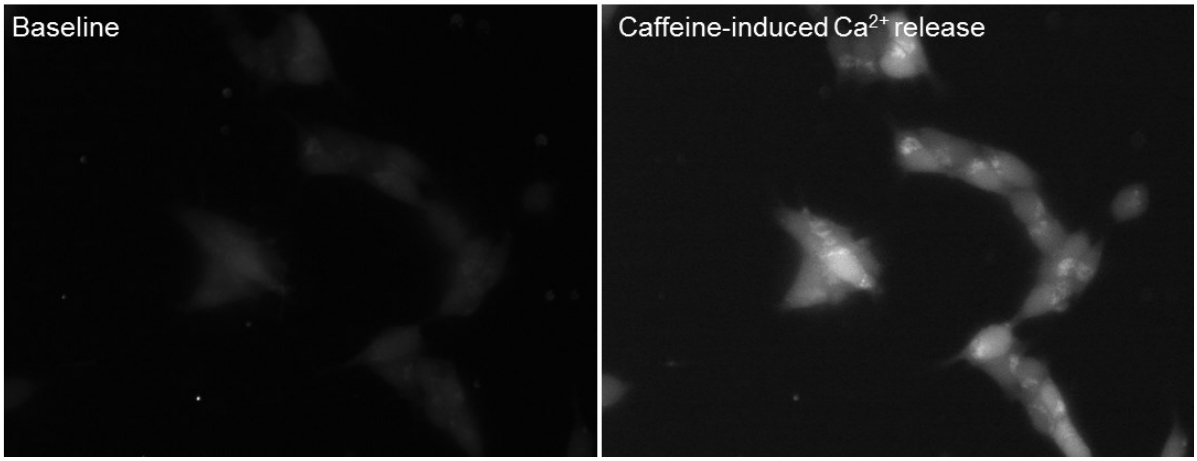

Figure 6. Representative video samples of caffeine-induced Ca2+ release during live cell Ca^{2+} imaging in SH-SY5Y cells

Representative images from calcium imaging experiments to show the fluorescent change in control SH-SY5Y cells following caffeine-induced calcium release.

Transformation and comparison analysis of Ca^{2+} imaging experiments utilizing quantitative calculated Ca^{2+} values

For each time point in the experiment protocol, the fluorescent values for excitation at 380nm (Ca^{2+} free Fura-2 indicator) and 340nm (Ca^{2+} bound Fura-2) were collected at 510nm. Background values were subtracted from raw fluorescent values to ensure only accurate signals was analyzed. Next, the ratio of bound to unbound Ca^{2+} indicator dye was calculated. The ratio of 340/380 allowed the calculation of R which describes the ratio of bound fluorescent indicator at each time point. The formula $[Ca^{2+}] = K_d*(R-R_{min})/(R_{max}-R)*F380_{min}/F380_{max}$ (K_d of Fura-2 = 0.118 μM; calculated as described earlier; R= 340/380 for each experimental time point; R_{min} = the 340/380 at 0 free Ca^{2+}; R_{max} = the 340/380 at saturating free Ca^{2+} ; $F380_{min}$ = the fluorescent intensity of 380nm at 0 free Ca^{2+}; and $F380_{max}$ = the fluorescent intensity of 380nm at saturating free Ca^{2+}) was used to calculate the quantitative Ca^{2+} concentration at each point (Note: All values in the formula were kept constant except for the experimental value of R). The formula used describes the interrelationship of free Ca^{2+} and the ratio of fluorescent intensities. The transformation of the data allows a more sensitive indicator of smaller changes in $[Ca^{2+}]$. Data sets were normalized by using $[Ca^{2+}\}/[Ca^{2+}]_0$ calculations, $[Ca^{2+}]_0$ being the calculated Ca^{2+} values for the first minute of recording (baseline), and $[Ca^{2+}]$ being the calculated Ca^{2+} values each time point. The following example calculation shows the increased sensitivity gained by transforming qualitative fluorescent signals to quantitative $[Ca^{2+}]$.

E.g. Using the same F and F_0 values, the qualitative estimate of caffeine-evoked Ca^{2+} response (F/F_0) and quantitative free [Ca^{2+}] conversions can be calculated:

F = maximum caffeine-evoked fluorescence signal = 0.074
F_0 = baseline = 0.063

A) The calculation F/F_0 can be used to obtain a qualitative estimate of the change in fluorescence over baseline after caffeine stimulation :

$F/F_0 = 0.074/0.063 = 1.17$

B) The conversion of the qualitative fluorescent signals to quantitative free [Ca^{2+}] more accurately describes the physiological changes due to smaller incremental increases in Ca^{2+}:

i) The following constants obtained from the calibration curve (Fig 5):

K_d of Fura-2 = 0.118uM
R_{min} = 0.033
R_{max} = 1.33
$F380_{min}$ = 132.08
$F380_{max}$ = 9.87

ii) Substitute constants, F, and F_0 into free [Ca^{2+}] conversion formula:

[Ca^{2+}] of F = [Ca^{2+}] = K_d*(F-R_{min})/ (R_{max}-F)* $F380_{min}$ / $F380_{max}$

[Ca^{2+}] = 0.118(0.074-0.033)/ (1.33-0.074)*(132.08/9.87)

= 0.118 (0.041/1.256)*13.38

= 0.118*0.033*13.38

= 0.052

$[Ca^{2+}]$ of F_0 = $[Ca^{2+}]_0$ = 0.118(0.063-0.033)/ (1.33-0.063)*(132.08/9.87)

= 0.118 (0.03/1.267)*13.38

= 0.118*0.024*13.38

= 0.038

iii) Therefore, the change in $[Ca^{2+}]$ over baseline after caffeine stimulation is:

$[Ca^{2+}]/ [Ca^{2+}]_0$ = 0.052/0.038 = 1.37

By transforming the qualitative fluorescent values to quantitative Ca^{2+} values the changes evoked by caffeine induced Ca^{2+} release become more biologically meaningful. Though the relationship between the signals is not altered, a small change in fluorescence equates to a larger change in Ca^{2+} concentration. Fura-2 is sensitive to small changes in Ca^{2+} concentration, which reflects the same sensitivity of cellular processes to minute changes in Ca^{2+} concentration. Therefore, the transformation of qualitative fluorescent values to quantitative Ca^{2+} concentrations more accurately reflects the magnitude of change in a cell after caffeine induced Ca^{2+} release.

Graphpad prism 5 software was used for all analysis and data presentation. The calculation for the area under the curve (AUC) was defined as follows: the beginning of the curve was the time point where the Ca^{2+} value rose above 5% of

baseline and the ending of the curve was defined by the last point in the curve that was above 5% of baseline. Both maximum value and width of response were calculated from this curve also. Linear regression was done to calculate the slope values of each response (which represents the rate of Ca^{2+} release for each experiment) using the max value and the first point 5% above baseline. All values were averaged and statistically analyzed using the student's t-test (Mean ± SEM, $p< 0.05$*, $p< 0.01$**, $p<0.001$***).

CHAPTER 3

RESULTS

The expression patterns of calsenilin and RyRs in neuronal tissue were compared and quantified using immunocytochemistry (SH-SY5Y cells and E18 cortical neurons) and immunohistochemistry (brain sections). To establish if colocalization translates to a direct protein-protein interaction co-immunoprecipitation of calsenilin and neuronal RyRs were carried out. Subsequent Western blot analyses of precipitated proteins were identified using protein weight estimation. Single channel electrophysiology and live-cell optical imaging techniques were used to determine the mechanisms of intracellular Ca^{2+} signaling controlled by the interaction of calsenilin and RyRs, including changes in the release of Ca^{2+} from intracellular stores. Immunocytochemistry or immunohistochemistry verified the biological relevance of this interaction by showing that calsenilin and RyR2 or RyR3 are co-localized in neuronal cells. Co-immunoprecipitation studies established a direct link between the two proteins of interest. To better understand the functional consequences of a calsenilin and RyR interaction the biophysical parameters of RyR Ca^{2+} release were measured in the presence of calsenilin. Single channel kinetics was measured using planar lipid bilayer electrophysiology. The modulation of Ca^{2+} release in a population of RyRs was tested by overexpressing calsenilin (transfection) in a whole cell model and imaging the release of Ca^{2+} through live cell optical imaging techniques.

Calsenilin and RyR2 and RyR3 co-localized in rat primary cortical neurons and SH-SY5Y cells

Immunoreactivity for calsenilin and RyR2 (Fig 7A), and calsenilin and RyR3 (Fig 7B) shows a punctate distribution pattern indicative of perinuclear endoplasmic reticulum staining [68, 149, 172]. These expression patterns were similar in primary cortical neurons (Fig 7A and 7B) and SH-SY5Y neuroblastoma cells (Fig 8A and 8B). Pearson's coefficient values (Table 1) for both primary neurons and neuroblastoma cells describe a moderate linear relationship characterizing two proteins that interact in the perinuclear regions of the cells, but diverge when located elsewhere. The Mander's coefficient values of calsenilin and RyR (Table 1) are between 30%-60% showing these proteins occupy the same region within the cell, but have a wide distribution throughout the cell.

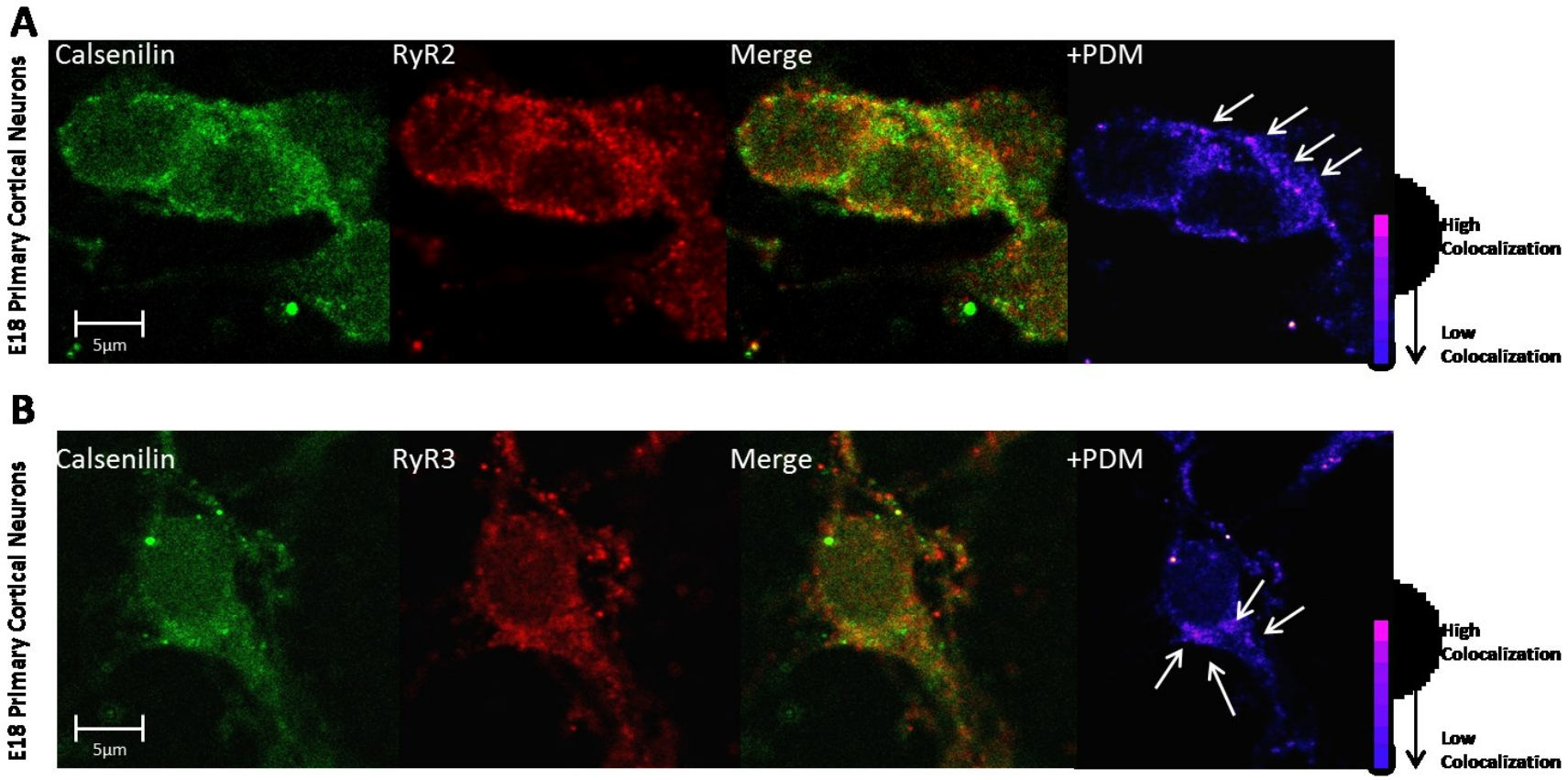

Figure 7. Calsenilin and RyR immunoreactivity and co-localization pattern in cortical neurons.

Calsenilin and A) RyR2 or B) RyR3 immunoreactivity in E18 primary cultured cortical neurons shows co-localization in regions adjacent to the nucleus indicative of endoplasmic reticulum staining. A) Calsenilin immunoreactivity (green) and RyR2 immunoreactivity (red) shows a perinuclear staining pattern (Merge) and a high degree of punctate co-localization in the perinuclear region (+PDM) as indicated by arrows and LUT in the last panel. B) Calsenilin immunoreactivity (green) and RyR3 immunoreactivity (red) shows a perinuclear staining pattern (Merge) and a high degree of punctate co-localization in the perinuclear region (+PDM) as indicated by arrows and LUT legend in the last panel.

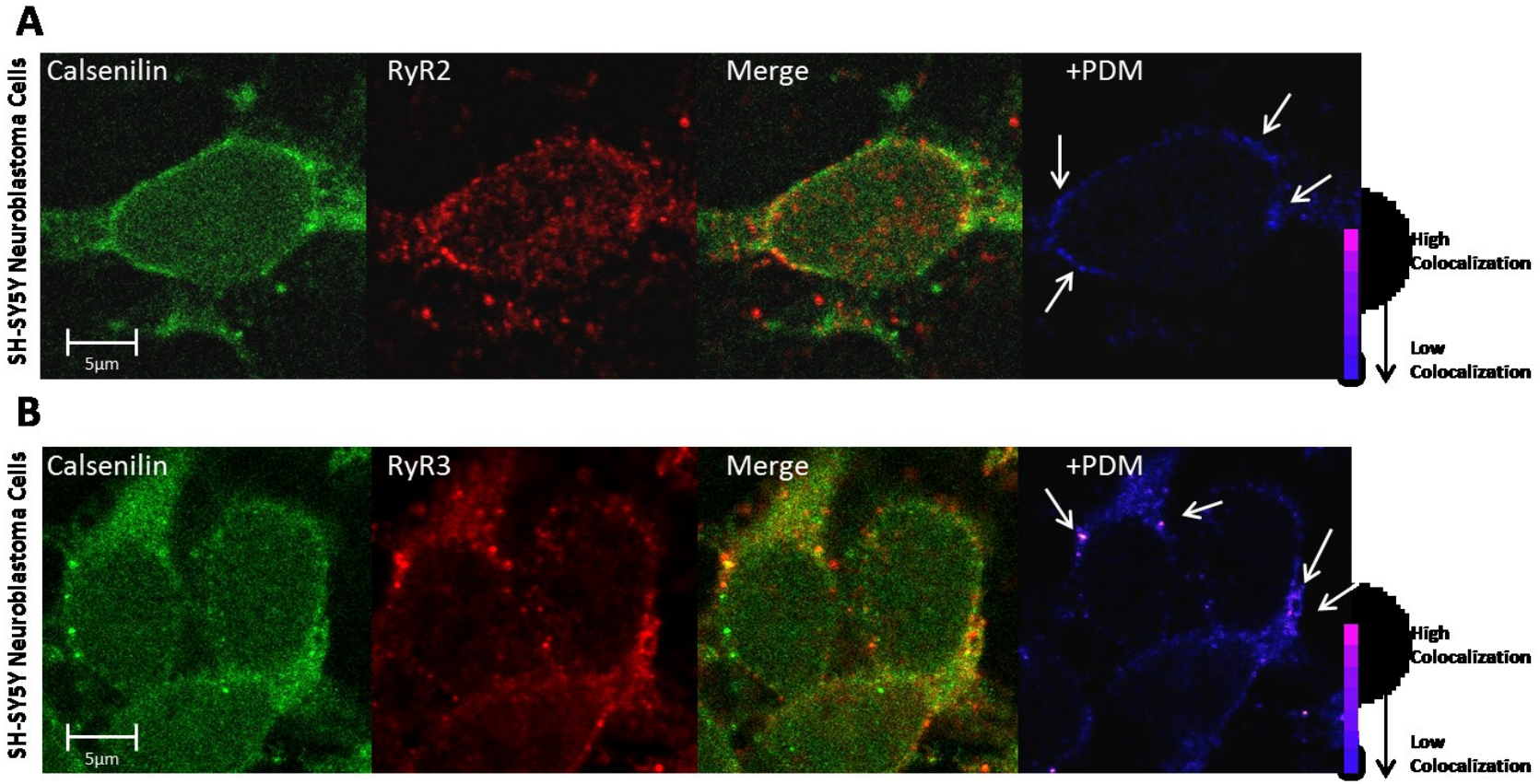

Figure 8. Calsenilin and RyR immunoreactivity and co-localization pattern in SH-SY5Y cells.

Calsenilin and A) RyR 2 or B) RyR 3 immunoreactivity in SH-SY5Y neuroblastoma cells shows co-localization in regions adjacent to the nucleus indicative of endoplasmic reticulum staining A) Calsenilin immunoreactivity (green) and RyR 2 immunoreactivity (red) shows a perinuclear staining pattern (Merge) and co-localization in the perinuclear region (+PDM) as indicated by arrows and LUT in the last panel B) Calsenilin immunoreactivity (green) and RyR 3 immunoreactivity (red) shows a perinuclear staining pattern (Merge) and a high degree of punctate co-localization in the perinuclear region (+PDM) as indicated by arrows and LUT in the last panel.

Calsenilin and RyR2 and RyR3 co-localize in the hippocampus and cortex

In the mouse brain, co-localization of calsenilin and RyR2 or RyR3 in the dentate gyrus, CA3 and CA1 of the hippocampus and II/III, V, and VI layer of the cortex showed differing degrees of co-localization for the two channel subtypes tested. Hippocampal immunoreactivity of RyR2 and calsenilin was similar to cellular studies, as represented by the dentate gyrus staining (Fig 9A). As shown in Table 1, Pearson's coefficient and Mander's coefficient values in brain tissue are similar to that of the cellular studies performed in this study, indicating that the distribution and co-localization of these two proteins are similar *in vitro* as well as *in vivo*. Immunoreactivity of RyR2 and calsenilin in the cortical layers shows a similar pattern of expression and co-localization, represented by cortical layer VI staining (Fig 9B), as seen in earlier experiments. R^r, M1, and M2 values are in accordance with those in the hippocampal areas, with the R^r values being slightly higher in all cortical levels tested (Table 1). RyR3 and calsenilin co-localization showed a differential distribution depending on brain region. The CA3 region of the hippocampus (Fig 10A) showed a higher degree of co-localization than the dentate gyrus (Fig 10B) and the CA1 regions (Table 1). In the cortical regions layer VI (Fig 11A), RyR3 and calsenilin showed a greater linear relationship than layers II/III (Fig 11B; Table 1).

To conclude, these results indicate that calsenilin and RyR expression overlap, with a specific ER-type expression pattern. In order to determine if this co-localization correlates to a direct protein-protein interaction, we incubated RyR-rich microsomes and recombinant calsenilin protein together. Using co-

immunoprecipitation to pull-down RyR complexes present in the mixture was visualized using western blot analysis.

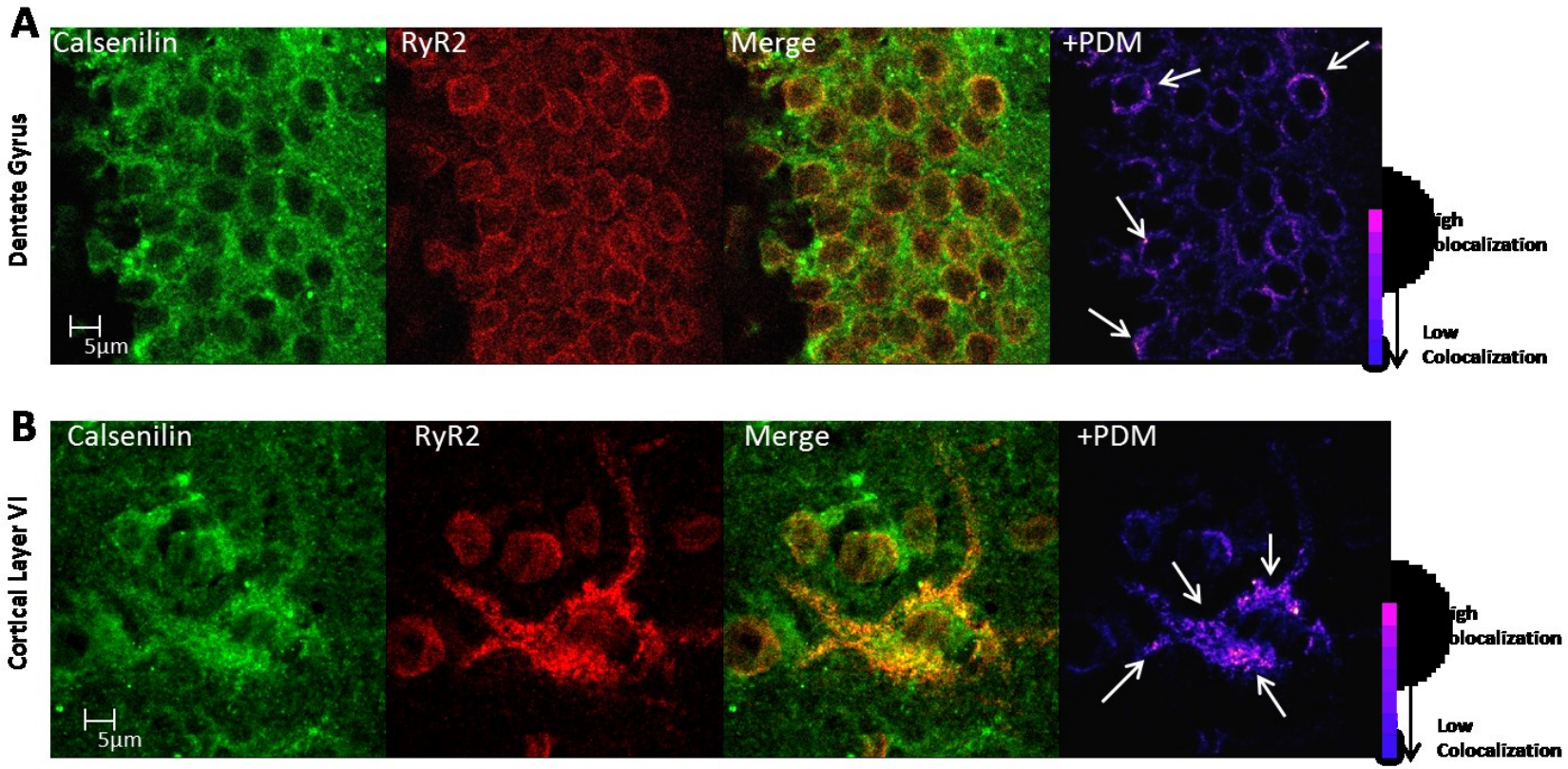

Figure 9. Calsenilin and RyR 2 immunoreactivity and co-localization pattern in the dentate gyrus and cortical layer VI.

Calsenilin and RyR2 immunoreactivity in the dentate gyrus and cortical layer VI of C57BL/6 mouse brain shows co-localization in adjacent regions to the nucleus, indicative of endoplasmic reticulum staining. A) Calsenilin immunoreactivity (green) and RyR2 immunoreactivity (red) in the dentate gyrus shows a perinuclear staining pattern and a co-localization (Merge) as indicated by arrows and (+PDM) LUT in the last panel. B) Calsenilin immunoreactivity (green) and RyR2 immunoreactivity (red) in layer VI of the cortex shows perinuclear, dendritic, and axonal staining patterns (Merge) with a high degree of punctate co-localization in the perinuclear region and at the base of processes (+PDM) , indicated by arrows and LUT in the last panel.

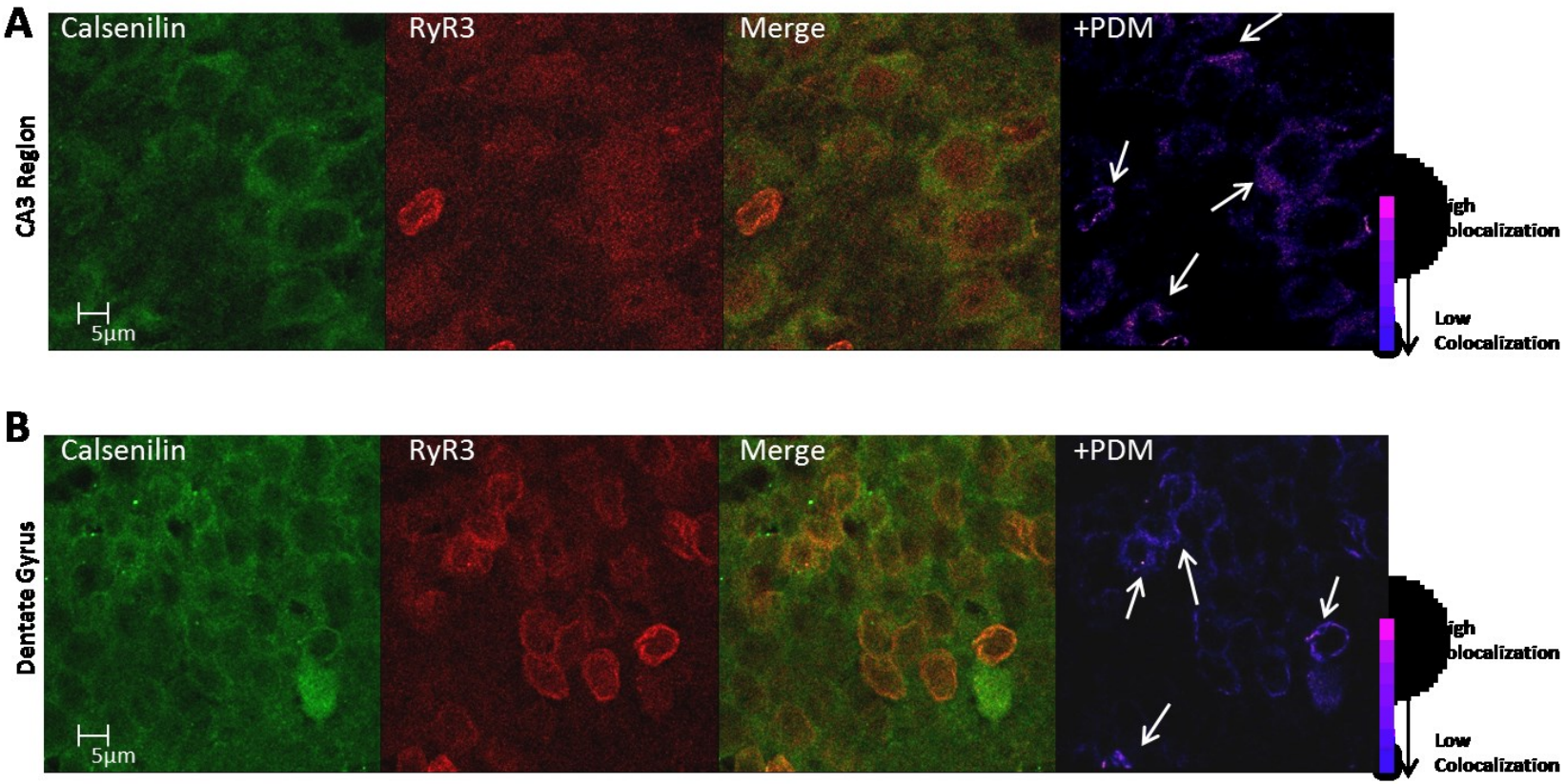

Figure 10. Calsenilin and RyR3 immunoreactivity and co-localization pattern in the dentate gyrus and CA3 region.

Calsenilin and RyR3 co-localization in C57BL/6 mouse brain is region specific with the A) CA3 region of the hippocampus showing higher degree of co-localization than the B) dentate gyrus. A) Calsenilin immunoreactivity (green) and RyR2 immunoreactivity (red) in the CA3 region shows a staining throughout the CA3 cells (Merge) and a high degree of co-localization, as indicated by arrows and (+PDM) LUT in the last panel. B) Calsenilin immunoreactivity (green) and RyR2 immunoreactivity (red) in the dentate gyrus shows staining in clusters of cells (Merge) with a moderate degree of co-localization, as indicated by arrows and (+PDM) LUT in the last panel.

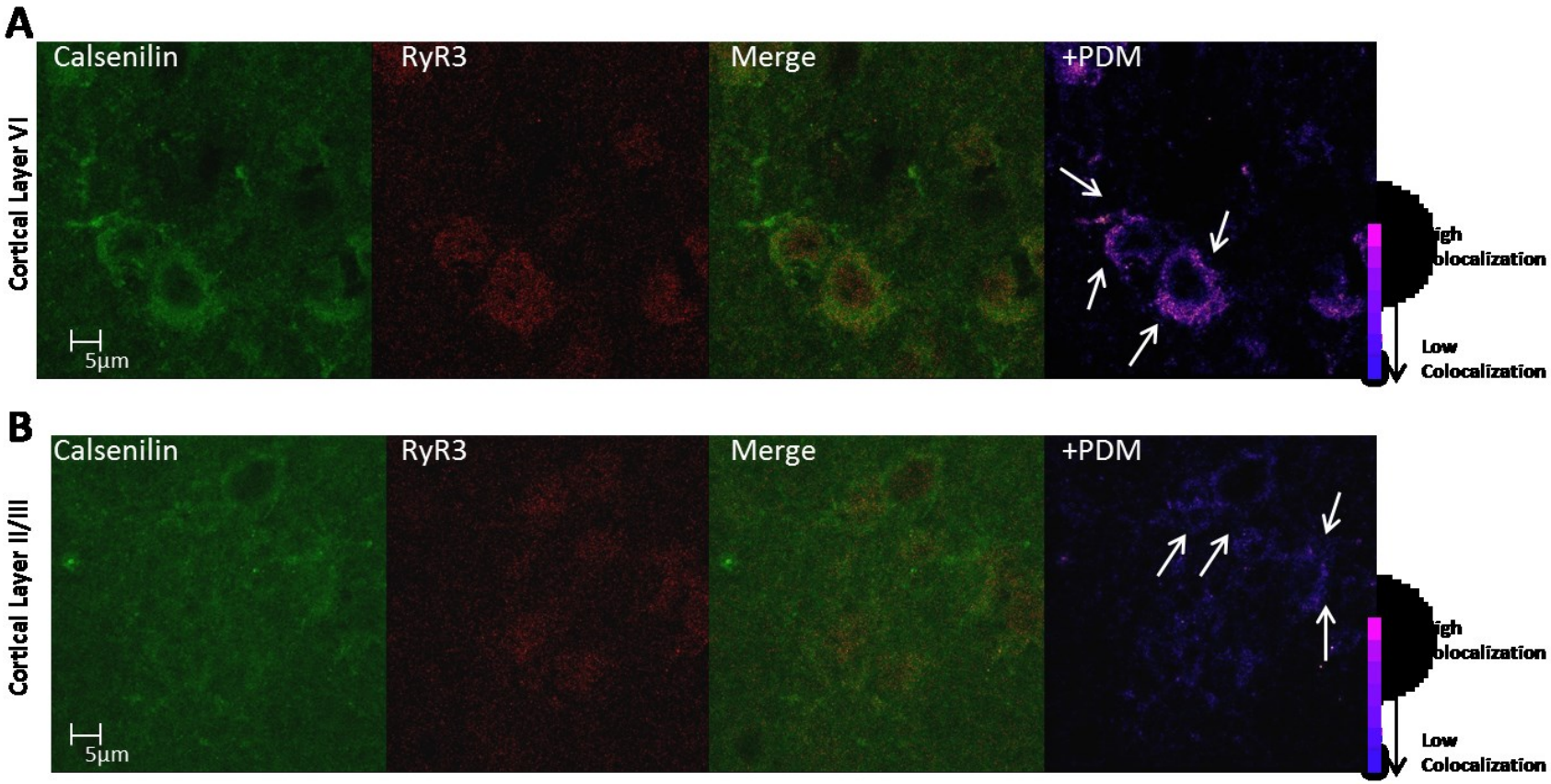

Figure 11. Calsenilin and RyR3 immunoreactivity and co-localization pattern in Cortical layer VI and II/III.

Calsenilin and RyR 3 co-localization in C57BL/6 mouse brain is region specific with A) cortical layer VI showing higher degree of co-localization than B) cortical layer II/III. A) Calsenilin immunoreactivity (green) and RyR2 immunoreactivity (red) in cortical layer VI shows perinuclear staining (Merge) and a high degree of co-localization, as indicated by arrows and (+PDM) LUT in the last panel. B) Calsenilin immunoreactivity (green) and RyR2 immunoreactivity (red) in cortical layer II/III shows slight staining (Merge) with a moderate degree of co-localization, as indicated by arrows and (+PDM) LUT in the last panel.

Table 1. Pearson's and Mander's values of co-localization for calsenilin and RyR subtypes.

Co-localization measurements between calsenilin and RyR2 or RyR3 for neuronal cell types (E18 primary cortical neurons and SH-SY5Y neuroblastoma cells) and 6wk old C57BL/6 mouse brain sections (dentate gyrus, CA3, CA1, cortical layers II/III, V, VI). The R^r = Pearson's coefficient and M1=Mander's coefficient describe the amount of calsenilin co-localized with the two RyR subtypes, whereas the M2= Mander's coefficient describes the amount of the RyR2 or RyR3 co-localized with calsenilin. Statistical significance represents the SEM for each replicate; co-localization was tested with the Costes method to ensure true co-localization. For calsenilin/RyR2 co-localization (values on left of table), R^r, M1, and M2 for both cell types and tissue tested were similar, with cortical layers V and VI showing higher R^r values. For calsenilin/RyR3 co-localization (values on right of table), R^2, M1 and M2 values for cell types, hippocampal region CA3, cortical layer VI showed similar values, while all values for the dentate gyrus, CA1, cortical layer II/III, and V were similar but at lower values than the other brain regions. Values are represented as Mean ± SEM.

	RyR2			RyR3		
Sample	R^r	M1	M2	R^r	M1	M2
Cell type						
Cortical Neurons	0.156 ± 0.022	0.504 ± 0.069	0.501 ± 0.037	0.209 ± 0.015	0.396 ± 0.033	0.437 ± 0.024
SH-SY5Y	0.155 ± 0.030	0.557 ± 0.079	0.601 ± 0.043	0.166 ± 0.008	0.468 ± 0.042	0.520 ± 0.033
Brain Region						
DG	0.131 ± 0.025	0.650 ± 0.061	0.460 ± 0.089	0.034 ± 0.043	0.424 ± 0.085	0.243 ± 0.106
CA3	0.138 ± 0.024	0.447 ± 0.075	0.493 ± 0.063	0.148 ± 0.038	0.288 ± 0.047	0.117 ± 0.023
CA1	0.122 ± 0.025	0.594 ± 0.059	0.587 ± 0.079	0.081 ± 0.018	0.393 ± 0.080	0.234 ± 0.076
Ctx II/III	0.178 ± 0.031	0.436 ± 0.065	0.355 ± 0.083	0.044 ± 0.007	0.199 ± 0.027	0.042 ± 0.004
Ctx V	0.259 ± 0.023	0.470 ± 0.050	0.445 ± 0.096	0.055 ± 0.007	0.201 ± 0.030	0.057 ± 0.013
Ctx VI	0.275 ± 0.033	0.416 ± 0.056	0.384 ± 0.066	0.111 ± 0.037	0.175 ± 0.014	0.054 ± 0.005

Calsenilin recombinant protein co-immunoprecipitates with RyR2, verified by Western blot analysis

Following co-immunoprecipitation, the RyR2 antibody successfully captured the RyR-calsenilin protein complex. The immunoblot in Figure 12 shows a calsenilin band at 51kDa (calsenilin recombinant protein + GST tag) and a RyR band at approximately 550kDa. IgG is detected in immunoblots at approximately 51kDa. To control for artificial positives on the immunoblot from pulldown antibody IgG, the antibody used to label immunoblots was derived from a different species than the precipitating antibody. By using a different species of antibody we can be certain that the band seen at the 51kDa weight marker is calsenilin with the GST tag. The IgG control showed no distinguishable band in either the RyR or calsenilin region of the immunoblot. Pull-down assays with brain microsomes absent of recombinant protein, showed no distinguishable bands due to protein levels being below detection levels of the immunoblot. Pull-down assays with whole brain preparations were marred with several unspecific protein bands and smears due to fatty content of the brain. Densitometric analysis of immunoblot bands with RyRs as the loading control showed saturation of RyR binding at 60nM-100nM. Revealing an approximate 1:1 ratio of expression for the RyR: calsenilin signal. Reverse pulldown assays using the calsenilin antibody as the pulldown antibody did not yield bands in immunoblots possibly due to weak electrostatic interactions between the two proteins from localized charges on their surfaces. The concentration of 60nM which yields approximately a 1:1 ratio in densiometric studies in reminiscent of the binding

ratio between $Kv_{4.2}$ channels and calsenilin. Calsenilin alters the release kinetics of the $Kv_{4.2}$ channel, so we tested the effect of this protein-protein interaction using 60nM recombinant calsenilin protein using planar lipid bilayer electrophysiology.

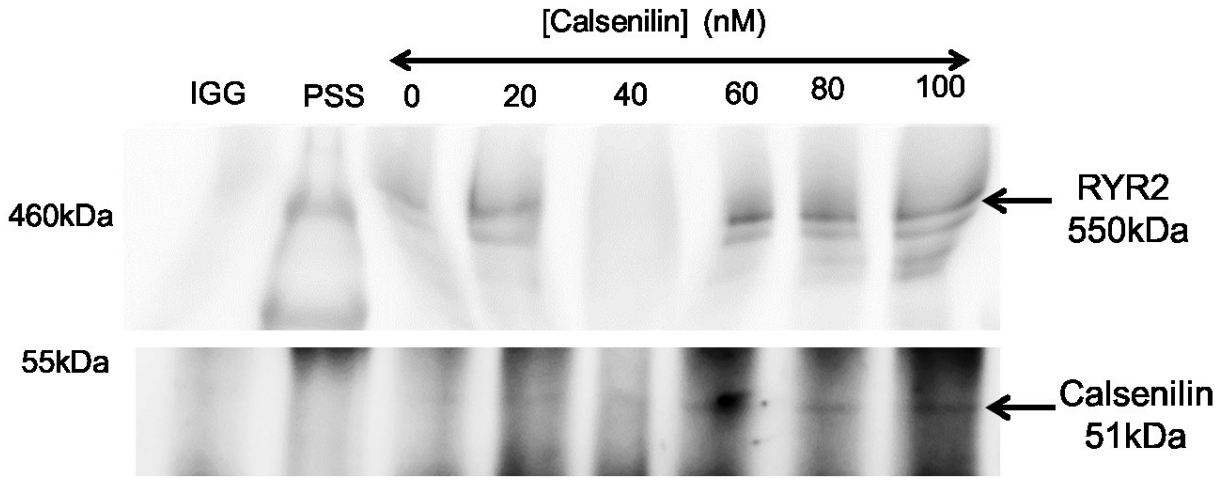

Figure 12. Western blot showing RyR2 and calsenilin protein, from a pulldown using RyR2 antibody.

Co-immunoprecipitation using rabbit anti-RyR antibody (1:200; #AB9080; Millipore) or control rabbit IgG (2mg/ml magnetic beads) in brain derived ER microsomes with increasing levels of calsenilin recombinant protein (0-100nM). Calsenilin is detected at 51kDa due to GST tag on the calsenilin recombinant protein that was added. No bands were seen using IgG as the precipitating antibody as viewed in the first lane.

Electrophysiological recordings show calsenilin reduces the amount of time that the RyR conducts ions during a given period of time at low intracellular Ca^{2+}

Figure 13 shows a representative long (30s) and short (4s) continuous recording of RyR channel activity. The 4s trace is labeled with the different parameters measured in single channel electrophysiology. The average amplitude describes the unique conductance property of RyRs. RyRs have three conductance states, a closed conductance state represented by the baseline label, a partially open state represented by the S2 label, and a fully opened state represented by the S4 label. The amplitude reflects the consequence of the conductance state where a closed state (baseline) = 0pA, a partially open state (S2) = -2pA, and a fully open state (S4) = -4pA. These descriptions are important as they are all used in assessing open probability of the channel over time. As seen in figures 15A and 13B, at low (100nM) intracellular Ca^{2+} (pCa7), 60nM calsenilin decreases the activity of the receptor as noted by less downward deflections in figure 15B as opposed to 15A. This decrease in activity is represented in figure 14A by a significant decrease in the time that the RyR channel will be open at any given period of time reflected by a decrease in open probability. There is a significant decrease in the open probability of the S2 state (Fig 14A). The mechanism of this decrease in channel activity can be attributed to a decrease in the number of times the receptor opens at S2 conductance state as indicated by a downward shift in the amplitude histogram (Fig15B) as well as decrease in the amount of time the channel remains open each

time it is activated as indicated by a leftward shift in the dwell time histogram (Fig15C).

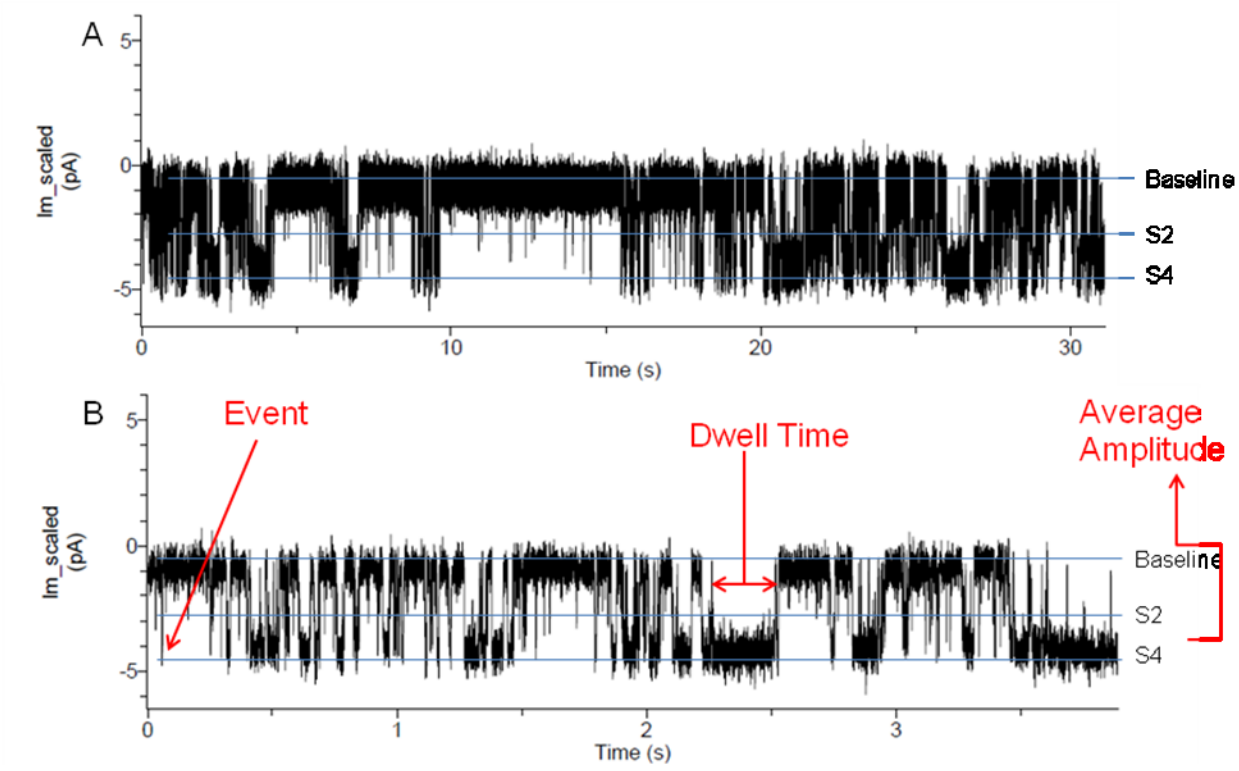

Figure 13. Representative single channel recordings of planar lipid bilayer electrophysiology.

Representative single channel recordings of long 30s (A) and short 4s (B) recordings showing representative example of baseline and conductance states average amplitude S2 (i^o =-2pA), S4 (i^o =-4pA), event, and dwell time.

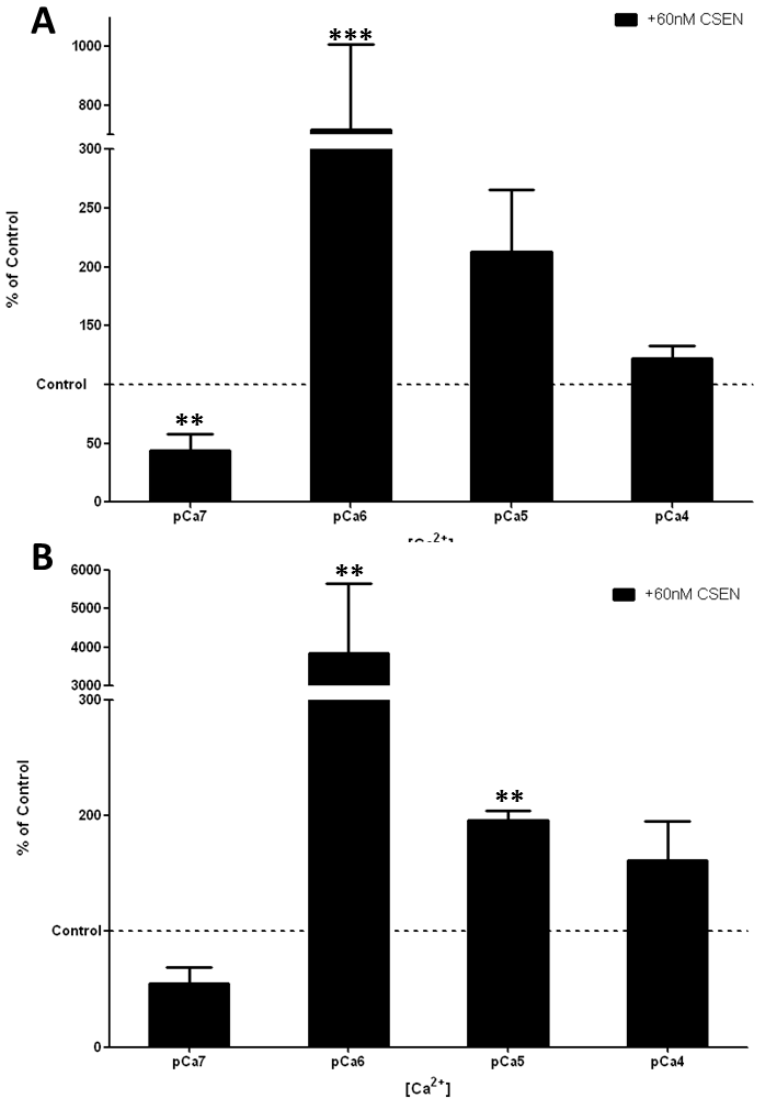

Figure 14. Calsenilin increases the open probability of RyR single channel activity at higher activity intracellular Ca^{2+} levels.

Calsenilin increases the open probability of RyR single channel activity at higher activity intracellular Ca^{2+} levels, but decreases the open probability of RyR single channel activity at low activity intracellular Ca^{2+} levels. After treatment with 60nM calsenilin the open probability for A) i_o=-2pA sublevel for pCa7 was decreased, while pCa6 was increased, but for B) i_o=-4pA both pCa6 and pCa5 open probability was increased. The number of channels averaged for each condition is presented at the bottom of each column bar. Significance parameters were obtained using Dunnett's Multiple Comparison Test. Values represented as Mean SEM ***p<0.001, **p<0.01, n=3-8.

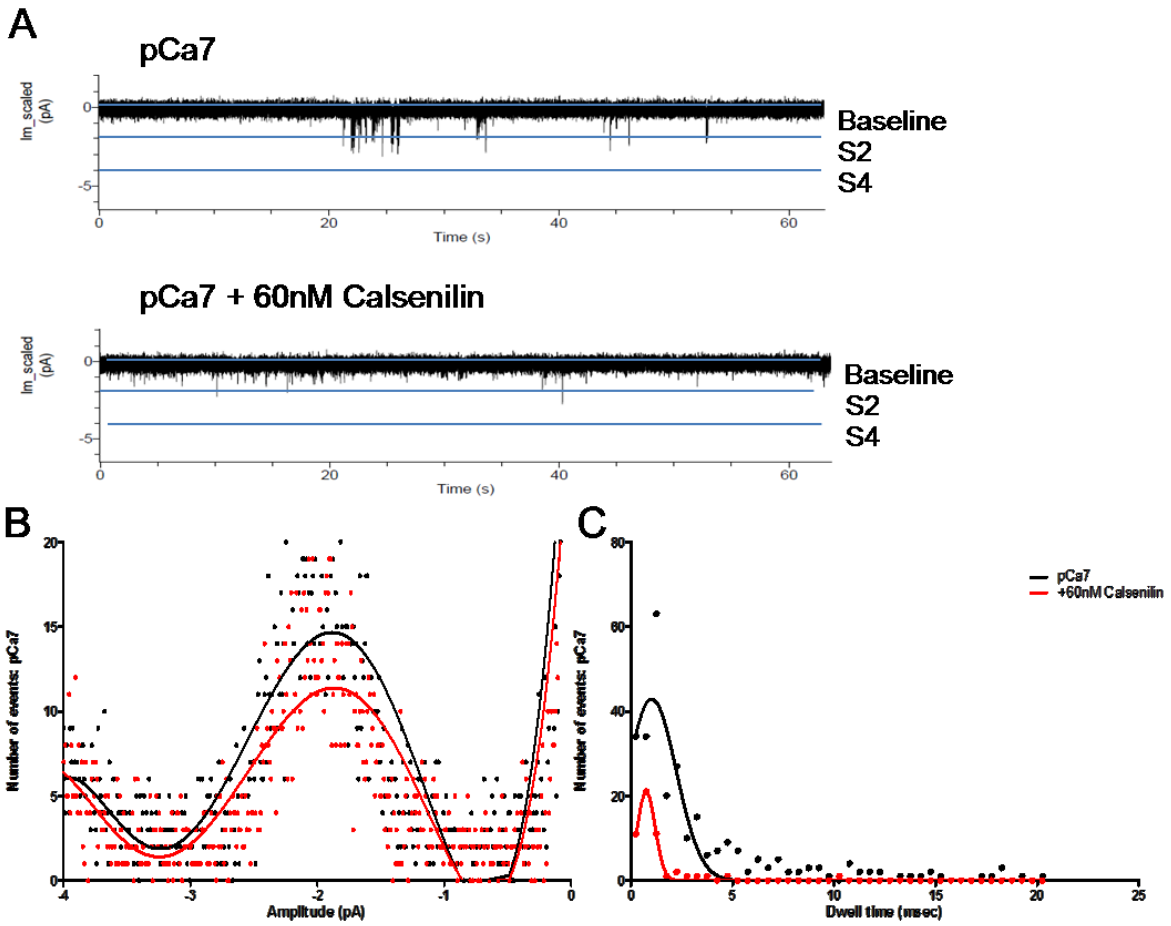

Figure 15. Calsenilin causes a downward shift in the amplitude histogram and a leftward shift in the dwell time histogram of RyR at pCa7.

(A) Current traces (60s continuous recordings) representing open channel states of RyR before (top) and after (bottom) addition of 60nM calsenilin. (B) Representative amplitude histogram curve fitted to a fourth order polynomial distribution with R^2 values of 0.591 (for pCa7) and 0.586 (for pCa7 + 60nM calsenilin) showing a downward shift in the amplitude histogram characterizing a decrease in the number of subconductance (i_o =-2pA) channel openings after treatment with 60nM calsenilin, (C) Dwell time histogram curve fitted to a Gaussian distribution with R^2 values of 0.817 (for pCa7) and 0.986 (for pCa7 + 60nM calsenilin) calculated from same 60s recording showing a leftward shift in dwell time histogram indicative of a decrease in the number of longer channel openings after treatment with 60nM calsenilin.

Electrophysiological recordings show calsenilin increases the amount of time that the RyR conducts ions during a given period of time at high intracellular Ca^{2+}

At higher activity intracellular Ca^{2+} (pCa6), there is an increase in the open probability of both the low S2 (Fig14A) and high S4 conductance states (Fig 14B). As can be seen in a representative 30s continuous trace (Fig 16A), the activity of the receptor is significantly increased in the presence of 60nM calsenilin. The mechanism of this potentiation can be demonstrated by the increase in the number of times the receptor opens at both S2 and S4 conductance states, indicated by the upward shift in the amplitude histogram (Fig 16B), as well as an increase in the amount of time the channel stays open each time it is activated, shown by a rightward shift in the dwell time histogram (Fig 16C). At the highest activity intracellular Ca^{2+} (pCa5), 60nM calsenilin significantly increases the probability that the channel will be open in the high S4 conductance state (Fig 14B). This increase in the activity of the receptor can be seen in a representative 30s continuous trace (Fig 17A), and can be attributed to an overall increase in the number of events that occur as indicated by an upward shift in both the amplitude (Fig 17B) and dwell time (Fig 17C) histograms.

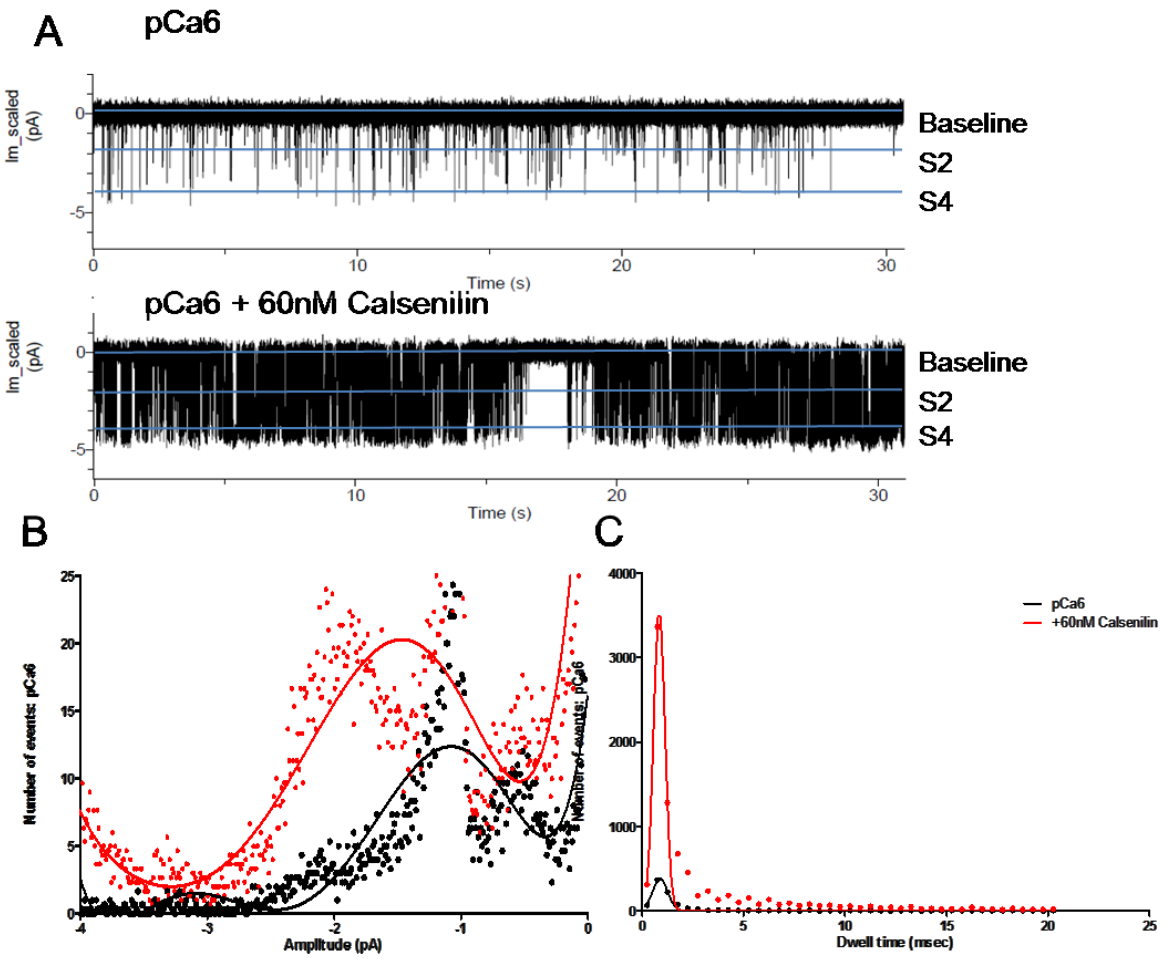

Figure 16. Calsenilin causes an upward shift in the amplitude histogram and a rightward shift in the dwell time histogram of RyR at pCa6.

A) Current traces (60s continuous recordings) representing open channel states of RyR before (top) and after (bottom) addition of 60nM calsenilin, (B) representative amplitude histogram curve fitted to a fourth order polynomial distribution with R^2 values of 0.157 (for pCa6) and 0.171 (for pCa 6 + 60nM calsenilin) showing an upward shift in the amplitude histogram characterizing an increase in the number of subconductance (i_o =-2pA) and conductance (i_o =-4pA) channel openings after treatment with 60nM calsenilin. (C) Dwell time histogram curve fitted to a Gaussian distribution with R^2 values of 0.968 (for pCa6) and 0.926 (for pCa 6 + 60nM calsenilin) calculated from same 60s recording showing a rightward shift in dwell time histogram indicative of an increase in the number of longer channel openings after treatment with 60nM calsenilin.

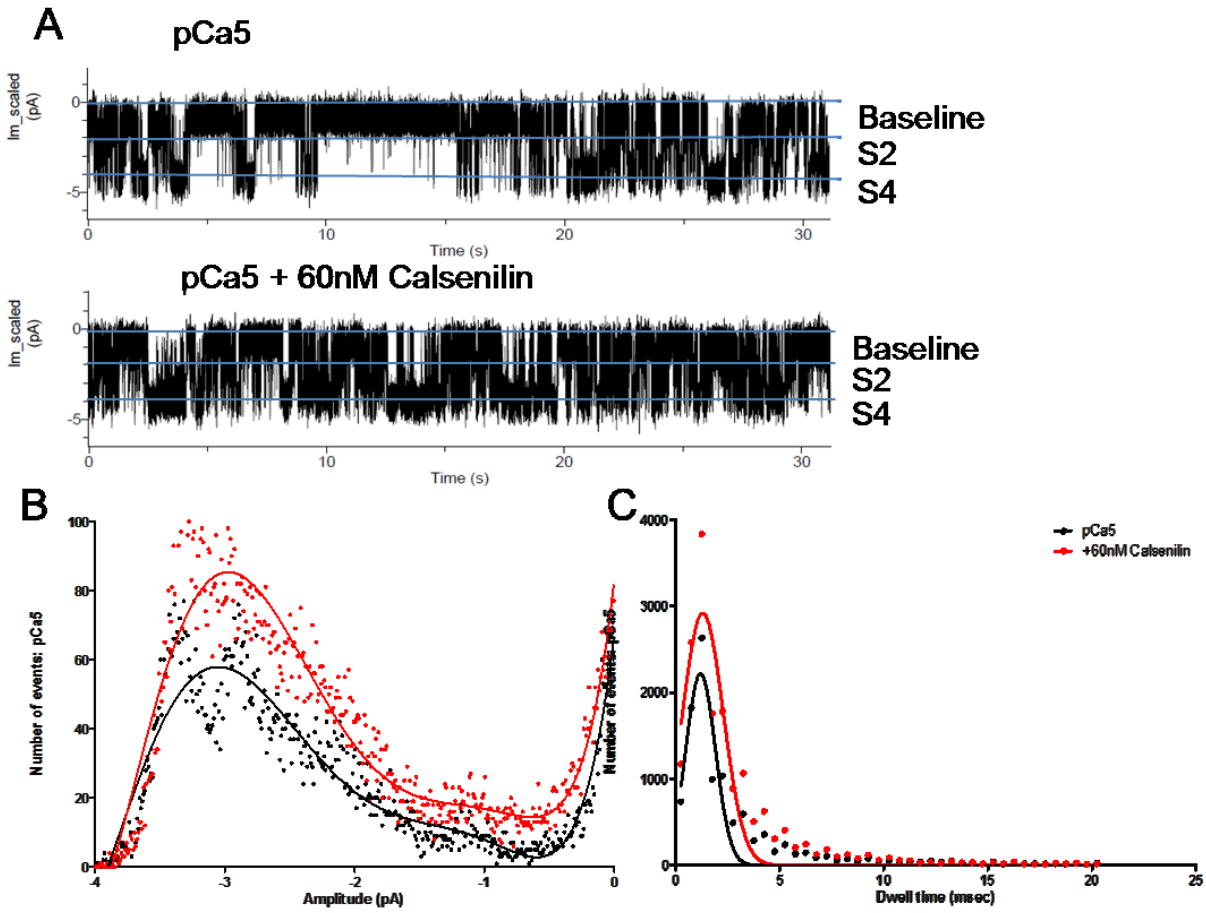

Figure 17. Calsenilin causes an upward shift in the amplitude histogram and a rightward shift in the dwell time histogram at pCa5.

(A) Current traces (60s continuous recordings representing open channel states of RyR before (top) and after (bottom) addition of 60nM calsenilin. (B) Representative amplitude histogram curve fitted to a Fourth Order Polynomial distribution with R^2 values of. 800 (for pCa5) and 842 (for pCa 5 + 60nM calsenilin) showing an upward shift in the amplitude histogram characterizing an increase in the number of conductance (i_o =-4pA) channel openings after treatment with 60nM calsenilin (C) Dwell time histogram curve fitted to a Gaussian distribution with R^2 values of 0.866 (for pCa5) and 0.871 (for pCa 5 + 60nM calsenilin) calculated from same 60s recording showing a slight rightward shift in dwell time histogram indicative of an increase in the number of longer channel openings after treatment with 60nM calsenilin.

Overexpression of calsenilin in SH-SY5Y cells caused faster kinetics of caffeine –induced Ca^{2+} release, but not the amount of Ca^{2+} released

Figure 18 shows an averaged change in Ca^{2+} $[Ca^{2+}]/[Ca^{2+}]_0$ following caffeine induced Ca^{2+} release in mock- and calsenilin-transfected cells. Overexpression of calsenilin sharpens the Ca^{2+} release by increasing the rate of release (Fig 19A), indicated by steep increase in the $[Ca^{2+}]/[Ca^{2+}]_0$ slope, and decreasing the overall Ca^{2+} response time (Fig 19C). There was an increase in the maximum amplitude of the Ca^{2+} response (Fig 19B), but no difference in the area under the curve (Fig 19D). The lack of difference in the area under the curve shows that there was no difference in the relative level of Ca^{2+} release, while the increase in the maximum amplitude of Ca^{2+} release supports a faster more precise signal due to calsenilin overexpression.

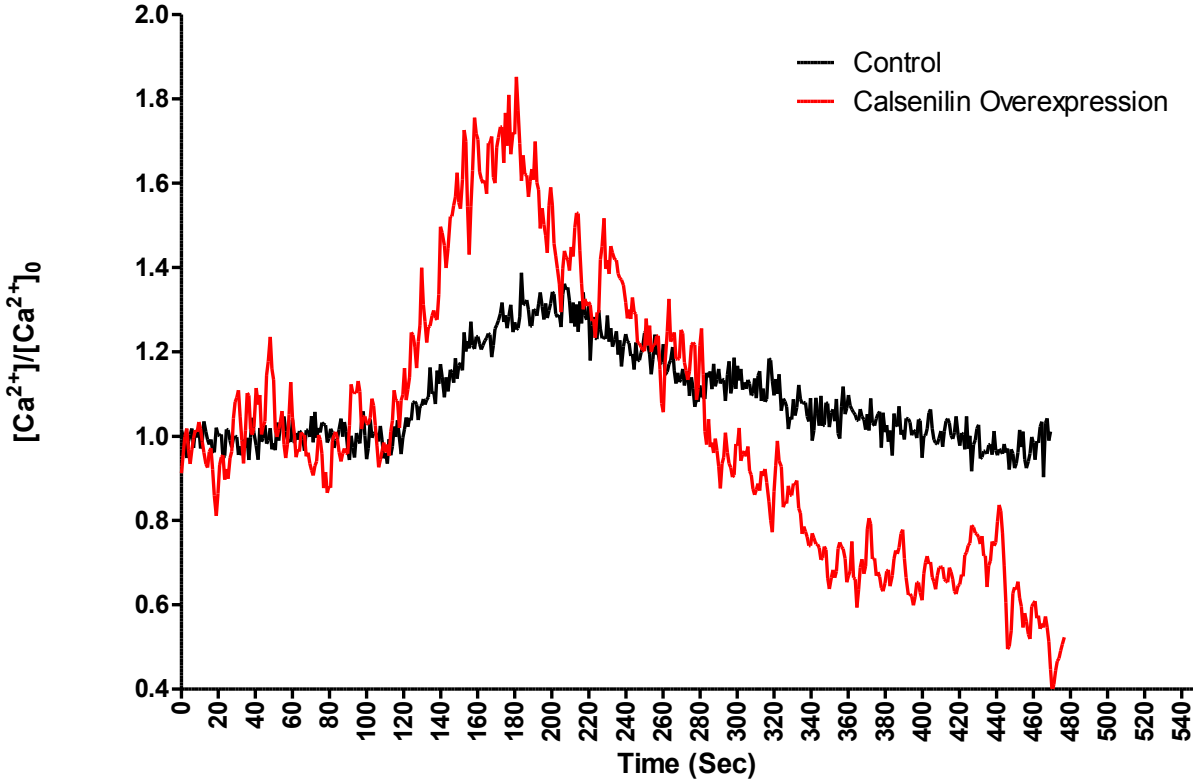

Figure 18. Representative Ca^{2+} response to caffeine stimulation in control and calsenilin overexpressing SH-SY5Y cells.

Representative response of SH-SY5Y cells to caffeine stimulation in control and calsenilin overexpressed cells as represented by change in $[Ca^{2+}]$. A response is represented by $[Ca^{2+}]/[Ca^{2+}]_0$ ($[Ca^{2+}]_0$=baseline, $[Ca^{2+}]$=response) to normalize experiments for comparison. Calsenilin causes a sharpening of Ca^{2+} release in response to Ca^{2+} as seen by a steep increase and shorter duration of caffeine-induced Ca^{2+}-release and increased magnitude of response compared with control cells with endogenous levels of calsenilin.

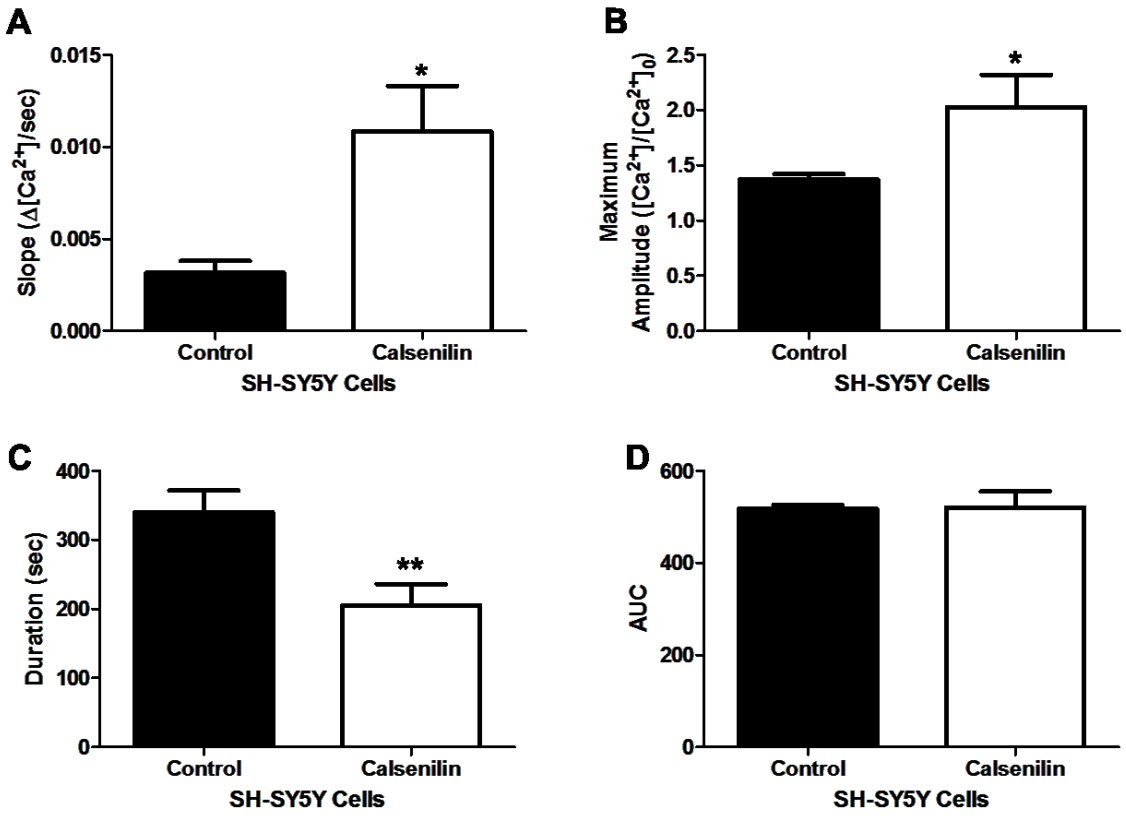

Figure 19. Quantification of caffeine induced Ca^{2+} release kinetics in control and calsenilin overexpressing SH-SY5Y cells.

Column graphs representing the A) slope B) maximum amplitude C) curve width D) area under the curve (AUC) of caffeine-induced Ca^{2+}-release kinetics in control (black columns) and calsenilin overexpression (white columns) of SH-SY5Y cells. Values represent averages of several experiments (N=8 for Control, and N=12 for calsenilin overexpression; each N represents 3-20 replicates) with a linear regression fit of the points between 5% above baseline and maximum $[Ca^{2+}]/[Ca^{2+}]_0$ values of the Ca^{2+} release slope The beginning of a Ca^{2+} response is defined as 5% above baseline and ending of a response is defined as below 5% of baseline. (Chi square values for best fit; control R^2=0.746, overexpression R^2=0.8431). Overexpression of calsenilin significantly increases the rate of Ca^{2+} release (slope) and the maximum amount of Ca^{2+} released (max amplitude), while decreasing the time of the Ca^{2+} release (curve width), however the total amount of Ca^{2+} released (AUC) remains unchanged suggesting a sharpening of the Ca^{2+} response without altering the amount of Ca^{2+} release. Values were statistically analyzed using a student's t-test (Mean ± SEM, $p< 0.05$*, $p< 0.01$**)

Overview: summary of results

The current study has shown through immunostaining and confocal microscopy that brain RyRs and calsenilin are located within the ER in neuronal cells. These two proteins physically interact as shown in co-immunoprecipitation studies. This interaction leads to a decrease in single channel Ca^{2+} release activity of brain RyRs at low Ca^{2+} concentrations (pCa7) through a decrease in the number of times the channel opens and a decrease in time that the channel stays open each time. Conversely, this interaction at high Ca^{2+} concentrations (pCa6 and pCa5) leads to an increase in single channel Ca^{2+} release activity of brain RyRs through an increase in the number of times the channel opens at all amplitudes, and an increase in time the channel stays open. This change in single channel biophysics was confirmed using optical Ca^{2+} imaging techniques, where increased calsenilin expression led to faster Ca^{2+} release, higher maximum release, and a shorter duration of release. Interestingly, these changes did not alter the overall amount of Ca^{2+} release as quantified by AUC. To conclude, calsenilin appears to sharpen Ca^{2+} release from the channel by shifting the Ca^{2+} activation of RyRs to a higher Ca^{2+} concentration, and increasing the channel kinetics following activation direct modulatory effect of calsenilin on neuronal RyRs.

CHAPTER 4

DISCUSSION

Limitations and considerations of experimental techniques and set up

Each of the methods used in the current study suffer from inherent technical limitations. By designing an experimental approach that utilizes several different techniques we have attempted to address these shortcomings. The evidence provided from the results of each of the experimental techniques taken together provide enough overlapping evidence to support the hypothesis that calsenilin and RyRs directly interact modulating RyR Ca^{2+} release.

Immunostaining of neuronal tissue provided evidence that calsenilin and RyRs are located and co-localized in the endoplasmic reticulum of neuronal cells. To ensure the specificity of the primary antibodies for their target protein, all primary antibodies used in the experiment were tested previously and published in peer reviewed papers [2, 39, 112]. Localization of calsenilin and RyRs was empirically compared with published expression patterns to further confirm the fidelity of the primary antibodies used. The algorithms used to define co-localization are sensitive to background fluorescence, fluorescence noise, and the relative intensity of immunostaining for each of the proteins. To address the sources of artifacts two distinct co-localization algorithms were used. The Pearson's coefficient is sensitive to relative intensities and noise, but not background fluorescence. The Mander's coefficient is conversely sensitive to background fluorescence, but not relative

intensity of the specific protein immunostaining. By utilizing the Pearson's and Mander's coefficient, we minimized aberrations in quantification due to differences in the intensity of immunostaining and background staining. To minimize artifacts from fluorescent noise, strict threshold values were set to delineate true fluorescent staining from unspecific staining. Finally, by using the Costes algorithm, we ensured that co-localization was true and not due to random overlap of the fluorescent signals. The resolution of a confocal microscope is well above wide field microscopy, but still cannot distinguish between species that are extremely close in proximity. By the use of the Raleigh criterion and Nyquist sampling theorem, the resolution and sampling rate of the confocal microscope were optimized to ensure proper image acquisition. The findings from the co-localization studies suggest that calsenilin and the RyRs are located in similar regions in neuronal cells. Using a FRET based approach or more accurate and sophisticated imaging technology would increase the characterization of these two proteins interaction *in vivo.* However, to initially establish and characterize a direct protein-protein interaction the *in vitro* approach of co-immunoprecipitation was employed.

Co-immunoprecipitation is an *in vitro* method for determining protein-protein interactions. Antibodies capture protein complexes that physically interact, and through immunoblotting, the proteins in this complex can be visualized. Using a RyR2 antibody to pulldown the RyR2 and calsenilin protein complex established a protein-protein interaction between calsenilin and RyR2. The antibodies used have been verified and published in peer reviewed papers [2, 39, 112]. The co-immunoprecipitation experimental set up minimized artifacts due to unspecific

binding of the proteins to paramagnetic collection beads in three ways: 1) substituting the rabbit RyR2 primary antibody with rabbit IgG during incubation with a protein sample, 2) using a protein sample with no antibody or IgG incubation and 3) pre-incubation of the unlabeled paramagnetic beads with unaltered protein samples to allow the protein samples to bind up any non-specific sites before incubation with the co-immunoprecipitated antibody-protein complex. Though all artifacts could not be removed in immunoblots using IgG only as the pulldown antibody, specific weight markers for calsenilin and RyRs showed no immunoreactivity. The use of purified ER microsomes harvested from several mouse brains increases the concentration of RyRs while lowering the concentration of superfluous proteins in the pulldown assay. The calsenilin content in ER microsomes is below the detection limit of immunoblotting, so each pulldown assay was performed with addition of recombinant calsenilin protein. This experimental design increases the likelihood of a calsenilin and RyR interaction. Though suggesting the possibility of a direct protein-protein interaction the presence of accessory proteins in the microsome is possible. Testing the functional consequence of this protein-protein interaction of calsenilin and RyRs was performed using single channel electrophysiology.

Single channel electrophysiology allows the testing of a single RyR channel activity. In the current study, calsenilin altered single channel RyR Ca^{2+} release in a Ca^{2+} dependent manner. The several advantages to using single channel electrophysiology are that the native brain RyRs are used, there is absolute control of the experimental environment, and single channel's biophysical properties can be measured. One disadvantage of the technique is that the purified ER microsomes

used could contain accessory proteins still attached to the receptor. This problem was addressed by using each channel as its own control therefore measuring a change before and after calsenilin introduction. Electrophysiology, in general, can suffer from improper collection technique and a lack of proper filtering. Both of these sources for error were overcome by using standard published collection rates and filtering techniques [67]. Finally the environment, though controlled by the experiment, lacks the cellular milieu of native neuronal cells. This problem is addressed by using optical imaging of cells overexpressing calsenilin to visualize Ca^{2+} release from RyRs in their native environment.

Ca^{2+} imaging techniques allow visualization and estimation of increased cytoplasmic Ca^{2+} levels following receptor stimulation through fluorescent Ca^{2+} binding proteins (See Figure 6). Our studies show calsenilin overexpression in SH-SY5Y neuroblastoma cells increases the rate of caffeine induced RyR Ca^{2+} release, decrease the duration of Ca^{2+} release, and increase the maximum amplitude of Ca^{2+} release from RyRs. Using overexpression of a target protein as an *in vitro* model ensures that the interaction between two proteins occurs at a level of saturation of the target protein, demarcating that any changes measured in Ca^{2+} release dynamics have a high probability of being due to the protein of interest. This technique suffers from inherent limitations such as cells loading differing amounts of Ca^{2+} indicator dye, photo-bleaching of the Ca^{2+} indicator dye, and possible alterations in Ca^{2+} release due to the transfections itself. Using Fura-2 as the Ca^{2+} indicator dye decreased the possible aberrations from dye loading in cells and photobleaching. Fura-2 is a ratiometric dye with excitation at 380nm in the unbound

state and 340nm in the bound state. The emission for both is 510nm. The use of the ratiometric dye addresses these anomalies due to dye loading and photo-bleaching since absolute fluorescent values are not used. The ratio of 340/380 is calculated as the output for each cell giving an accurate picture of changes within each individual cell bypassing any differences in dye loading and photo-bleaching. Previous experiments in our lab have shown the transfection technique does not affect Ca^{2+} signaling [72]. Overexpressing proteins in cells could alter several processes in cells. Using caffeine, a specific RyR agonist [85], ensures that Ca^{2+} release is evoked through RyRs and not another Ca^{2+} release channel. Taken together, these results strongly suggest that calsenilin and RyRs directly interact, and that this interaction modifies Ca^{2+} release from RyRs.

Calsenilin and RyRs interactions in brain signaling and disease progression

Figures 7-11 show calsenilin and neuronal RyRs co-localize in the ER of neuronal cells. Figure 9B clearly shows colocalization between calsenilin and RyRs in the major branch points of dendrites in cortical neurons. The ER network in neurons spans the entire cell from the soma to the dendrites [172]. IP_3Rs and RyRs are distributed throughout the ER in all regions of the cell [141, 149, 150, 175, 180] . Backpropagating action potentials are action potentials that travel from soma to axon and concurrently from soma through the dendritic arborization [184] . Backpropagating action potentials shape the responses of post synaptic cells to presynaptic cell stimuli , affecting the spike-timing dependence of plasticity [184]. In

Purkinje cells, as well as cortical and hippocampal cells, these backpropagating action potentials are shaped by the location of numerous ion channels including the RyR and IP_3R [118, 158]. This alteration in spike-timing coordination between neurons is now thought to shape LTP and LTD in the formation of memory [10, 50, 94, 105, 134, 138]. This study has shown there is a high density of co-localization between RyR and calsenilin in cortical neurons at the major dendritic branch points decreasing as the proximity to the soma increases (Fig 9B). This relationship of RyRs expression follows a well characterized phenomenon in neurons that correlates to a lessening of backpropagating action potentials as the proximity to the soma is decreased[21, 94, 118, 149, 175]. The interaction of calsenilin with RyRs, as seen in the single channel electrophysiology experiments (Fig13-17), shifts the Ca^{2+} activation curve for the RyR. The shift in the Ca^{2+} activation curve of RyRs lowers single channel activity at resting, 100nM (Fig 15), Ca^{2+} concentrations while increasing single channel activity at 1μM and 10μM Ca^{2+} levels (Fig 16 and 17, respectively). The alterations in single channel Ca^{2+} release of RyRs translates to faster and higher amplitude Ca^{2+} release in whole cells as seen in Ca^{2+} imaging experiments (Fig 18-19). The result of this alteration in RyR kinetics can be hypothesized to alter the timing and firing of a backpropagating action potentials. The alteration in backpropagating action potential will affect the polarization of the post synaptic membrane to pre synaptic signals [184]. In AD mice, the increase in resting concentrations of Ca^{2+} [102] could result in increased higher amplitude Ca^{2+} release through RyRs when modulated by calsenilin. This increase in firing rate and amplitude alter the pre and post synaptic firing of neurons. In fact, this phenomenon

of timing in spiking potentials is a major determinant of whether LTP or LTD occurs [10, 50].

One of the major correlative features of alterations in Ca^{2+} signaling in AD mice and cellular models is the aberrant release of Ca^{2+} from RyRs sensitive stores [33, 34, 83, 152, 161, 162]. RyRs are known to form complexes with other proteins and channels allowing the transmission of cell signals from discrete locations [12, 178]. In heart and skeletal muscle RyRs form clusters of alternating receptors linked with L-type Ca^{2+} channels coordinating depolarization between cells leading to muscle contractions [13, 148]. The establishment of defined puncta of co-localization of RyRs and calsenilin throughout the neuronal tissue tested here is reminiscent of the organization of RyRs in heart and skeletal muscle tissue [13]. This organization of ion channels and accessory proteins shape the propagation of waves throughout these excitable cells [29]. RyRs are homotetramers of four 550kDa subunits [61, 178]. In our co-immunoprecipitation studies, 60nM of recombinant calsenilin protein showed an approximately 1:1 ratio between the amounts of calsenilin pulled down with RyRs. This one to one relationship between calsenilin and RyRs is reminiscent of the ratio of binding between calsenilin and $Kv_{4.2}$ potassium channel subunits [75, 87, 128, 181]. In this interaction, four calsenilin units bind to each of the four $Kv_{4.2}$ potassium channel subunits in a ratio of 1:1[181]. This interaction stabilizes the tetramer conformation and changes signaling within the receptor [87]. A calsenilin interaction with $Kv_{4.2}$ channels changes gating properties of this channel, most notably by increasing the peak current, peak current density, inactivation time constant, and recovery from inactivation [75].

In this study, a calsenilin and RyR interaction altered Ca^{2+} release in single channel electrophysiological recordings (Fig 13-17). The alteration of the $Kv_{4.2}$ channel in the presence of calsenilin allows the channel to recover more rapidly from inactivation allowing it to fire more frequently at higher intensities [2]. In the single channel electrophysiology experiments, calsenilin interaction with RyRs shifts the Ca^{2+} response curve of the RyR) to the right, (Fig 15-17), which suggests that activation of the RyR to Ca^{2+} release occurs at 1μM Ca^{2+} rather than 100nM Ca^{2+} (Figs. 15-16) The silencing of the receptor at 100nM Ca^{2+} (Fig 15), along with the significant increase in channel activity at 1μM Ca^{2+} (Fig 16) and 10μM Ca^{2+} (Fig 17) shows an increase density in the current transmitted per period of time through the receptor (Fig 14). This change in single channel activity of RyRs can be translated in cells as a sharpening of RyR activity. This effect is shown also in the Ca^{2+} imaging experiments (Fig 18-19) where Ca^{2+} response curves show faster and more robust Ca^{2+} release. This data, along with the planar lipid bilayer data, suggests a sharpening, or tuning, of the RyR response. Since the RyR is a CICR channel any alteration in the channels response to Ca^{2+}, also alters the pattern of the Ca^{2+} signal creating an all or nothing response at specific Ca^{2+} concentrations.

RyRs and IP_3Rs serve multiple roles in normal physiological neuronal function such as propagation of action potentials, backpropagating action potentials, neurotransmitter release, and membrane excitability [10]. In several neurodegenerative disorders such as Huntington's disease (HD), Amyotrophic lateral sclerosis (ALS), and AD, aberrant intracellular Ca^{2+} release is associated with cell death and disease progression [11, 15, 54, 83, 123, 160, 169]. Increased Ca^{2+}

release from intracellular stores, increased Ca^{2+} in response to Aβ, and increased Ca^{2+} induced apoptosis are enhanced in AD models by overexpression of calsenilin [49, 78, 81, 98, 100]. The interaction between calsenilin and RyRs provides a link between abnormal Ca^{2+} signaling and these diseases. In HD, direct interaction between the polyglutamine expansion of the amino terminus of the Huntington protein (Htt), which promotes binding to Huntington-associated protein (HAP1), is thought to be the cause of this disorder [170]. The interaction between this complex and IP_3Rs elevates Ca^{2+} release and apoptosis in neuronal cells [1, 169, 170]. This increased in IP_3R Ca^{2+} release can further be amplified by CICR from the RyRs [15]. The interaction between calsenilin and RyRs enhances signaling at higher Ca^{2+} levels (Fig 16 and 17) thereby exacerbating increased IP_3R Ca^{2+} release. It is interesting to note that increased Ca^{2+} release and resting Ca^{2+} levels in all the neurodegenerative disorders mentioned can be further amplified by RyRs CICR [11, 109]. Any increase in calsenilin levels in diseases associated with abnormal Ca^{2+} could create more binding between the two species leading to increased abnormal Ca^{2+} signaling.

Calsenilin modulates Ca^{2+} homeostasis through several protein interactions throughout the cell. Some of the modulators of calsenilin also modulate RyRs [144, 155] directly linking Ca^{2+} signaling pathways to calsenilin. In studies with calsenilin as a transcriptional modulator, interactions of calsenilin at CRE sites alter transcription of Ca^{2+} exchangers on the surface [56] increasing resting Ca^{2+} levels by limiting the extrusion of Ca^{2+} from the cytoplasm. It is therefore exciting to propose

that calsenilin may act as a modulator for competing cellular signals [144]. One such Ca^{2+} related signal is apoptosis [59].

Several studies have shown that increased cytoplasmic Ca^{2+} along with calsenilin overexpression can lead to apoptotic cell death [80]. Calsenilin is a substrate for caspase-3 cleavage [37], but it is not known if the caspase cleavage product of calsenilin causes apoptosis. In cell models increased apoptosis due to calsenilin overexpression can be normalized back to control levels with caspase inhibitors [36, 37, 81]. It is also interesting to note that calsenilin as a transcriptional modulator is responsible for the repression of pro-apoptotic transcription HRK [140], and is related to the transcription of anti-apoptotic proteins of the Bcl family [139]. Calsenilin also forms a complex with the anti-apoptotic N-terminus of PS2 further suggesting a role as a signaling molecule in apoptosis [24].

Structural basis for interaction between calsenilin and RyRs

Calsenilin interacts with $Kv_{4.2}$ channels modulating channel activity [76]. The binding calsenilin forms a tetrameric structure stabilizing the four $Kv_{4.2}$ channel subunits [87]. The scaffolding protein Homer mediates the interaction between RyRs and Cav1.2 (L-type voltage gated Ca^{2+} channels) in cardiac cells. This interaction regulates Ca^{2+} microdomains by coupling L-type VOCC calcium entry with RyR release [71]. Therefor L-type-calcium activation directly modulates the release of Ca^{2+} from RyR [188]. Homer proteins form tetrameric structures [64] stabilizing post synaptic densities [65] in neurons. The tetramerization of Homer

proteins into a scaffolding structure is through interactions in leucine zipper domains of the Homer proteins [167]. Calsenilin interacts with αCREM at the kinase inducible domain (KID) of the leucine zipper in αCREM [95]. This interaction occurs between the two leucine charge residue rich domains (LCD) located in both calsenilin and αCREM [92]. These findings suggest that calsenilin and Homer may interact through motifs located in the leucine zipper domain of Homer. Recently, calsenilin has been shown to play a role in the interaction between $Kv_{4.2}$ channels and Cav3 (M-type voltage gated Ca^{2+} channels) linking Ca^{2+} release through M-type voltage gated Ca^{2+} channels with modulation of $Kv_{4.2}$ channels by calsenilin [3]. Calsenilin interacts with $Kv_{4.2}$ channels around the pore forming segment of $Kv_{4.2}$ channels [18]. Interestingly, the pore regions of RyRs and A-type potassium channels share structural features. Crystal structures of the pore region for both channels were elucidated using the same bacterial K1 channel KcsA as a template [18, 187]. As seen in co-immunoprecipitation studies, the addition of 60nM calsenilin to ER microsomes showed expression of calsenilin: RyR in a 1:1 ratio. This same type of ratio of calsenilin: $Kv_{4.2}$ is described in the formation of calsenilin and $Kv_{4.2}$ channel complexes and is needed for the alterations in channel release seen in this structure [7, 181].

Future directions

As higher resolution imaging technology becomes available, the nanodomain interaction between calsenilin and RyRs can be viewed. The higher resolution imaging would allow a more precise analysis of the exact localization of these two proteins *in vivo*. Colocalization in distal dendrites and the density of this colocalization, with respect to the proximity to the soma, would provide evidence for the functional consequence of this protein-protein interaction in neuronal communication. In hippocampal neurons, RyRs are located in the most distal branches of dendrites and responsible for the propagation of Ca^{2+} signals throughout the dendritic tree [150, 180]. Whether calsenilin modulation effects the propagation of Ca^{2+} signals through dendritic branches has yet to be determined. A more specific survey of calsenilin and RyR colocalization in neural pathways would provide evidence for an exact physiological role of calsenilin and RyR interaction. Determination of the Ca^{2+} dependence of the calsenilin and RyR interaction would shed more light on the mechanism of RyR modulation. Mutations in each of the Ca^{2+} binding EF –hand domains of calsenilin would provide an *in vitro* method to determine the importance of specific Ca^{2+} binding sites on the interaction and modulation of RyRs.

Calsenilin EF-hand mutations that disrupt Ca^{2+} binding result in loss of function in transcription modulation and potassium channel modulation by calsenilin. During transcriptional regulation, mutations preventing the binding of Ca^{2+} to all 4 –

EF-hands of calsenilin result in calsenilin being irreversibly bound to the DRE site [121]. Calsenilin interaction with $Kv_{4.2}$ channels is not abolished when mutations prevent Ca^{2+} binding to all 4 –EF-hands of calsenilin, but the modulatory effect of the interaction is removed [182]. Calsenilin has 4-EF hands with different binding affinities for Ca^{2+} [120], the importance of each of these binding sites on the function of calsenilin has yet to be resolved. Using single channel electrophysiology, single EF-hand mutations that prevent Ca^{2+} binding to calsenilin, and their effect on the modulation of RyRs channel activity would be measured.

The whole cell paradigm in this study could be improved by a more quantitative measure of overexpression of calsenilin to identify if the changes in Ca^{2+} signaling are sensitive to the concentration of calsenilin. In *in vitro* studies it has been shown that the concentration of calsenilin effects the formation of dimers and tetramers [120, 121], these interactions of calsenilin confer the action of calsenilin in transcriptional regulation as well as $Kv_{4.2}$ channel modification[75, 121]

In our current study, we have established that calsenilin and RyRs interact through a direct protein-protein interaction. It would be interesting to further elucidate properties of this interaction by testing the Ca^{2+} dependence on this interaction as stated earlier. It would also be interesting to establish whether the caspase cleavage product of calsenilin binds with the RyR, as well as understanding how phosphorylation of RyRs and calsenilin effect this interaction. Further experiments in hippocampal neurons with specific emphasis on pre and post synaptic connections with calsenilin and RyRs would allow a more precise definition of what this interaction means for synaptic signaling.

The interaction between calsenilin and RyRs could provide a specific pharmacological site for the modulation of intracellular Ca^{2+} in neurons. The Taiwan banded krait beta-bungarotoxin specifically and irreversibly binds calsenilin, but none of the other isoforms in the calsenilin NCS family [101]. Hadrucalcin, a peptide from Hadrurus gertschi scorpion venom, specifically and irreversibly interacts with RyRs [145]. The discovery of the binding sites of these compounds on calsenilin and RyR could lead to the production of a compound that targets the interaction between these two proteins. By creating a genetic dimer of the toxins the compound could bind both calsenilin and RyRs covalently. The consequence of this interaction could be tested easily in whole cell assays and single channel electrophysiology.

To conclude, we have provided evidence for a calsenilin interaction with neuronal RyRs. The interaction has a biophysical effect on single channel RyRs, as well as a modulatory effect on a population of RyRs in a whole cell paradigm. These are important findings in that could aid future investigations into the dysfunction of calsenilin regulation in neurodegenerative diseases such as AD, and potentially be a target for therapeutic intervention.

REFERENCES

1. A novel gene containing a trinucleotide repeat that is expanded and unstable on Huntington's disease chromosomes. The Huntington's Disease Collaborative Research Group. *Cell*, *72* 6 (1993). 971-983.
2. An, W.F., Bowlby, M.R., Betty, M., Cao, J., Ling, H.P., Mendoza, G., Hinson, J.W., Mattsson, K.I., Strassle, B.W., Trimmer, J.S. and Rhodes, K.J. Modulation of A-type potassium channels by a family of calcium sensors. *Nature*, *403* 6769 (2000). 553-556.
3. Anderson, D., Mehaffey, W.H., Iftinca, M., Rehak, R., Engbers, J.D., Hameed, S., Zamponi, G.W. and Turner, R.W. Regulation of neuronal activity by Cav3-Kv4 channel signaling complexes. *Nat Neurosci*, *13* 3 (2010). 333-337.
4. Arundine, M. and Tymianski, M. Molecular mechanisms of calcium-dependent neurodegeneration in excitotoxicity. *Cell Calcium*, *34* 4-5 (2003). 325-337.
5. Bacskai, B.J., Hochner, B., Mahaut-Smith, M., Adams, S.R., Kaang, B.K., Kandel, E.R. and Tsien, R.Y. Spatially resolved dynamics of cAMP and protein kinase A subunits in Aplysia sensory neurons. *Science*, *260* 5105 (1993). 222-226.
6. Bading, H., Hardingham, G.E., Johnson, C.M. and Chawla, S. Gene regulation by nuclear and cytoplasmic calcium signals. *Biochem Biophys Res Commun*, *236* 3 (1997). 541-543.
7. Barghaan, J., Tozakidou, M., Ehmke, H. and Bahring, R. Role of N-terminal domain and accessory subunits in controlling deactivation-inactivation coupling of Kv4.2 channels. *Biophys J*, *94* 4 (2008). 1276-1294.
8. Beisker, W., Dolbeare, F. and Gray, J.W. An improved immunocytochemical procedure for high-sensitivity detection of incorporated bromodeoxyuridine. *Cytometry*, *8* 2 (1987). 235-239.
9. Berridge, M.J. Calcium signalling and Alzheimer's disease. *Neurochem Res*, *36* 7 (2011). 1149-1156.
10. Berridge, M.J. Neuronal calcium signaling. *Neuron*, *21* 1 (1998). 13-26.
11. Berridge, M.J., Bootman, M.D. and Roderick, H.L. Calcium signalling: dynamics, homeostasis and remodelling. *Nat Rev Mol Cell Biol*, *4* 7 (2003). 517-529.
12. Berridge, M.J., Lipp, P. and Bootman, M.D. The versatility and universality of calcium signalling. *Nat Rev Mol Cell Biol*, *1* 1 (2000). 11-21.
13. Bers, D.M. Macromolecular complexes regulating cardiac ryanodine receptor function. *J Mol Cell Cardiol*, *37* 2 (2004). 417-429.
14. Bezprozvanny, I. and Ehrlich, B.E. ATP modulates the function of inositol 1,4,5-trisphosphate-gated channels at two sites. *Neuron*, *10* 6 (1993). 1175-1184.
15. Bezprozvanny, I. and Hayden, M.R. Deranged neuronal calcium signaling and Huntington disease. *Biochem Biophys Res Commun*, *322* 4 (2004). 1310-1317.

16. Bezprozvanny, I. and Mattson, M.P. Neuronal calcium mishandling and the pathogenesis of Alzheimer's disease. *Trends Neurosci*, *31* 9 (2008). 454-463.
17. Bezprozvanny, I., Watras, J. and Ehrlich, B.E. Bell-shaped calcium-response curves of Ins(1,4,5)P3- and calcium-gated channels from endoplasmic reticulum of cerebellum. *Nature*, *351* 6329 (1991). 751-754.
18. Birnbaum, S.G., Varga, A.W., Yuan, L.L., Anderson, A.E., Sweatt, J.D. and Schrader, L.A. Structure and function of Kv4-family transient potassium channels. *Physiol Rev*, *84* 3 (2004). 803-833.
19. Bito, H., Deisseroth, K. and Tsien, R.W. CREB phosphorylation and dephosphorylation: a Ca($^{2+}$)- and stimulus duration-dependent switch for hippocampal gene expression. *Cell*, *87* 7 (1996). 1203-1214.
20. Bolte, S. and Cordelieres, F.P. A guided tour into subcellular colocalization analysis in light microscopy. *J Microsc*, *224* Pt 3 (2006). 213-232.
21. Brown, T.H. and Jaffe, D.B. Calcium imaging in hippocampal neurons using confocal microscopy. *Ann N Y Acad Sci*, *747*(1994). 313-324.
22. Bull, R. and Marengo, J.J. Sarcoplasmic reticulum release channels from frog skeletal muscle display two types of calcium dependence. *FEBS Lett*, *331* 3 (1993). 223-227.
23. Burgoyne, R.D. and Weiss, J.L. The neuronal calcium sensor family of Ca^{2+}-binding proteins. *Biochem J*, *353* Pt 1 (2001). 1-12.
24. Buxbaum, J.D., Choi, E.K., Luo, Y., Lilliehook, C., Crowley, A.C., Merriam, D.E. and Wasco, W. Calsenilin: a calcium-binding protein that interacts with the presenilins and regulates the levels of a presenilin fragment. *Nat Med*, *4* 10 (1998). 1177-1181.
25. Buxbaum, J.D., Lilliehook, C., Chan, J.Y., Go, R.C., Bassett, S.S., Tanzi, R.E., Wasco, W. and Blacker, D. Genomic structure, expression pattern, and chromosomal localization of the human calsenilin gene: no association between an exonic polymorphism and Alzheimer's disease. *Neurosci Lett*, *294* 3 (2000). 135-138.
26. Callamaras, N., Marchant, J.S., Sun, X.P. and Parker, I. Activation and co-ordination of InsP3-mediated elementary Ca^{2+} events during global Ca^{2+} signals in Xenopus oocytes. *J Physiol*, *509 (Pt 1)*(1998). 81-91.
27. Callsen, B., Isbrandt, D., Sauter, K., Hartmann, L.S., Pongs, O. and Bahring, R. Contribution of N- and C-terminal Kv4.2 channel domains to KChIP interaction [corrected]. *J Physiol*, *568* Pt 2 (2005). 397-412.
28. Campos, D., Jimenez-Diaz, L. and Carrion, A.M. Ca($^{2+}$)-dependent prodynorphin transcriptional derepression in neuroblastoma cells is exerted through DREAM protein activity in a kinase-independent manner. *Mol Cell Neurosci*, *22* 2 (2003). 135-145.
29. Cannell, M.B., Cheng, H. and Lederer, W.J. The control of calcium release in heart muscle. *Science*, *268* 5213 (1995). 1045-1049.
30. Carafoli, E., Santella, L., Branca, D. and Brini, M. Generation, control, and processing of cellular calcium signals. *Crit Rev Biochem Mol Biol*, *36* 2 (2001). 107-260.
31. Carrion, A.M., Link, W.A., Ledo, F., Mellstrom, B. and Naranjo, J.R. DREAM is a Ca^{2+}-regulated transcriptional repressor. *Nature*, *398* 6722 (1999). 80-84.

32. Cebolla, B., Fernandez-Perez, A., Perea, G., Araque, A. and Vallejo, M. DREAM mediates cAMP-dependent, Ca^{2+}-induced stimulation of GFAP gene expression and regulates cortical astrogliogenesis. *J Neurosci*, *28* 26 (2008). 6703-6713.
33. Chakroborty, S., Goussakov, I., Miller, M.B. and Stutzmann, G.E. Deviant ryanodine receptor-mediated calcium release resets synaptic homeostasis in presymptomatic 3xTg-AD mice. *J Neurosci*, *29* 30 (2009). 9458-9470.
34. Chan, S.L., Mayne, M., Holden, C.P., Geiger, J.D. and Mattson, M.P. Presenilin-1 mutations increase levels of ryanodine receptors and calcium release in PC12 cells and cortical neurons. *J Biol Chem*, *275* 24 (2000). 18195-18200.
35. Chavira-Suarez, E., Ramirez, M. and Lamas, M. D-Serine/N-methyl-D-aspartate receptor signaling decreases DNA-binding activity of the transcriptional repressor DREAM in Muller glia from the retina. *Neurosci Lett*, *432* 2 (2008). 121-126.
36. Choi, E.K., Miller, J.S., Zaidi, N.F., Salih, E., Buxbaum, J.D. and Wasco, W. Phosphorylation of calsenilin at Ser63 regulates its cleavage by caspase-3. *Mol Cell Neurosci*, *23* 3 (2003). 495-506.
37. Choi, E.K., Zaidi, N.F., Miller, J.S., Crowley, A.C., Merriam, D.E., Lilliehook, C., Buxbaum, J.D. and Wasco, W. Calsenilin is a substrate for caspase-3 that preferentially interacts with the familial Alzheimer's disease-associated C-terminal fragment of presenilin 2. *J Biol Chem*, *276* 22 (2001). 19197-19204.
38. Collin, T. Coloclalsation, McMaster Biophotonics Facility, McMaster University, Hamilton, ON.
39. Collins, T.P. and Terrar, D.A. $Ca(^{2+})$-stimulated adenylyl cyclases regulate the L-type $Ca(^{2+})$ current in guinea-pig atrial myocytes. *J Physiol*, *590* Pt 8 (2012). 1881-1893.
40. Costes, S.V., Daelemans, D., Cho, E.H., Dobbin, Z., Pavlakis, G. and Lockett, S. Automatic and quantitative measurement of protein-protein colocalization in live cells. *Biophys J*, *86* 6 (2004). 3993-4003.
41. Craig, T.A., Benson, L.M., Venyaminov, S.Y., Klimtchuk, E.S., Bajzer, Z., Prendergast, F.G., Naylor, S. and Kumar, R. The metal-binding properties of DREAM: evidence for calcium-mediated changes in DREAM structure. *J Biol Chem*, *277* 13 (2002). 10955-10966.
42. De Crescenzo, V., Fogarty, K.E., Zhuge, R., Tuft, R.A., Lifshitz, L.M., Carmichael, J., Bellve, K.D., Baker, S.P., Zissimopoulos, S., Lai, F.A., Lemos, J.R. and Walsh, J.V., Jr. Dihydropyridine receptors and type 1 ryanodine receptors constitute the molecular machinery for voltage-induced Ca^{2+} release in nerve terminals. *J Neurosci*, *26* 29 (2006). 7565-7574.
43. Du, G.G., Khanna, V.K. and MacLennan, D.H. Mutation of divergent region 1 alters caffeine and $Ca(^{2+})$ sensitivity of the skeletal muscle $Ca(^{2+})$ release channel (ryanodine receptor). *J Biol Chem*, *275* 16 (2000). 11778-11783.
44. Duncan, C.E., Schofield, P.R. and Weickert, C.S. K(v) channel interacting protein 3 expression and regulation by haloperidol in midbrain dopaminergic neurons. *Brain Res*, *1304*(2009). 1-13.

45. Duncan, R.S., Goad, D.L., Grillo, M.A., Kaja, S., Payne, A.J. and Koulen, P. Control of intracellular calcium signaling as a neuroprotective strategy. *Molecules*, *15* 3 (2010). 1168-1195.
46. Duncan, R.S., Hwang, S.Y. and Koulen, P. Effects of Vesl/Homer proteins on intracellular signaling. *Exp Biol Med (Maywood)*, *230* 8 (2005). 527-535.
47. Edling, Y., Ingelman-Sundberg, M. and Simi, A. Glutamate activates c-fos in glial cells via a novel mechanism involving the glutamate receptor subtype mGlu5 and the transcriptional repressor DREAM. *Glia*, *55* 3 (2007). 328-340.
48. Esler, W.P., Kimberly, W.T., Ostaszewski, B.L., Ye, W., Diehl, T.S., Selkoe, D.J. and Wolfe, M.S. Activity-dependent isolation of the presenilin- gamma - secretase complex reveals nicastrin and a gamma substrate. *Proc Natl Acad Sci U S A*, *99* 5 (2002). 2720-2725.
49. Fedrizzi, L., Lim, D., Carafoli, E. and Brini, M. Interplay of the Ca^{2+}-binding protein DREAM with presenilin in neuronal Ca^{2+} signaling. *J Biol Chem*, *283* 41 (2008). 27494-27503.
50. Feldman, D.E. The spike-timing dependence of plasticity. *Neuron*, *75* 4 (2012). 556-571.
51. Ferreiro, E., Resende, R., Costa, R., Oliveira, C.R. and Pereira, C.M. An endoplasmic-reticulum-specific apoptotic pathway is involved in prion and amyloid-beta peptides neurotoxicity. *Neurobiol Dis*, *23* 3 (2006). 669-678.
52. Franzini-Armstrong, C. and Protasi, F. Ryanodine receptors of striated muscles: a complex channel capable of multiple interactions. *Physiol Rev*, *77* 3 (1997). 699-729.
53. Giannini, G., Conti, A., Mammarella, S., Scrobogna, M. and Sorrentino, V. The ryanodine receptor/calcium channel genes are widely and differentially expressed in murine brain and peripheral tissues. *J Cell Biol*, *128* 5 (1995). 893-904.
54. Gleichmann, M. and Mattson, M.P. Neuronal calcium homeostasis and dysregulation. *Antioxid Redox Signal*, *14* 7 (2011). 1261-1273.
55. Golding, N.L., Kath, W.L. and Spruston, N. Dichotomy of action-potential backpropagation in CA1 pyramidal neuron dendrites. *J Neurophysiol*, *86* 6 (2001). 2998-3010.
56. Gomez-Villafuertes, R., Torres, B., Barrio, J., Savignac, M., Gabellini, N., Rizzato, F., Pintado, B., Gutierrez-Adan, A., Mellstrom, B., Carafoli, E. and Naranjo, J.R. Downstream regulatory element antagonist modulator regulates Ca^{2+} homeostasis and viability in cerebellar neurons. *J Neurosci*, *25* 47 (2005). 10822-10830.
57. Gomez, A.M., Schuster, I., Fauconnier, J., Prestle, J., Hasenfuss, G. and Richard, S. FKBP12.6 overexpression decreases Ca^{2+} spark amplitude but enhances $[Ca^{2+}]$i transient in rat cardiac myocytes. *Am J Physiol Heart Circ Physiol*, *287* 5 (2004). H1987-1993.
58. Guse, A.H. Cyclic ADP-ribose. *J Mol Med (Berl)*, *78* 1 (2000). 26-35.
59. Hajnoczky, G., Davies, E. and Madesh, M. Calcium signaling and apoptosis. *Biochem Biophys Res Commun*, *304* 3 (2003). 445-454.

60. Hakamata, Y., Nakai, J., Takeshima, H. and Imoto, K. Primary structure and distribution of a novel ryanodine receptor/calcium release channel from rabbit brain. *FEBS Lett*, *312* 2-3 (1992). 229-235.
61. Hamilton, S.L. Ryanodine receptors. *Cell Calcium*, *38* 3-4 (2005). 253-260.
62. Hammond, P.I., Craig, T.A., Kumar, R. and Brimijoin, S. Regional and cellular distribution of DREAM in adult rat brain consistent with multiple sensory processing roles. *Brain Res Mol Brain Res*, *111* 1-2 (2003). 104-110.
63. Hardy, J. A hundred years of Alzheimer's disease research. *Neuron*, *52* 1 (2006). 3-13.
64. Hayashi, M.K., Ames, H.M. and Hayashi, Y. Tetrameric hub structure of postsynaptic scaffolding protein homer. *J Neurosci*, *26* 33 (2006). 8492-8501.
65. Hayashi, M.K., Tang, C., Verpelli, C., Narayanan, R., Stearns, M.H., Xu, R.M., Li, H., Sala, C. and Hayashi, Y. The postsynaptic density proteins Homer and Shank form a polymeric network structure. *Cell*, *137* 1 (2009). 159-171.
66. Hayek, S.M., Zhao, J., Bhat, M., Xu, X., Nagaraj, R., Pan, Z., Takeshima, H. and Ma, J. A negatively charged region of the skeletal muscle ryanodine receptor is involved in Ca($^{2+}$)-dependent regulation of the Ca($^{2+}$) release channel. *FEBS Lett*, *461* 3 (1999). 157-164.
67. Hayrapetyan, V., Rybalchenko, V., Rybalchenko, N. and Koulen, P. The N-terminus of presenilin-2 increases single channel activity of brain ryanodine receptors through direct protein-protein interaction. *Cell Calcium*, *44* 5 (2008). 507-518.
68. Henkart, M.P., Reese, T.S. and Brinley, F.J., Jr. Endoplasmic reticulum sequesters calcium in the squid giant axon. *Science*, *202* 4374 (1978). 1300-1303.
69. Holmqvist, M.H., Cao, J., Knoppers, M.H., Jurman, M.E., Distefano, P.S., Rhodes, K.J., Xie, Y. and An, W.F. Kinetic modulation of Kv4-mediated A-current by arachidonic acid is dependent on potassium channel interacting proteins. *J Neurosci*, *21* 12 (2001). 4154-4161.
70. Hong, Y.M., Jo, D.G., Lee, M.C., Kim, S.Y. and Jung, Y.K. Reduced expression of calsenilin/DREAM/KChIP3 in the brains of kainic acid-induced seizure and epilepsy patients. *Neurosci Lett*, *340* 1 (2003). 33-36.
71. Huang, G., Kim, J.Y., Dehoff, M., Mizuno, Y., Kamm, K.E., Worley, P.F., Muallem, S. and Zeng, W. Ca^{2+} signaling in microdomains: Homer1 mediates the interaction between RyR2 and Cav1.2 to regulate excitation-contraction coupling. *J Biol Chem*, *282* 19 (2007). 14283-14290.
72. Hwang, S.Y., Wei, J., Westhoff, J.H., Duncan, R.S., Ozawa, F., Volpe, P., Inokuchi, K. and Koulen, P. Differential functional interaction of two Vesl/Homer protein isoforms with ryanodine receptor type 1: a novel mechanism for control of intracellular calcium signaling. *Cell Calcium*, *34* 2 (2003). 177-184.
73. Inui, M., Saito, A. and Fleischer, S. Purification of the ryanodine receptor and identity with feet structures of junctional terminal cisternae of sarcoplasmic reticulum from fast skeletal muscle. *J Biol Chem*, *262* 4 (1987). 1740-1747.
74. Jang, C., Choi, J.K., Na, Y.J., Jang, B., Wasco, W., Buxbaum, J.D., Kim, Y.S. and Choi, E.K. Calsenilin regulates presenilin 1/gamma-secretase-mediated

N-cadherin epsilon-cleavage and beta-catenin signaling. *FASEB J*, *25* 12 (2011). 4174-4183.
75. Jerng, H.H., Kunjilwar, K. and Pfaffinger, P.J. Multiprotein assembly of Kv4.2, KChIP3 and DPP10 produces ternary channel complexes with ISA-like properties. *J Physiol*, *568* Pt 3 (2005). 767-788.
76. Jerng, H.H. and Pfaffinger, P.J. Multiple Kv channel-interacting proteins contain an N-terminal transmembrane domain that regulates Kv4 channel trafficking and gating. *J Biol Chem*, *283* 51 (2008). 36046-36059.
77. Jeyakumar, L.H., Copello, J.A., O'Malley, A.M., Wu, G.M., Grassucci, R., Wagenknecht, T. and Fleischer, S. Purification and characterization of ryanodine receptor 3 from mammalian tissue. *J Biol Chem*, *273* 26 (1998). 16011-16020.
78. Jo, D.G., Chang, J.W., Hong, H.S., Mook-Jung, I. and Jung, Y.K. Contribution of presenilin/gamma-secretase to calsenilin-mediated apoptosis. *Biochem Biophys Res Commun*, *305* 1 (2003). 62-66.
79. Jo, D.G., Jang, J., Kim, B.J., Lundkvist, J. and Jung, Y.K. Overexpression of calsenilin enhances gamma-secretase activity. *Neurosci Lett*, *378* 1 (2005). 59-64.
80. Jo, D.G., Kim, M.J., Choi, Y.H., Kim, I.K., Song, Y.H., Woo, H.N., Chung, C.W. and Jung, Y.K. Pro-apoptotic function of calsenilin/DREAM/KChIP3. *FASEB J*, *15* 3 (2001). 589-591.
81. Jo, D.G., Lee, J.Y., Hong, Y.M., Song, S., Mook-Jung, I., Koh, J.Y. and Jung, Y.K. Induction of pro-apoptotic calsenilin/DREAM/KChIP3 in Alzheimer's disease and cultured neurons after amyloid-beta exposure. *J Neurochem*, *88* 3 (2004). 604-611.
82. Kaja, S., Sumien, N., Borden, P.K., Khullar, N., Iqbal, M., Collins, J.L., Forster, M.J. and Koulen, P. Homer-1a immediate early gene expression correlates with better cognitive performance in aging. *Age (Dordr)*(2012).
83. Kelliher, M., Fastbom, J., Cowburn, R.F., Bonkale, W., Ohm, T.G., Ravid, R., Sorrentino, V. and O'Neill, C. Alterations in the ryanodine receptor calcium release channel correlate with Alzheimer's disease neurofibrillary and beta-amyloid pathologies. *Neuroscience*, *92* 2 (1999). 499-513.
84. Kermode, H., Williams, A.J. and Sitsapesan, R. The interactions of ATP, ADP, and inorganic phosphate with the sheep cardiac ryanodine receptor. *Biophys J*, *74* 3 (1998). 1296-1304.
85. Koulen, P. and Thrower, E.C. Pharmacological modulation of intracellular $Ca(^{2+})$ channels at the single-channel level. *Mol Neurobiol*, *24* 1-3 (2001). 65-86.
86. Kuchibhotla, K.V., Goldman, S.T., Lattarulo, C.R., Wu, H.Y., Hyman, B.T. and Bacskai, B.J. Abeta plaques lead to aberrant regulation of calcium homeostasis in vivo resulting in structural and functional disruption of neuronal networks. *Neuron*, *59* 2 (2008). 214-225.
87. Kunjilwar, K., Strang, C., DeRubeis, D. and Pfaffinger, P.J. KChIP3 rescues the functional expression of Shal channel tetramerization mutants. *J Biol Chem*, *279* 52 (2004). 54542-54551.

88. Lafon-Cazal, M., Pietri, S., Culcasi, M. and Bockaert, J. NMDA-dependent superoxide production and neurotoxicity. *Nature*, *364* 6437 (1993). 535-537.
89. Lai, F.A., Dent, M., Wickenden, C., Xu, L., Kumari, G., Misra, M., Lee, H.B., Sar, M. and Meissner, G. Expression of a cardiac Ca($^{2+}$)-release channel isoform in mammalian brain. *Biochem J*, *288 (Pt 2)*(1992). 553-564.
90. Lai, F.A., Misra, M., Xu, L., Smith, H.A. and Meissner, G. The ryanodine receptor-Ca^{2+} release channel complex of skeletal muscle sarcoplasmic reticulum. Evidence for a cooperatively coupled, negatively charged homotetramer. *J Biol Chem*, *264* 28 (1989). 16776-16785.
91. Lamas, M., Lee-Rivera, I., Ramirez, M. and Lopez-Colome, A.M. D-serine regulates CREB phosphorylation induced by NMDA receptor activation in Muller glia from the retina. *Neurosci Lett*, *427* 1 (2007). 55-60.
92. Lamb, G.D. Excitation-contraction coupling in skeletal muscle: comparisons with cardiac muscle. *Clin Exp Pharmacol Physiol*, *27* 3 (2000). 216-224.
93. Lanner, J.T., Georgiou, D.K., Joshi, A.D. and Hamilton, S.L. Ryanodine receptors: structure, expression, molecular details, and function in calcium release. *Cold Spring Harb Perspect Biol*, *2* 11 (2010). a003996.
94. Larkum, M.E., Watanabe, S., Nakamura, T., Lasser-Ross, N. and Ross, W.N. Synaptically activated Ca^{2+} waves in layer 2/3 and layer 5 rat neocortical pyramidal neurons. *J Physiol*, *549* Pt 2 (2003). 471-488.
95. Ledo, F., Carrion, A.M., Link, W.A., Mellstrom, B. and Naranjo, J.R. DREAM-alphaCREM interaction via leucine-charged domains derepresses downstream regulatory element-dependent transcription. *Mol Cell Biol*, *20* 24 (2000). 9120-9126.
96. Ledo, F., Kremer, L., Mellstrom, B. and Naranjo, J.R. Ca^{2+}-dependent block of CREB-CBP transcription by repressor DREAM. *EMBO J*, *21* 17 (2002). 4583-4592.
97. Lee, S.Y., Hwang, D.Y., Kim, Y.K., Lee, J.W., Shin, I.C., Oh, K.W., Lee, M.K., Lim, J.S., Yoon, D.Y., Hwang, S.J. and Hong, J.T. PS2 mutation increases neuronal cell vulnerability to neurotoxicants through activation of caspase-3 by enhancing of ryanodine receptor-mediated calcium release. *FASEB J*, *20* 1 (2006). 151-153.
98. Leissring, M.A., Yamasaki, T.R., Wasco, W., Buxbaum, J.D., Parker, I. and LaFerla, F.M. Calsenilin reverses presenilin-mediated enhancement of calcium signaling. *Proc Natl Acad Sci U S A*, *97* 15 (2000). 8590-8593.
99. Lilliehook, C., Bozdagi, O., Yao, J., Gomez-Ramirez, M., Zaidi, N.F., Wasco, W., Gandy, S., Santucci, A.C., Haroutunian, V., Huntley, G.W. and Buxbaum, J.D. Altered Abeta formation and long-term potentiation in a calsenilin knock-out. *J Neurosci*, *23* 27 (2003). 9097-9106.
100. Lilliehook, C., Chan, S., Choi, E.K., Zaidi, N.F., Wasco, W., Mattson, M.P. and Buxbaum, J.D. Calsenilin enhances apoptosis by altering endoplasmic reticulum calcium signaling. *Mol Cell Neurosci*, *19* 4 (2002). 552-559.
101. Lin, Y.L., Wu, P.F., Wu, T.T. and Chang, L.S. KChIP3: a binding protein for Taiwan banded krait beta-bungarotoxin. *Toxicon*, *47* 3 (2006). 265-270.

102. Lopez, J.R., Lyckman, A., Oddo, S., Laferla, F.M., Querfurth, H.W. and Shtifman, A. Increased intraneuronal resting [Ca^{2+}] in adult Alzheimer's disease mice. *J Neurochem*, *105* 1 (2008). 262-271.
103. Lusin, J.D., Vanarotti, M., Li, C., Valiveti, A. and Ames, J.B. NMR structure of DREAM: Implications for Ca($^{2+}$)-dependent DNA binding and protein dimerization. *Biochemistry*, *47* 8 (2008). 2252-2264.
104. Magee, J.C. and Carruth, M. Dendritic voltage-gated ion channels regulate the action potential firing mode of hippocampal CA1 pyramidal neurons. *J Neurophysiol*, *82* 4 (1999). 1895-1901.
105. Markram, H., Gerstner, W. and Sjostrom, P.J. A history of spike-timing-dependent plasticity. *Front Synaptic Neurosci*, *3*(2011). 4.
106. Marx, S.O., Gaburjakova, J., Gaburjakova, M., Henrikson, C., Ondrias, K. and Marks, A.R. Coupled gating between cardiac calcium release channels (ryanodine receptors). *Circ Res*, *88* 11 (2001). 1151-1158.
107. Marx, S.O., Ondrias, K. and Marks, A.R. Coupled gating between individual skeletal muscle Ca^{2+} release channels (ryanodine receptors). *Science*, *281* 5378 (1998). 818-821.
108. Matsu-ura, T., Konishi, Y., Aoki, T., Naranjo, J.R., Mikoshiba, K. and Tamura, T.A. Seizure-mediated neuronal activation induces DREAM gene expression in the mouse brain. *Brain Res Mol Brain Res*, *109* 1-2 (2002). 198-206.
109. Mattson, M.P. Calcium and neurodegeneration. *Aging Cell*, *6* 3 (2007). 337-350.
110. Mattson, M.P. Excitotoxic and excitoprotective mechanisms: abundant targets for the prevention and treatment of neurodegenerative disorders. *Neuromolecular Med*, *3* 2 (2003). 65-94.
111. Mattson, M.P., Zhu, H., Yu, J. and Kindy, M.S. Presenilin-1 mutation increases neuronal vulnerability to focal ischemia in vivo and to hypoxia and glucose deprivation in cell culture: involvement of perturbed calcium homeostasis. *J Neurosci*, *20* 4 (2000). 1358-1364.
112. Medina-Ortiz, W.E., Gregg, E.V., Brun-Zinkernagel, A.M. and Koulen, P. Identification and functional distribution of intracellular ca channels in mouse lacrimal gland acinar cells. *Open Ophthalmol J*, *1*(2007). 8-16.
113. Mezey, E., Imbembo, A.L., Potter, J.J., Rent, K.C., Lombardo, R. and Holt, P.R. Endogenous ethanol production and hepatic disease following jejunoileal bypass for morbid obesity. *Am J Clin Nutr*, *28* 11 (1975). 1277-1283.
114. Mignery, G.A., Sudhof, T.C., Takei, K. and De Camilli, P. Putative receptor for inositol 1,4,5-trisphosphate similar to ryanodine receptor. *Nature*, *342* 6246 (1989). 192-195.
115. Morelli, M.B., Amantini, C., Liberati, S., Santoni, M. and Nabissi, M. TRP Channels: New Potential Therapeutic Approaches in CNS Neuropathies. *CNS Neurol Disord Drug Targets*(2013).
116. Muik, M., Schindl, R., Fahrner, M. and Romanin, C. Ca($^{2+}$) release-activated Ca($^{2+}$) (CRAC) current, structure, and function. *Cell Mol Life Sci*, *69* 24 (2012). 4163-4176.
117. Nadal, M.S., Ozaita, A., Amarillo, Y., Vega-Saenz de Miera, E., Ma, Y., Mo, W., Goldberg, E.M., Misumi, Y., Ikehara, Y., Neubert, T.A. and Rudy, B. The

CD26-related dipeptidyl aminopeptidase-like protein DPPX is a critical component of neuronal A-type K+ channels. *Neuron*, *37* 3 (2003). 449-461.
118. Nakamura, T., Lasser-Ross, N., Nakamura, K. and Ross, W.N. Spatial segregation and interaction of calcium signalling mechanisms in rat hippocampal CA1 pyramidal neurons. *J Physiol*, *543* Pt 2 (2002). 465-480.
119. Nakanishi, S., Kuwajima, G. and Mikoshiba, K. Immunohistochemical localization of ryanodine receptors in mouse central nervous system. *Neurosci Res*, *15* 1-2 (1992). 130-142.
120. Osawa, M., Dace, A., Tong, K.I., Valiveti, A., Ikura, M. and Ames, J.B. Mg^{2+} and Ca^{2+} differentially regulate DNA binding and dimerization of DREAM. *J Biol Chem*, *280* 18 (2005). 18008-18014.
121. Osawa, M., Tong, K.I., Lilliehook, C., Wasco, W., Buxbaum, J.D., Cheng, H.Y., Penninger, J.M., Ikura, M. and Ames, J.B. Calcium-regulated DNA binding and oligomerization of the neuronal calcium-sensing protein, calsenilin/DREAM/KChIP3. *J Biol Chem*, *276* 44 (2001). 41005-41013.
122. Otsu, K., Willard, H.F., Khanna, V.K., Zorzato, F., Green, N.M. and MacLennan, D.H. Molecular cloning of cDNA encoding the Ca^{2+} release channel (ryanodine receptor) of rabbit cardiac muscle sarcoplasmic reticulum. *J Biol Chem*, *265* 23 (1990). 13472-13483.
123. Pagani, M.R., Reisin, R.C. and Uchitel, O.D. Calcium signaling pathways mediating synaptic potentiation triggered by amyotrophic lateral sclerosis IgG in motor nerve terminals. *J Neurosci*, *26* 10 (2006). 2661-2672.
124. Palade, P., Dettbarn, C., Alderson, B. and Volpe, P. Pharmacologic differentiation between inositol-1,4,5-trisphosphate-induced Ca^{2+} release and Ca^{2+}- or caffeine-induced Ca^{2+} release from intracellular membrane systems. *Mol Pharmacol*, *36* 4 (1989). 673-680.
125. Perez, C.F., Mukherjee, S. and Allen, P.D. Amino acids 1-1,680 of ryanodine receptor type 1 hold critical determinants of skeletal type for excitation-contraction coupling. Role of divergence domain D2. *J Biol Chem*, *278* 41 (2003). 39644-39652.
126. Petersen, O.H., Michalak, M. and Verkhratsky, A. Calcium signalling: past, present and future. *Cell Calcium*, *38* 3-4 (2005). 161-169.
127. Prestle, J., Janssen, P.M., Janssen, A.P., Zeitz, O., Lehnart, S.E., Bruce, L., Smith, G.L. and Hasenfuss, G. Overexpression of FK506-binding protein FKBP12.6 in cardiomyocytes reduces ryanodine receptor-mediated Ca($^{2+}$) leak from the sarcoplasmic reticulum and increases contractility. *Circ Res*, *88* 2 (2001). 188-194.
128. Ramachandran, P.L., Craig, T.A., Atanasova, E.A., Cui, G., Owen, B.A., Bergen, H.R., 3rd, Mer, G. and Kumar, R. The potassium channel interacting protein 3 (DREAM/KChIP3) heterodimerizes with and regulates calmodulin function. *J Biol Chem*, *287* 47 (2012). 39439-39448.
129. Ramirez, M. and Lamas, M. NMDA receptor mediates proliferation and CREB phosphorylation in postnatal Muller glia-derived retinal progenitors. *Mol Vis*, *15*(2009). 713-721.

130. Rivas, M., Aurrekoetxea, K., Mellstrom, B. and Naranjo, J.R. Redox signaling regulates transcriptional activity of the Ca^{2+}-dependent repressor DREAM. *Antioxid Redox Signal*, *14* 7 (2011). 1237-1243.
131. Rivera-Arconada, I., Benedet, T., Roza, C., Torres, B., Barrio, J., Krzyzanowska, A., Avendano, C., Mellstrom, B., Lopez-Garcia, J.A. and Naranjo, J.R. DREAM regulates BDNF-dependent spinal sensitization. *Mol Pain*, *6*(2010). 95.
132. Rodriguez, P., Bhogal, M.S. and Colyer, J. Stoichiometric phosphorylation of cardiac ryanodine receptor on serine 2809 by calmodulin-dependent kinase II and protein kinase A. *J Biol Chem*, *278* 40 (2003). 38593-38600.
133. Rosen, L.B., Ginty, D.D., Weber, M.J. and Greenberg, M.E. Membrane depolarization and calcium influx stimulate MEK and MAP kinase via activation of Ras. *Neuron*, *12* 6 (1994). 1207-1221.
134. Ross, W.N. Understanding calcium waves and sparks in central neurons. *Nat Rev Neurosci*, *13* 3 (2012). 157-168.
135. Rousseau, E. and Meissner, G. Single cardiac sarcoplasmic reticulum Ca^{2+}-release channel: activation by caffeine. *Am J Physiol*, *256* 2 Pt 2 (1989). H328-333.
136. Rybalchenko, V., Grillo, M.A., Gastinger, M.J., Rybalchenko, N., Payne, A.J. and Koulen, P. The unliganded long isoform of estrogen receptor beta stimulates brain ryanodine receptor single channel activity alongside with cytosolic Ca^{2+}. *J Recept Signal Transduct Res*, *29* 6 (2009). 326-341.
137. Rybalchenko, V., Hwang, S.Y., Rybalchenko, N. and Koulen, P. The cytosolic N-terminus of presenilin-1 potentiates mouse ryanodine receptor single channel activity. *Int J Biochem Cell Biol*, *40* 1 (2008). 84-97.
138. Sadowski, J.H., Jones, M.W. and Mellor, J.R. Ripples make waves: binding structured activity and plasticity in hippocampal networks. *Neural Plast*, *2011*(2011). 960389.
139. Sanz, C., Horita, M. and Fernandez-Luna, J.L. Fas signaling and blockade of Bcr-Abl kinase induce apoptotic Hrk protein via DREAM inhibition in human leukemia cells. *Haematologica*, *87* 9 (2002). 903-907.
140. Sanz, C., Mellstrom, B., Link, W.A., Naranjo, J.R. and Fernandez-Luna, J.L. Interleukin 3-dependent activation of DREAM is involved in transcriptional silencing of the apoptotic Hrk gene in hematopoietic progenitor cells. *EMBO J*, *20* 9 (2001). 2286-2292.
141. Satoh, T., Ross, C.A., Villa, A., Supattapone, S., Pozzan, T., Snyder, S.H. and Meldolesi, J. The inositol 1,4,5,-trisphosphate receptor in cerebellar Purkinje cells: quantitative immunogold labeling reveals concentration in an ER subcompartment. *J Cell Biol*, *111* 2 (1990). 615-624.
142. Schneggenburger, R., Han, Y. and Kochubey, O. $Ca(^{2+})$ channels and transmitter release at the active zone. *Cell Calcium*, *52* 3-4 (2012). 199-207.
143. Schrader, L.A., Anderson, A.E., Mayne, A., Pfaffinger, P.J. and Sweatt, J.D. PKA modulation of Kv4.2-encoded A-type potassium channels requires formation of a supramolecular complex. *J Neurosci*, *22* 23 (2002). 10123-10133.

144. Schrader, L.A., Ren, Y., Cheng, F., Bui, D., Sweatt, J.D. and Anderson, A.E. Kv4.2 is a locus for PKC and ERK/MAPK cross-talk. *Biochem J*, *417* 3 (2009). 705-715.
145. Schwartz, E.F., Capes, E.M., Diego-Garcia, E., Zamudio, F.Z., Fuentes, O., Possani, L.D. and Valdivia, H.H. Characterization of hadrucalcin, a peptide from Hadrurus gertschi scorpion venom with pharmacological activity on ryanodine receptors. *Br J Pharmacol*, *157* 3 (2009). 392-403.
146. Schwarzer, C. 30 years of dynorphins--new insights on their functions in neuropsychiatric diseases. *Pharmacol Ther*, *123* 3 (2009). 353-370.
147. Scriven, D.R., Lynch, R.M. and Moore, E.D. Image acquisition for colocalization using optical microscopy. *Am J Physiol Cell Physiol*, *294* 5 (2008). C1119-1122.
148. Sencer, S., Papineni, R.V., Halling, D.B., Pate, P., Krol, J., Zhang, J.Z. and Hamilton, S.L. Coupling of RYR1 and L-type calcium channels via calmodulin binding domains. *J Biol Chem*, *276* 41 (2001). 38237-38241.
149. Seymour-Laurent, K.J. and Barish, M.E. Inositol 1,4,5-trisphosphate and ryanodine receptor distributions and patterns of acetylcholine- and caffeine-induced calcium release in cultured mouse hippocampal neurons. *J Neurosci*, *15* 4 (1995). 2592-2608.
150. Sharp, A.H., McPherson, P.S., Dawson, T.M., Aoki, C., Campbell, K.P. and Snyder, S.H. Differential immunohistochemical localization of inositol 1,4,5-trisphosphate- and ryanodine-sensitive Ca^{2+} release channels in rat brain. *J Neurosci*, *13* 7 (1993). 3051-3063.
151. Shibata, R., Misonou, H., Campomanes, C.R., Anderson, A.E., Schrader, L.A., Doliveira, L.C., Carroll, K.I., Sweatt, J.D., Rhodes, K.J. and Trimmer, J.S. A fundamental role for KChIPs in determining the molecular properties and trafficking of Kv4.2 potassium channels. *J Biol Chem*, *278* 38 (2003). 36445-36454.
152. Smith, I.F., Hitt, B., Green, K.N., Oddo, S. and LaFerla, F.M. Enhanced caffeine-induced Ca^{2+} release in the 3xTg-AD mouse model of Alzheimer's disease. *J Neurochem*, *94* 6 (2005). 1711-1718.
153. Smith, J.S., Coronado, R. and Meissner, G. Sarcoplasmic reticulum contains adenine nucleotide-activated calcium channels. *Nature*, *316* 6027 (1985). 446-449.
154. Smith, J.S., Coronado, R. and Meissner, G. Single channel measurements of the calcium release channel from skeletal muscle sarcoplasmic reticulum. Activation by Ca^{2+} and ATP and modulation by Mg^{2+}. *J Gen Physiol*, *88* 5 (1986). 573-588.
155. Song, D.W., Lee, J.G., Youn, H.S., Eom, S.H. and Kim do, H. Ryanodine receptor assembly: a novel systems biology approach to 3D mapping. *Prog Biophys Mol Biol*, *105* 3 (2011). 145-161.
156. Sours-Brothers, S., Ma, R. and Koulen, P. Ca^{2+}-sensitive transcriptional regulation: direct DNA interaction by DREAM. *Front Biosci*, *14*(2009). 1851-1856.

157. Spreafico, F., Barski, J.J., Farina, C. and Meyer, M. Mouse DREAM/calsenilin/KChIP3: gene structure, coding potential, and expression. *Mol Cell Neurosci*, *17* 1 (2001). 1-16.
158. Sterratt, D.C., Groen, M.R., Meredith, R.M. and van Ooyen, A. Spine calcium transients induced by synaptically-evoked action potentials can predict synapse location and establish synaptic democracy. *PLoS Comput Biol*, *8* 6 (2012). e1002545.
159. Strassle, B.W., Menegola, M., Rhodes, K.J. and Trimmer, J.S. Light and electron microscopic analysis of KChIP and Kv4 localization in rat cerebellar granule cells. *J Comp Neurol*, *484* 2 (2005). 144-155.
160. Stutzmann, G.E., Caccamo, A., LaFerla, F.M. and Parker, I. Dysregulated IP3 signaling in cortical neurons of knock-in mice expressing an Alzheimer's-linked mutation in presenilin1 results in exaggerated Ca^{2+} signals and altered membrane excitability. *J Neurosci*, *24* 2 (2004). 508-513.
161. Stutzmann, G.E., Smith, I., Caccamo, A., Oddo, S., Laferla, F.M. and Parker, I. Enhanced ryanodine receptor recruitment contributes to Ca^{2+} disruptions in young, adult, and aged Alzheimer's disease mice. *J Neurosci*, *26* 19 (2006). 5180-5189.
162. Stutzmann, G.E., Smith, I., Caccamo, A., Oddo, S., Parker, I. and Laferla, F. Enhanced ryanodine-mediated calcium release in mutant PS1-expressing Alzheimer's mouse models. *Ann N Y Acad Sci*, *1097*(2007). 265-277.
163. Sudhof, T.C. The synaptic vesicle cycle. *Annu Rev Neurosci*, *27*(2004). 509-547.
164. Sudhof, T.C. The synaptic vesicle cycle: a cascade of protein-protein interactions. *Nature*, *375* 6533 (1995). 645-653.
165. Supnet, C. and Bezprozvanny, I. The dysregulation of intracellular calcium in Alzheimer disease. *Cell Calcium*, *47* 2 (2010). 183-189.
166. Supnet, C., Grant, J., Kong, H., Westaway, D. and Mayne, M. Amyloid-beta-(1-42) increases ryanodine receptor-3 expression and function in neurons of TgCRND8 mice. *J Biol Chem*, *281* 50 (2006). 38440-38447.
167. Szumlinski, K.K., Kalivas, P.W. and Worley, P.F. Homer proteins: implications for neuropsychiatric disorders. *Curr Opin Neurobiol*, *16* 3 (2006). 251-257.
168. Tanaka, D., Nakada, K., Takao, K., Ogasawara, E., Kasahara, A., Sato, A., Yonekawa, H., Miyakawa, T. and Hayashi, J. Normal mitochondrial respiratory function is essential for spatial remote memory in mice. *Mol Brain*, *1*(2008). 21.
169. Tang, T.S., Slow, E., Lupu, V., Stavrovskaya, I.G., Sugimori, M., Llinas, R., Kristal, B.S., Hayden, M.R. and Bezprozvanny, I. Disturbed Ca^{2+} signaling and apoptosis of medium spiny neurons in Huntington's disease. *Proc Natl Acad Sci U S A*, *102* 7 (2005). 2602-2607.
170. Tang, T.S., Tu, H., Chan, E.Y., Maximov, A., Wang, Z., Wellington, C.L., Hayden, M.R. and Bezprozvanny, I. Huntingtin and huntingtin-associated protein 1 influence neuronal calcium signaling mediated by inositol-(1,4,5) triphosphate receptor type 1. *Neuron*, *39* 2 (2003). 227-239.

171. Tantral, L., Malathi, K., Kohyama, S., Silane, M., Berenstein, A. and Jayaraman, T. Intracellular calcium release is required for caspase-3 and -9 activation. *Cell Biochem Funct*, *22* 1 (2004). 35-40.
172. Terasaki, M., Slater, N.T., Fein, A., Schmidek, A. and Reese, T.S. Continuous network of endoplasmic reticulum in cerebellar Purkinje neurons. *Proc Natl Acad Sci U S A*, *91* 16 (1994). 7510-7514.
173. Toescu, E.C. and Verkhratsky, A. The importance of being subtle: small changes in calcium homeostasis control cognitive decline in normal aging. *Aging Cell*, *6* 3 (2007). 267-273.
174. Tripathy, A., Xu, L., Mann, G. and Meissner, G. Calmodulin activation and inhibition of skeletal muscle Ca^{2+} release channel (ryanodine receptor). *Biophys J*, *69* 1 (1995). 106-119.
175. Tsai, T.D. and Barish, M.E. Imaging of caffeine-inducible release of intracellular calcium in cultured embryonic mouse telencephalic neurons. *J Neurobiol*, *27* 2 (1995). 252-265.
176. Tsien, R. and Pozzan, T. Measurement of cytosolic free Ca^{2+} with quin2. *Methods Enzymol*, *172*(1989). 230-262.
177. Vallejo, M. PACAP signaling to DREAM: a cAMP-dependent pathway that regulates cortical astrogliogenesis. *Mol Neurobiol*, *39* 2 (2009). 90-100.
178. Van Petegem, F. Ryanodine receptors: structure and function. *J Biol Chem*, *287* 38 (2012). 31624-31632.
179. Varga, A.W., Yuan, L.L., Anderson, A.E., Schrader, L.A., Wu, G.Y., Gatchel, J.R., Johnston, D. and Sweatt, J.D. Calcium-calmodulin-dependent kinase II modulates Kv4.2 channel expression and upregulates neuronal A-type potassium currents. *J Neurosci*, *24* 14 (2004). 3643-3654.
180. Walton, P.D., Airey, J.A., Sutko, J.L., Beck, C.F., Mignery, G.A., Sudhof, T.C., Deerinck, T.J. and Ellisman, M.H. Ryanodine and inositol trisphosphate receptors coexist in avian cerebellar Purkinje neurons. *J Cell Biol*, *113* 5 (1991). 1145-1157.
181. Wang, H., Yan, Y., Liu, Q., Huang, Y., Shen, Y., Chen, L., Chen, Y., Yang, Q., Hao, Q., Wang, K. and Chai, J. Structural basis for modulation of Kv4 K+ channels by auxiliary KChIP subunits. *Nat Neurosci*, *10* 1 (2007). 32-39.
182. Wang, K. Modulation by clamping: Kv4 and KChIP interactions. *Neurochem Res*, *33* 10 (2008). 1964-1969.
183. Wang, S.Q., Song, L.S., Lakatta, E.G. and Cheng, H. Ca^{2+} signalling between single L-type Ca^{2+} channels and ryanodine receptors in heart cells. *Nature*, *410* 6828 (2001). 592-596.
184. Waters, J., Schaefer, A. and Sakmann, B. Backpropagating action potentials in neurones: measurement, mechanisms and potential functions. *Prog Biophys Mol Biol*, *87* 1 (2005). 145-170.
185. Wehrens, X.H., Lehnart, S.E., Huang, F., Vest, J.A., Reiken, S.R., Mohler, P.J., Sun, J., Guatimosim, S., Song, L.S., Rosemblit, N., D'Armiento, J.M., Napolitano, C., Memmi, M., Priori, S.G., Lederer, W.J. and Marks, A.R. FKBP12.6 deficiency and defective calcium release channel (ryanodine receptor) function linked to exercise-induced sudden cardiac death. *Cell*, *113* 7 (2003). 829-840.

186. Wehrens, X.H., Lehnart, S.E., Reiken, S.R. and Marks, A.R. Ca^{2+}/calmodulin-dependent protein kinase II phosphorylation regulates the cardiac ryanodine receptor. *Circ Res*, *94* 6 (2004). e61-70.
187. Welch, W., Rheault, S., West, D.J. and Williams, A.J. A model of the putative pore region of the cardiac ryanodine receptor channel. *Biophys J*, *87* 4 (2004). 2335-2351.
188. Westhoff, J.H., Hwang, S.Y., Duncan, R.S., Ozawa, F., Volpe, P., Inokuchi, K. and Koulen, P. Vesl/Homer proteins regulate ryanodine receptor type 2 function and intracellular calcium signaling. *Cell Calcium*, *34* 3 (2003). 261-269.
189. Witcher, D.R., Kovacs, R.J., Schulman, H., Cefali, D.C. and Jones, L.R. Unique phosphorylation site on the cardiac ryanodine receptor regulates calcium channel activity. *J Biol Chem*, *266* 17 (1991). 11144-11152.
190. Woo, H.N., Chang, J.W., Choi, Y.H., Gwon, A.R., Jung, Y.K. and Jo, D.G. Characterization of subcellular localization and Ca^{2+} modulation of calsenilin/DREAM/KChIP3. *Neuroreport*, *19* 12 (2008). 1193-1197.
191. Xiao, B., Sutherland, C., Walsh, M.P. and Chen, S.R. Protein kinase A phosphorylation at serine-2808 of the cardiac Ca^{2+}-release channel (ryanodine receptor) does not dissociate 12.6-kDa FK506-binding protein (FKBP12.6). *Circ Res*, *94* 4 (2004). 487-495.
192. Xiong, H., Kovacs, I. and Zhang, Z. Differential distribution of KChIPs mRNAs in adult mouse brain. *Brain Res Mol Brain Res*, *128* 2 (2004). 103-111.
193. Yu, L., Sun, C., Mendoza, R., Wang, J., Matayoshi, E.D., Hebert, E., Pereda-Lopez, A., Hajduk, P.J. and Olejniczak, E.T. Solution structure and calcium-binding properties of EF-hands 3 and 4 of calsenilin. *Protein Sci*, *16* 11 (2007). 2502-2509.
194. Zaidi, N.F., Berezovska, O., Choi, E.K., Miller, J.S., Chan, H., Lilliehook, C., Hyman, B.T., Buxbaum, J.D. and Wasco, W. Biochemical and immunocytochemical characterization of calsenilin in mouse brain. *Neuroscience*, *114* 1 (2002). 247-263.
195. Zaidi, N.F., Kuplast, K.G., Washicosky, K.J., Kajiwara, Y., Buxbaum, J.D. and Wasco, W. Calsenilin interacts with transcriptional co-repressor C-terminal binding protein(s). *J Neurochem*, *98* 4 (2006). 1290-1301.
196. Zhang, Y., Li, Y., Yang, Y.R., Zhu, H.H., Han, J.S. and Wang, Y. Distribution of downstream regulatory element antagonist modulator (DREAM) in rat spinal cord and upregulation of its expression during inflammatory pain. *Neurochem Res*, *32* 9 (2007). 1592-1599.
197. Zhang, Y., Su, P., Liang, P., Liu, T., Liu, X., Liu, X.Y., Zhang, B., Han, T., Zhu, Y.B., Yin, D.M., Li, J., Zhou, Z., Wang, K.W. and Wang, Y. The DREAM protein negatively regulates the NMDA receptor through interaction with the NR1 subunit. *J Neurosci*, *30* 22 (2010). 7575-7586.
198. Zorzato, F., Fujii, J., Otsu, K., Phillips, M., Green, N.M., Lai, F.A., Meissner, G. and MacLennan, D.H. Molecular cloning of cDNA encoding human and rabbit forms of the Ca^{2+} release channel (ryanodine receptor) of skeletal muscle sarcoplasmic reticulum. *J Biol Chem*, *265* 4 (1990). 2244-2256.

VITA

Michael Anthony Grillo graduated from Palestine High School in Palestine, Texas, in 1995. In May 2000, Michael graduated from the Texas Wesleyan University in Texas with a Bachelor of Science in Biology. In August 2008, Michael started graduate studies at the University of North Texas Health Science Center, Fort Worth, Texas, and continued his studies at the University of Missouri – Kansas City in Kansas City, Missouri in 2009. He received a Master's degree in Cell Biology and Biophysics in 2010.